nanomaterials

Electrospun Nanomaterials

Applications in Food, Environmental Remediation, and Bioengineering

Edited by

Ricardo Mallavia and Alberto Falco

Printed Edition of the Special Issue Published in *Nanomaterials*

www.mdpi.com/journal/nanomaterials

MDPI

Electrospun Nanomaterials

Electrospun Nanomaterials

Applications in Food, Environmental Remediation, and Bioengineering

Editors

Ricardo Mallavia
Alberto Falco

MDPI • Basel • Beijing • Wuhan • Barcelona • Belgrade • Manchester • Tokyo • Cluj • Tianjin

Editors
Ricardo Mallavia
Instituto de Biología Molecular y Celular,
Universidad Miguel Hernández
Spain

Alberto Falco
Instituto de Biología Molecular y Celular,
Universidad Miguel Hernández
Spain

Editorial Office
MDPI
St. Alban-Anlage 66
4052 Basel, Switzerland

This is a reprint of articles from the Special Issue published online in the open access journal *Nanomaterials* (ISSN 2079-4991) (available at: https://www.mdpi.com/journal/nanomaterials/special_issues/Electrospun_Nanomaterials).

For citation purposes, cite each article independently as indicated on the article page online and as indicated below:

LastName, A.A.; LastName, B.B.; LastName, C.C. Article Title. *Journal Name* **Year**, *Article Number*, Page Range.

ISBN 978-3-03943-226-4 (Hbk)
ISBN 978-3-03943-227-1 (PDF)

Contents

About the Editors . . . . . **vii**

Alberto Falco and Ricardo Mallavia
Electrospun Nanomaterials: Applications in Food, Environmental Remediation, and Bioengineering
Reprinted from: *Nanomaterials* **2020**, *10*, 1714, doi:10.3390/nano10091714 . . . . . **1**

Luying Zhao, Gaigai Duan, Guoying Zhang, Haoqi Yang, Shuijian He and Shaohua Jiang
Electrospun Functional Materials toward Food Packaging Applications: A Review
Reprinted from: *Nanomaterials* **2020**, *10*, 150, doi:10.3390/nano10010150 . . . . . **7**

Giulia Massaglia, Francesca Frascella, Alessandro Chiadò, Adriano Sacco, Simone Luigi Marasso, Matteo Cocuzza, Candido F. Pirri and Marzia Quaglio
Electrospun Nanofibers: from Food to Energy by Engineered Electrodes in Microbial Fuel Cells
Reprinted from: *Nanomaterials* **2020**, *10*, 523, doi:10.3390/nano10030523 . . . . . **39**

Nicole Angel, S. N. Vijayaraghavan, Feng Yan and Lingyan Kong
Electrospun Cadmium Selenide Nanoparticles-Loaded Cellulose Acetate Fibers for Solar Thermal Application
Reprinted from: *Nanomaterials* **2020**, *10*, 1329, doi:10.3390/nano10071329 . . . . . **51**

Amalia Mira, Carlos Sainz-Urruela, Helena Codina, Stuart I. Jenkins, Juan Carlos Rodriguez-Diaz, Ricardo Mallavia and Alberto Falco
Physico-Chemically Distinct Nanomaterials Synthesized from Derivates of a Poly(Anhydride) Diversify the Spectrum of Loadable Antibiotics
Reprinted from: *Nanomaterials* **2020**, *10*, 486, doi:10.3390/nano10030486 . . . . . **61**

Carla N. Cruz-Salas, Cristina Prieto, Montserrat Calderón-Santoyo, José M. Lagarón and Juan A. Ragazzo-Sánchez
Micro- and Nanostructures of Agave Fructans to Stabilize Compounds of High Biological Value via Electrohydrodynamic Processing
Reprinted from: *Nanomaterials* **2019**, *9*, 1659, doi:10.3390/nano9121659 . . . . . **73**

Feifei Wang, Zhaoyang Sun, Jing Yin and Lan Xu
Preparation, Characterization and Properties of Porous PLA/PEG/Curcumin Composite Nanofibers for Antibacterial Application
Reprinted from: *Nanomaterials* **2019**, *9*, 508, doi:10.3390/nano9040508 . . . . . **85**

Rina Afiani Rebia, Nurul Shaheera binti Sadon and Toshihisa Tanaka
Natural Antibacterial Reagents (*Centella*, Propolis, and Hinokitiol) Loaded into Poly[(*R*)-3- hydroxybutyrate-*co*-(*R*)-3-hydroxyhexanoate] Composite Nanofibers for Biomedical Applications
Reprinted from: *Nanomaterials* **2019**, *9*, 1665, doi:10.3390/nano9121665 . . . . . **99**

Ekaterina N. Maevskaia, Anton S. Shabunin, Elena N. Dresvyanina, Irina P. Dobrovol'skaya, Vladimir E. Yudin, Moisey B. Paneyah, Andrey M. Fediuk, Petr L. Sushchinskii, Gerald P. Smirnov, Evgeniy V. Zinoviev and Pierfrancesco Morganti
Influence of the Introduced Chitin Nanofibrils on Biomedical Properties of Chitosan-Based Materials
Reprinted from: *Nanomaterials* **2020**, *10*, 945, doi:10.3390/nano10050945 . . . . . **117**

Svetlana Miroshnichenko, Valeriia Timofeeva, Elizaveta Permyakova, Sergey Ershov, Philip Kiryukhantsev-Korneev, Eva Dvořaková, Dmitry V. Shtansky, Lenka Zajíčková, Anastasiya Solovieva and Anton Manakhov
Plasma-Coated Polycaprolactone Nanofibers with Covalently Bonded Platelet-Rich Plasma Enhance Adhesion and Growth of Human Fibroblasts
Reprinted from: *Nanomaterials* **2019**, *9*, 637, doi:10.3390/nano9040637 . . . . . **131**

Yuchao Li, Chengzhu Liao and Sie Chin Tjong
Electrospun Polyvinylidene Fluoride-Based Fibrous Scaffolds with Piezoelectric Characteristics for Bone and Neural Tissue Engineering
Reprinted from: *Nanomaterials* **2019**, *9*, 952, doi:10.3390/nano9070952 . . . . . **151**

About the Editors

Ricardo Mallavia (full professor) is a chemist and a polymer specialist, having obtained his PhD in 1994 at the University Autónoma of Madrid (UAM, Spain). He is currently a professor at Miguel Hernández University (UMH, Spain) and a member of the Spanish Chemical Society (RSEQ), sections Polymers (POL) and Nanoscience and Molecular Materials (MAM). He has participated in more than 20 research projects in the last 15 years; six projects as principal investigator. He completed two stays as a visiting professor at the University of California in Santa Barbara, in 2002 and 2013. He has co-authored a hundred articles (h = 26). His research activity has mainly focused on polymer science, mostly in the synthesis and characterization of conjugated polyfluorenes with interest for potential biological applications, and recently in the preparation of nanostructures, particularly in nanofibers, based on polymeric biomaterials.

Alberto Falco (senior researcher), after studying Biological Sciences, completed his PhD studies at the Miguel Hernandez University of Elche (Spain) on animal antimicrobial peptides with antiviral activity, in 2008 (summa cum laude). From 2009 to 2011, he worked as a postdoctoral research assistant at the School of Life Sciences of Keele University (United Kingdom) and, from 2011 to 2013, at the Wageningen Institute of Animal Sciences of Wageningen University (Holland). Since 2014, Dr. Alberto Falco has held a position as senior scientist at the Institute of Research, Development and Innovation in Biotechnology of Elche (IDiBE) back to the Miguel Hernández University of Elche. Overall, so far, he has more than 15 years of experience in both public research agencies and industrial R&D organizations, and has authored over 40 publications in peer-reviewed journals, 4 chapters and 1 book. His expertise involves the innate immune responses to animal viruses, and his current main research interests comprise the encapsulation technologies of natural bioactive compounds with applications in antiviral treatment.

nanomaterials

MDPI

Editorial

Electrospun Nanomaterials: Applications in Food, Environmental Remediation, and Bioengineering

Alberto Falco * and Ricardo Mallavia *

Institute of Research, Development and Innovation in Biotechnology of Elche (IDiBE), Miguel Hernández University (UMH), 03202 Elche, Spain

* Correspondence: alber.falco@umh.es (A.F.); r.mallavia@umh.es (R.M.)

Received: 24 August 2020; Accepted: 28 August 2020; Published: 29 August 2020

Among the large number of methods to fabricate nanofibers, electrospinning stands out because of its simplicity and versatility. The formation of nanoscaled fibers via electrospinning is based on the application of high voltage (usually ranging from 1 to 30 kV) to generate an electrostatic field that induces the formation and stretching of a jet from a viscoelastic polymer solution or melt. The nanofibers are finally formed by either evaporation of solvent or freezing of the melt. Regarding the setup, one of the electrodes can be placed either directly in this solution, or onto the metal needle attached to the tip of the syringe feeding the solution at a constant and controllable flux by means of an infusion pump. The other electrode is connected to a metal object that can work as collector (that can be covered by a fabric), usually a static plane surface that is located perpendicular and at a certain distance from the spinneret. As a result of the forces involved, a highly electrified continuous jet is ejected from the pendent drop of solution at the top of the spinneret and deposited on the collector as randomly distributed nanofibers. In addition, by modifying the basic setup of electrospinning and/or the composition of the electrospinnable solution, the morphology (including porosity), diameter and functionality of the final outcome can be controlled. For instance, nanofibers can even be aligned by adapting the collector to a rotary cylinder or disposed in a core/shell structure by using a spinneret with two coaxial capillaries supplying two solutions separately [1–4].

The origin of this method, which allows the efficient obtention of long, uniform nanofibers with either solid or hollow interiors, dates back to the beginning of the 20th century, when some essential technical milestones for its development, such as the generation and manipulation of electricity, were reached. However, a series of other preceding scientific advances paved the way towards this invention, which can be considered as a variant of the electrospraying process (i.e., the collapse of liquid jets into droplets by the effect) [3–5]. Among them, the distortion and attraction of liquid droplets when applying electrostatic forces, reported by William Gilbert in 1600, could be considered as the oldest one. In the middle of the 18th century, George Mathias Bose described the generation of aerosols by the application of high electric potentials to fluids, and Giovanni Battista Beccaria observed that when fluids were charged, they evaporated faster. Such discoveries might be considered as the basis for the development of electrospraying. It was not until the verge of 19th century that John William Strutt (Lord Rayleigh) first observed the electrospinning phenomena, and Charles Vernon Boys first designed and constructed an electrospinning device and drew fibers from a number of melts, mostly molten waxes. It was in 1900 and 1902 when John Francis Cooley and William James Morton, respectively, filed the first electrospinning patents on industrial applications, and a bit later when John Zeleny studied in detail the mechanisms underlying the process (mostly electrospraying). The origin of electrospinning was established with broad consensus in 1934, when Anton Formhals started patenting several inventions on the technology associated to this process. After up to 22 patents in about 10 years, Formhals greatly improved the process and made electrospinning an efficient and viable technique.

Later, the work of Sir Geoffrey Ingram Taylor in the 1960s, whose fundamental studies on the jet forming process laid the theory groundwork for electrospinning, is of note. Since then, the conical shape

of the jet occurring as a consequence of the distortion of the spinneret droplet when the electrostatic forces exceed its surface tension has been referenced as the "Taylor cone" in later literature [6]. More recently, Larrondo and Manley in the early 1980s, and the Reneker's group in the early 1990s, notably revitalized this technology by demonstrating the possibility of electrospinning a range of molten polymers [7] and organic polymer solutions [8,9], respectively. Reneker also popularized the term "electrospinning", which derives from the former "electrostatic spinning" used until then. In the last decades, the advances in the fabrication, processing, and characterization of electrospun nanofibers have contributed to the wide expansion of this technique across laboratories and industry. This growth is mainly promoted by the surging interest in nanotechnology and the great expectations placed on the unique properties of nanomaterials, with notable support from the outstanding progress of the materials and polymer sciences in recent times [4].

As for the raw materials used for electrospun nanofibers, polymers comprise an unlimited number of molecules with different properties that can even be endowed with extra specific features by means of feasible functionalization protocols. In addition, electrospun nanofibers can be prepared from not only single/pure polymer sources, but also compatible polymer blends to combine the properties of their moieties [10]. Altogether, this family of compounds guarantee an extraordinary diversity of nanofiber compositions and thus properties, which explains the broad application potential of these nanomaterials. Indeed, depending on their specific composition/properties, electrospun nanofibers can be exploited in multiple applications covering areas as different as nanoelectronics, energy storage, catalyst substrates, sensors, nanofilters, protective and smart clothing, and adsorbent and biomedical materials [11–15].

At this point, and regardless of the application, it is worth mentioning that the assessment of the environmental impact of the nanomaterials used, as well as their fabrication and degradation by-products, is critical to avoid possible harmful effects on ecosystems by allowing, for instance, the design of appropriate disposal protocols for these compounds and to preferentially opt for those that are eco-friendly. In this sense, polymers also offer a large collection of both natural, but also synthetic, electrospinnable compounds that are non-toxic and biodegradable, as well as biocompatible [4,10]. Electrospun nanofibers made of such biomaterials are thus suitable for applications involving direct (and indirect) contact with biological systems, which mostly comprise applications within the biomedical [1,4,11,13,16–19], but also the environmental protection [11,16] and the food packaging fields [11,20,21].

The present book compiles the Special Issue "Electrospun Nanomaterials: Applications in Food, Environmental Remediation, and Bioengineering" from the journal "Nanomaterials", and, therefore, it comprises several review and research articles addressing several applications of electrospun nanofibers in these areas. In regard to the application of these nanomaterials to the food field, the implementation of electrospinning in food packaging is thoroughly revised in Zhao et al. (2020) [22], which also includes a summary of the additional characteristics provided by functional food packaging materials, degradability, superhydrophobicity, edibility, antibacterial activity and high barrier protection, as well as the contribution of electrospun nanofibers to their development. In terms of environmental remediation, this topic is tackled by two research articles that converge on the green/sustainable generation of energy by improving two different applications (i.e., microbial fuel cells [23] and solar thermal techniques [24]) using electrospun nanofibers.

The current research and utilization of nanofibers mainly for biomedical applications is proportionally covered in this compilation. In this sense, the biomedical applications of electrospun nanofibers included here can be classified into two broad types: drug delivery systems and tissue scaffolds. Regarding drug delivery, polymers comprise a large number of biocompatible materials with an extraordinary versatility to be structured as different nanomaterials with drug-loading capacity. Thus, compounds with different solubility properties can be encapsulated into polymeric nanomaterials by either changing the polymer source or the nanomaterial type. Here, this is shown by Mira et al. (2020) [25] for the encapsulation of different classes of antibiotics by using two separate

derivatives of poly(methyl vinyl ether-alt-maleic anhydride) (PMVE/MA) that can be used (alone or in combination with other polymers such as fluorescent polyfluorenes [26–28]) for the fabrication of both nanoparticles [29] and electrospun nanofibers [30,31]. Polymeric nanofibers also protect loaded compounds from degradation, as described by Cruz-Salas et al. (2019) [32] for electrospun nanofibers made from agave fructans, which thermoprotect and photoprotect encapsulated β-carotene. Another advantage of polymeric nanofibers is their modifiable drug-release kinetics by means of feasible design changes to adjust their degradability or porosity for providing optimal therapeutic drug concentrations. As reported here [33,34], this property is being intensively investigated at present for the development of improved dressings, bandages or coatings with, for example, antibacterial activity. In this sense, the use of functional polymers such as chitosan (with reported protective immunomodulatory properties) is also attracting great interest, as widely reviewed by Maevskaia et al. (2020) [35].

Finally, the current great effort made by the scientific community in the development of tissue scaffolds based on electrospun nanofibers is also addressed here. The work of Miroshnichenko et al. (2019) [36] provides a representative example of the research lines in this area by reporting the cell interaction improvements when coating polycaprolactone nanofibers with covalently bonded platelet-rich plasma. Likewise, Li et al. (2019) [37] broadly review the progress in the particular area of electrospun polyvinylidene fluoride-based materials used for bone and neural tissue engineering.

In summary, the papers collected in this Special Issue entitled "Electrospun Nanomaterials: Applications in Food, Environmental Remediation, and Bioengineering" illustrate the high diversity and potential for implementation of electrospun nanofibers in these fields, including the covering of a wide number of subtopics. Undoubtably, such pieces of fundamental research will contribute to the promotion of electrospinning as the focal point in the future development of technological applications at the interface of biological systems, which promise long-term benefits for both health and the environment.

Author Contributions: Both guest editors conceived, wrote and reviewed this Editorial Letter. All authors have read and agreed to the published version of the manuscript.

Funding: This research was funded by the Spanish Ministerio de Economía y Competitividad, grant number MAT-2017-86805-R, and Spanish Ministerio de Ciencia e Innovación (MCI)—Agencia Estatal de Investigación (AEI)/Fondo Europeo de Desarrollo Regional (FEDER), grant number RTI2018-101969-J-I00.

Acknowledgments: We are grateful to all the authors who contributed to this Special Issue, as well as to the referees who notably helped to improve the quality of all submitted manuscripts. We also acknowledge the editorial staff of Nanomaterials, and especially Tina Tian, for their great support.

Conflicts of Interest: The authors declare no conflict of interest.

References

1. Frenot, A.; Chronakis, I.S. Polymer nanofibers assembled by electrospinning. *Curr. Opin. Colloid Interface Sci.* **2003**, *8*, 64–75. [CrossRef]
2. Li, D.; Xia, Y. Electrospinning of nanofibers: Reinventing the wheel? *Adv. Mater.* **2004**, *16*, 1151–1170. [CrossRef]
3. Subbiah, T.; Bhat, G.S.; Tock, R.W.; Parameswaran, S.; Ramkumar, S.S. Electrospinning of nanofibers. *J. Appl. Polym. Sci.* **2005**, *96*, 557–569. [CrossRef]
4. Bhardwaj, N.; Kundu, S.C. Electrospinning: A fascinating fiber fabrication technique. *Biotechnol. Adv.* **2010**, *28*, 325–347. [CrossRef]
5. Tucker, N.; Stanger, J.J.; Staiger, M.P.; Razzaq, H.; Hofman, K. The history of the science and technology of electrospinning from 1600 to 1995. *J. Eng. Fibers Fabr.* **2012**, *7*, 63–73. [CrossRef]
6. Taylor, G.I. Electrically driven jets. *Proc. R. Soc. Lond. A Math. Phys. Sci.* **1969**, *313*, 453–475.
7. Larrondo, L.; St. John Manley, R. Electrostatic fiber spinning from polymer melts. I. Experimental observations on fiber formation and properties. *J. Polym. Sci. Polym. Phys. Ed.* **1981**, *19*, 909–920. [CrossRef]
8. Doshi, J.; Reneker, D.H. Electrospinning process and applications of electrospun fibers. *J. Electrost.* **1995**, *35*, 151–160. [CrossRef]

9. Reneker, D.H.; Chun, I. Nanometre diameter fibres of polymer, produced by electrospinning. *Nanotechnology* **1996**, *7*, 216. [CrossRef]
10. Gunn, J.; Zhang, M. Polyblend nanofibers for biomedical applications: Perspectives and challenges. *Trends Biotechnol.* **2010**, *28*, 189–197. [CrossRef]
11. Liu, H.; Gough, C.R.; Deng, Q.; Gu, Z.; Wang, F.; Hu, X. Recent advances in electrospun sustainable composites for biomedical, environmental, energy, and packaging applications. *Int. J. Mol. Sci.* **2020**, *21*, 4019. [CrossRef] [PubMed]
12. Xue, J.; Wu, T.; Dai, Y.; Xia, Y. Electrospinning and electrospun nanofibers: Methods, materials, and applications. *Chem. Rev.* **2019**, *119*, 5298–5415. [CrossRef] [PubMed]
13. Ding, J.; Zhang, J.; Li, J.; Li, D.; Xiao, C.; Xiao, H.; Yang, H.; Zhuang, X.; Chen, X. Electrospun polymer biomaterials. *Prog. Polym. Sci.* **2019**, *90*, 1–34. [CrossRef]
14. Ding, Y.; Li, W.; Zhang, F.; Liu, Z.; Zanjanizadeh Ezazi, N.; Liu, D.; Santos, H.A. Electrospun fibrous architectures for drug delivery, tissue engineering and cancer therapy. *Adv. Funct. Mater.* **2019**, *29*, 1802852. [CrossRef]
15. Barhoum, A.; Pal, K.; Rahier, H.; Uludag, H.; Kim, I.S.; Bechelany, M. Nanofibers as new-generation materials: From spinning and nano-spinning fabrication techniques to emerging applications. *Appl. Mater. Today* **2019**, *17*, 1–35. [CrossRef]
16. Thenmozhi, S.; Dharmaraj, N.; Kadirvelu, K.; Kim, H.Y. Electrospun nanofibers: New generation materials for advanced applications. *Mater. Sci. Eng. B* **2017**, *217*, 36–48. [CrossRef]
17. Parham, S.; Kharazi, A.Z.; Bakhsheshi-Rad, H.R.; Ghayour, H.; Ismail, A.F.; Nur, H.; Berto, F. Electrospun nano-fibers for biomedical and tissue engineering applications: A comprehensive review. *Materials* **2020**, *13*, 2153. [CrossRef]
18. Edmans, J.G.; Clitherow, K.H.; Murdoch, C.; Hatton, P.V.; Spain, S.G.; Colley, H.E. Mucoadhesive electrospun fibre-based technologies for oral medicine. *Pharmaceutics* **2020**, *12*, 504. [CrossRef]
19. Teixeira, M.A.; Amorim, M.T.P.; Felgueiras, H.P. Poly (vinyl alcohol)-based nanofibrous electrospun scaffolds for tissue engineering applications. *Polymers* **2020**, *12*, 7. [CrossRef]
20. Becerril, R.; Nerín, C.; Silva, F. Encapsulation systems for antimicrobial food packaging components: An update. *Molecules* **2020**, *25*, 1134. [CrossRef]
21. Wang, M.; Wang, K.; Yang, Y.; Liu, Y.; Yu, D.-G. Electrospun environment remediation nanofibers using unspinnable liquids as the sheath fluids: A review. *Polymers* **2020**, *12*, 103. [CrossRef] [PubMed]
22. Zhao, L.; Duan, G.; Zhang, G.; Yang, H.; He, S.; Jiang, S. Electrospun functional materials toward food packaging applications: A review. *Nanomaterials* **2020**, *10*, 150. [CrossRef] [PubMed]
23. Massaglia, G.; Frascella, F.; Chiadò, A.; Sacco, A.; Marasso, S.L.; Cocuzza, M.; Pirri, C.F.; Quaglio, M. Electrospun nanofibers: From food to energy by engineered electrodes in microbial fuel cells. *Nanomaterials* **2020**, *10*, 523. [CrossRef] [PubMed]
24. Angel, N.; Vijayaraghavan, S.; Yan, F.; Kong, L. Electrospun cadmium selenide nanoparticles-loaded cellulose acetate fibers for solar thermal application. *Nanomaterials* **2020**, *10*, 1329. [CrossRef] [PubMed]
25. Mira, A.; Sainz-Urruela, C.; Codina, H.; Jenkins, S.I.; Rodriguez-Diaz, J.C.; Mallavia, R.; Falco, A. Physico-chemically distinct nanomaterials synthesized from derivates of a poly (anhydride) diversify the spectrum of loadable antibiotics. *Nanomaterials* **2020**, *10*, 486. [CrossRef]
26. Kahveci, Z.; Vázquez-Guilló, R.; Mira, A.; Martinez, L.; Falcó, A.; Mallavia, R.; Mateo, C.R. Selective recognition and imaging of bacterial model membranes over mammalian ones by using cationic conjugated polyelectrolytes. *Analyst* **2016**, *141*, 6287–6296. [CrossRef] [PubMed]
27. Vázquez-Guilló, R.; Martínez-Tomé, M.J.; Kahveci, Z.; Torres, I.; Falco, A.; Mallavia, R.; Mateo, C.R. Synthesis and characterization of a novel green cationic polyfluorene and its potential use as a fluorescent membrane probe. *Polymers* **2018**, *10*, 938. [CrossRef] [PubMed]
28. Vázquez-Guilló, R.; Falco, A.; Martínez-Tomé, M.J.; Mateo, C.R.; Herrero, M.A.; Vázquez, E.; Mallavia, R. Advantageous microwave-assisted suzuki polycondensation for the synthesis of aniline-fluorene alternate copolymers as molecular model with solvent sensing properties. *Polymers* **2018**, *10*, 215. [CrossRef]
29. Ruiz-Gatón, L.; Espuelas, S.; Larrañeta, E.; Reviakine, I.; Yate, L.A.; Irache, J.M. Pegylated poly (anhydride) nanoparticles for oral delivery of docetaxel. *Eur. J. Pharm. Sci.* **2018**, *118*, 165–175. [CrossRef]
30. Mira, A.; Mateo, C.R.; Mallavia, R.; Falco, A. Poly (methyl vinyl ether-alt-maleic acid) and ethyl monoester as building polymers for drug-loadable electrospun nanofibers. *Sci. Rep.* **2017**, *7*, 1–13. [CrossRef]

31. Martínez-Ortega, L.; Mira, A.; Fernandez-Carvajal, A.; Mateo, C.R.; Mallavia, R.; Falco, A. Development of a new delivery system based on drug-loadable electrospun nanofibers for psoriasis treatment. *Pharmaceutics* **2019**, *11*, 14. [CrossRef]
32. Cruz-Salas, C.N.; Prieto, C.; Calderón-Santoyo, M.; Lagarón, J.M.; Ragazzo-Sánchez, J.A. Micro-and nanostructures of agave fructans to stabilize compounds of high biological value via electrohydrodynamic processing. *Nanomaterials* **2019**, *9*, 1659. [CrossRef] [PubMed]
33. Wang, F.; Sun, Z.; Yin, J.; Xu, L. Preparation, characterization and properties of porous pla/peg/curcumin composite nanofibers for antibacterial application. *Nanomaterials* **2019**, *9*, 508. [CrossRef] [PubMed]
34. Rebia, R.A.; Tanaka, T. Natural antibacterial reagents (centella, propolis, and hinokitiol) loaded into poly [(r)-3-hydroxybutyrate-co-(r)-3-hydroxyhexanoate] composite nanofibers for biomedical applications. *Nanomaterials* **2019**, *9*, 1665. [CrossRef]
35. Maevskaia, E.N.; Shabunin, A.S.; Dresvyanina, E.N.; Dobrovol'skaya, I.P.; Yudin, V.E.; Paneyah, M.B.; Fediuk, A.M.; Sushchinskii, P.L.; Smirnov, G.P.; Zinoviev, E.V. Influence of the introduced chitin nanofibrils on biomedical properties of chitosan-based materials. *Nanomaterials* **2020**, *10*, 945. [CrossRef] [PubMed]
36. Miroshnichenko, S.; Timofeeva, V.; Permyakova, E.; Ershov, S.; Kiryukhantsev-Korneev, P.; Dvořaková, E.; Shtansky, D.V.; Zajíčková, L.; Solovieva, A.; Manakhov, A. Plasma-coated polycaprolactone nanofibers with covalently bonded platelet-rich plasma enhance adhesion and growth of human fibroblasts. *Nanomaterials* **2019**, *9*, 637. [CrossRef] [PubMed]
37. Li, Y.; Liao, C.; Tjong, S.C. Electrospun polyvinylidene fluoride-based fibrous scaffolds with piezoelectric characteristics for bone and neural tissue engineering. *Nanomaterials* **2019**, *9*, 952. [CrossRef]

nanomaterials

MDPI

Review

Electrospun Functional Materials toward Food Packaging Applications: A Review

Luying Zhao [1], Gaigai Duan [1,*], Guoying Zhang [2], Haoqi Yang [3,*], Shuijian He [1] and Shaohua Jiang [1,*]

[1] Co-Innovation Center of Efficient Processing and Utilization of Forest Resources, College of Materials Science and Engineering, Nanjing Forestry University, Nanjing 210037, China; zhaoluying1@163.com (L.Z.); shuijianhe@njfu.edu.cn (S.H.)

[2] College of Chemistry and Molecular Engineering, Qingdao University of Science and Technology, Qingdao 266000, China; zhanggy@qust.edu.cn

[3] College of Material Science and Engineering, Jilin University, Changchun 130022, China

* Correspondence: duangaigai@njfu.edu.cn (G.D.); yhq1214@126.com (H.Y.); shaohua.jiang@njfu.edu.cn (S.J.)

Received: 26 November 2019; Accepted: 10 January 2020; Published: 15 January 2020

Abstract: Electrospinning is an effective and versatile method to prepare continuous polymer nanofibers and nonwovens that exhibit excellent properties such as high molecular orientation, high porosity and large specific surface area. Benefitting from these outstanding and intriguing features, electrospun nanofibers have been employed as a promising candidate for the fabrication of food packaging materials. Actually, the electrospun nanofibers used in food packaging must possess biocompatibility and low toxicity. In addition, in order to maintain the quality of food and extend its shelf life, food packaging materials also need to have certain functionality. Herein, in this timely review, functional materials produced from electrospinning toward food packaging are highlighted. At first, various strategies for the preparation of polymer electrospun fiber are introduced, then the characteristics of different packaging films and their successful applications in food packaging are summarized, including degradable materials, superhydrophobic materials, edible materials, antibacterial materials and high barrier materials. Finally, the future perspective and key challenges of polymer electrospun nanofibers for food packaging are also discussed. Hopefully, this review would provide a fundamental insight into the development of electrospun functional materials with high performance for food packaging.

Keywords: electrospinning; food packaging; functional membrane; nanofibers

1. Introduction

Electrospinning is a versatile technique for continuously producing nanofibers with a fiber diameter range from sub-nanometers to micrometers. The electrospun fibers have been broadly applied in nearly all the fields, such as composites [1–5], tissue engineering [6–9], biomaterials [10,11], energy storage and conversion [12–16], food packaging [17–19], drug deliver and release [20,21], catalysts [22–25], sensors [26–29], flexible electronics [30–32], reactors [33,34], environmental protection [35–37], etc. During the fiber preparation process, the polymer solution or melt is induced by a high-voltage power supply device to accelerate injection onto a collecting plate with opposite polarity to form nanofiber membrane. Basically, there are three key components to fulfill the process: a high voltage supplier, a pipette or needle with small diameter, and a metal collector [38]. In details, during the electrospinning process, the polymer solution is extruded from the capillary tube by the electric field force, and a Taylor cone can be formed at the tip of the capillary. As the strength of electric field increases, positive charges could accumulate on the surface of the Taylor cone, which further overcomes the surface tension and cause fluid ejection. When the spinning process proceeds, the injected fluid could be stretched several

times longer than the original length, and the solvent evaporates simultaneously to form a continuous ultrafine polymer fiber.

The electrospinning process is a simple and effective strategy for fabricating nanofibers, which can prepare polymer nanofibers directly, continuously and even in a large scale. It has the advantages of mild experimental conditions, low cost, easy operation and function, wide range of raw materials, etc. The spinning process is controllable, and the parameters can be adjusted according to the different requirements in various research fields. For example, electrospun nanofibers can be prepared with custom shapes and various orientations to quantitatively investigate the relationship of mechanical properties and molecular orientation [39]. Generally, the nanofibers obtained by electrospinning would have the characteristics of fine size, large specific surface area, high porosity, large aspect ratio and superior mechanical properties.

Functional packaging materials are gradually evolving into the public eyes, which have the functions of moisture absorbing [40,41], antioxidant releasing [42,43] and flavor or odor absorbing [44]. However, for the functional packaging materials applied in the food field, some additional features must be considered, such as degradable, superhydrophobic, edible, antibacterial and high barrier. By virtue of their submicron to nano-scale diameter and very large surface area, electrospun fibers may offer numerous advantages compared to conventional film and sheet packages, such as being more responsive to changes (e.g., relative humidity and temperature) in the surrounding atmosphere. Furthermore, because the electrospinning process takes place at ambient conditions, electrospun fibers are more suitable for encapsulating thermally labile active agents as compared to the fibers made by conventional melt spinning process. Given these advantages mentioned above, electrospun fiber not only could incorporate into bioactive substances, but also could satisfy the requirements of designers and consumers for packaging materials. Therefore, the development of functional packaging materials based on electrospinning technology has become a hot spot in the food packaging field. In the following sections, different approaches for the preparation of functional electrospun fiber will be introduced and their applications on functional package materials will be described (Figure 1). Furthermore, a conclusion including future perspective and key challenges for electrospun functional packaging materials are also discussed. In a word, we believe electrospun materials are good candidates for food packaging materials, and this review would significantly promote the research on application of electrospun fibrous materials for food packaging materials.

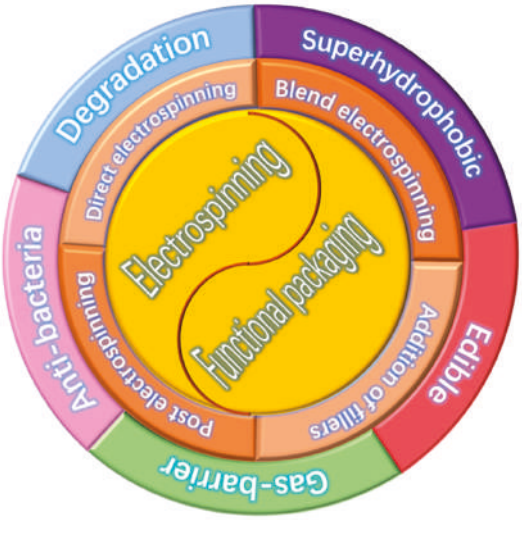

Figure 1. Overview of functional electrospun and food packaging materials diagram.

2. Strategies for the Preparation of Functional Electrospun Materials

In 1934, Formalas invented an experimental device for preparing polymer fibers by electrostatic force and applied for a patent that discloses how a polymer solution forms a jet between two electrodes. The above device could successfully produce a fiber by using high voltage static electricity, which is consequently recognized as the beginning of electrospinning technology [45]. Unfortunately, electrospinning technology did not attract numerous attentions until the middle of the 20th century. With the rapid development of nanomaterials and nanotechnology, electrospinning method has gradually received the attention of scholars from various areas.

So far, the preparation method for nanofibers based on electrospinning technology has been well developed. According to the electrospinning raw materials, it can be divided into melt electrospinning [46–48], solution electrospinning [49,50] and mixed electrospinning [51–53]. According to the design of the spray head, it can be classified as needleless electrospinning [54–56], coaxial or triaxial electrospinning [57–62], multi-jet electrospinning [63–65], etc. The application of electrospinning technology will be described below according to different situations.

2.1. Direct Electrospun Packaging Membrane

Direct electrospinning is defined here as single-component melt electrospinning or single-component solution electrospinning using one jet head. The functional electrospun materials commonly used in packaging field are chitosan (antibacterial), corn protein (edible), polyvinyl alcohol (transparent), etc.

Chitosan (CS) is obtained by deacetylation of chitin, which could form a transparent, elastic and oxygen resistant film. CS film can not only prevent fungi from contaminating and corroding food, but also effectively regulate the composition of oxygen and carbon dioxide around fruits and vegetables, inhibiting the aerobic respiration to a certain extent, so as to improve the shelf life. CS has a huge application potential in the food industry attribute to its advantages of short-time biodegradation, biocompatibility with human tissues, anti-microbial and antifungal activities and non-toxicity. Therefore, chitosan-based nanofiber membrane/film has attracted great attention in food preservation and packaging technology [66,67].

Ohkawa et al. [68] successfully prepared pure CS electrospun nanofibers with trifluoroacetic acid (TFA) as spinning solvent for the first time, because TFA can form salt with amino group in chitosan, effectively reducing the interaction between CS molecules, making electrospinning easier. In addition, the high volatility of TFA is beneficial to the rapid solidification of CS-TFA electrostatic jet. The concentration of CS also affects the morphology of fibers. When the mass fraction of chitosan is 6% or lower, beads and fibers coexist. When the mass fraction of CS is 7%, beads obviously decrease. When the mass fraction of CS is 8%, the spinning effect is better. The diameter of obtained fibers ranges from 390 to 610 nm, with an average diameter of 490 nm, but there still are small beads and interconnected fibers can be seen. To avoid the above phenomena of beads and interconnected fibers and improve the uniformity of electrospun fibers, dichloromethane (DCM) was added into chitosan-TFA solution. Under the optimum conditions, uniform CS nanofibers with an average diameter of 330 nm can be obtained.

In addition to the TFA as solvent, another effective solvent for chitosan is concentrated acetic acid. Geng et al. [69] studied the electrospinning of CS with concentrated acetic acid as solvent. The results show that with the increase of acetic acid concentration, the surface tension of chitosan-acetic acid solution decreases, while the viscosity does not change significantly. At the same time, the charge density of the jet increases. When the mass fraction of acetic acid is 30%, nanofibers begin to appear, accompanied with a large number of beads; when the mass fraction is 90%, uniform fibers with an average diameter of 130 nm can be obtained, and no beads appear. The molecular weight and concentration of CS also affect the formation of fibers. Only when the molecular weight of CS is about 1.06×10^5 g/mol and the mass fraction is 7–7.5%, the beadless nanofibers can be produced. However, high content of CS (more than 90%) cannot be well dissolved in solvent, which is difficult to meet the

requirements of spinning viscosity. In addition, the electric field strength also affects the formation of fibers. When the electric field strength is 1 kV/cm, spindle beads and coarse fibers appear. When the electric field strength is 3–4.5 kV/cm, uniform and regular fibers can be formed. However, when the electric field strength is greater than 4.5 kV/cm, a great number of beads could exist in the obtained fine fibers due to the tensile force increases and the charged jet is unstable.

Besides the solvent composition and concentrate, the fiber morphology is also influenced by other parameters, such as applied voltage, needle diameter, receiving distance and feed rate. For instance, Sencadasa et al. [70] investigated the effects of electrospinning parameters on the average diameter and width distribution of CS nanofibers. By controlling the solution parameters and process parameters, the spinning process gets more stable, and the target fiber size could be customized. However, the parameters of the needle tube diameter and feeding speed have no effect on the fiber diameter. When the applied voltage is increased, the diameter of the fibers would decrease. Furthermore, with the reduction of receiving distance, the fibers diameter at the tip of the needle decreases due to the decrease of electrostatic field intensity.

Zein, a kind of storage protein in corn, has a good film-forming property owing to its rich sulfur-containing amino acids that could connect the disulfide bond and water release bond. As a renewable polymer protein, zein has good biocompatibility, which can be used not only as fresh-keeping film, but also as film coating for food preservation [71]. Moreover, it can also be used as edible packaging films in food packaging.

Takanori et al. [72] investigated the parameters such as electric field and polymer solution concentration in the electrospinning process to prepare zein nanofiber membranes. They choose 15 kV and 30 kV as the field strength and 80 wt.% ethanol aqueous solution as solvent. It is found that when the electric field strength is 15 kV, the polymer concentration is mainly 21 wt.%. However, the electric field strength is increased to 30 KV, fibers could be generated at 18 wt.% of polymer concentration. Neo et al. [73] also prepared the electrospun zein membranes with the 80% ethanol as solvent, and further studied the fiber morphology affected by three processing parameters including solution concentration, electric field strength and solution parameters. That is, with the increase of zein concentration, the viscosity of solution would increase, which promotes the formation of bead-free fiber, and the average fiber diameter become larger. They also found that there is an interaction effect between the electric field and feed rate of the solution. At a high voltage, changes of the fiber diameter have a more sensitive response to the feed rate of the solution. Similarly, changes in fiber diameter were also found to be more responsive to the applied voltage at a high feed rate. However, at a low applied voltage, the effect for the feed rate on average fiber diameter will not be significant since the amount of charges are not enough to accelerate the solution.

Polyvinyl alcohol (PVA) film is a kind of antistatic film with good performance, which is widely used in the sales and packaging of textiles and clothing. Compared with polyethylene, polypropylene and other general-purpose films, polyvinyl alcohol film exhibits the advantages of high transparency, good antistatic property, which can significantly reduce the dust absorption effect [74–76]. Furthermore, polyvinyl alcohol is often used in water-soluble packaging.

Tao et al. [77] studied the effects of molecular weight and concentration in a PVA-water system on the morphology and structure of PVA electrospun nanofibers (Figure 2). They found that with the increase of molecular weight, the morphology of PVA fibers can be changed from bead to beaded fibers, then to smooth fibers and finally to flat ribbons at the same concentration. Supaphol et al. [78] further explored the effects of solution concentration and parameters change during electrospinning process (applied voltage and collection distance) on the morphology and fiber diameter of as-spun PVA fiber mats and individual fibers. In the range of solution concentration (6–14%), the average fiber diameter for as-spun PVA fiber mats decreases with the increase of solution concentration and applied voltage, which ranges from 12.5 to 25 kV. At a fixed applied potential of 15 kV, when the receiving distance was changed within a certain range (5–20 cm), the average fiber diameter would become

smaller as the receiving distance increased. In addition, there is a decrease of the viscosity that can be observed after sonication, which could result in a decrease of average fiber diameter.

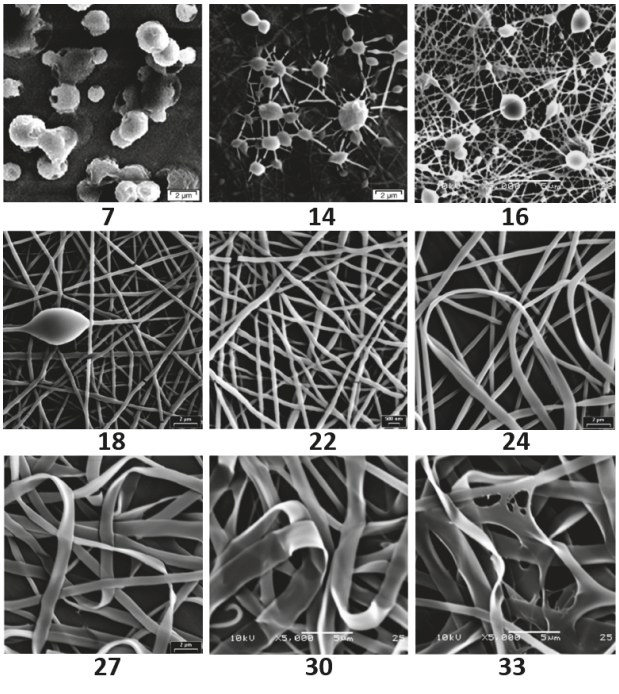

Figure 2. Photographs showing the range of structures that can be produced as the concentration (wt.%) is increased at Mw = 18,000 g/mol [77]. © 2006 Elsevier B.V. All rights reserved.

In another study, Yang et al. [79] employed bubble electrospinning, a special electrospinning method, to prepare PVA nanofibers, and studied the effects of solution concentration and viscosity on the morphology and fiber diameter. They concluded that the higher PVA concentration in solution, the smoother surfaces and larger diameters in the obtained nanofibers. There is an allometric scaling relation between the diameter and PVA aqueous solution concentration: $d \propto C\hat{}5$. Niu et al. [80] fabricated PVA nanofibers via a needless method, which utilized a cone-shaped metal wire coil as a spinneret instead of needle. This method would increase the fiber production efficiency and achieve a finer average fiber diameter than that of traditional electrospinning. In the same year, this group [81] reported a needleless electrospinning method including a rotating disk and cylinder to prepare PVA nanofibers, and discussed the effect of nozzle shape on spinning process and fiber morphology. On one side, this needleless electrospinning method could improve the productivity, which overcomes the shortcomings of the traditional multi-needle electrospinning method such as large operating space and careful design. On the other side, needleless electrospinning avoids strong charge repulsion between the spinneret and adjacent needles, resulting in an even fiber deposition.

Apart from three polymers mentioned above, some degradable polymers have also been applied in food packaging field, such as polycaprolactone (PCL), poly (propylene carbonate) (PPC), polylactic acid (PLA) and natural cellulose, starch. Moreover, electrospinning plastic materials, such as polyvinyl chloride (PVC), polyethylene (PE), polypropylene (PP), polystyrene (PS), polyethylene terephthalate (PET) and nylon, are commonly used in the field of packaging as well.

2.2. Mixed Electrospun Packaging Membrane

Electrospinning of polymer blends enables the produced nanofibers possess multi-function from each constituent. Up to now, there are many ways for solution mixing, such as electrospinning of multi-components mixed solutions, and design of jet device to obtain multi-components mixed fiber membranes. In the food packaging industry, electrostatic spinning technology is usually employed to prepare composite mats of two or more components.

2.2.1. Blending with Different Polymer Solutions

Before electrospinning, by mixing two or three polymers in spinning solutions, the fiber membranes with better performance could be obtained. Recently, some natural and natural-derived polymers have been used to prepare electrospun fibers through blending with other functional polymers in spinning solutions.

Feng et al. [82] blended gelatin (GT) and PCL (50:50) in trifluoroethanol (TFE) cosolvent, and found a phase-separation behavior of the GT/PCL polymers, which leads to inferior morphology of fibers during the electrospinning. In order to solve this problem, they added a tiny amount of acetic acid to the mixed solution. As a result, the opaque solution became transparent immediately without any obvious precipitation for over one week, and the obtained nanofibers demonstrated a thin, smooth and homogeneous morphology.

Chitosan is soluble in many solvents. It is soluble in organic acids, such as dilute acetic acid, formic acid and lactic acid, and also soluble in the mixture of water and methanol, ethanol or acetone, and its physical and chemical properties can be used for electrospinning, so it is often mixed with other polymers to prepare electrospinning fibers. González et al. [83] studied the thermophysical properties of CS + starch + PET fibers via a blending electrospinning, which could have excellent mechanical properties, thermal stability and biodegradability due to the strong intermolecular force among three components verified by Infrared spectra. Sajeev et al. [84] electrospun PVA and CS in a mixed homogeneous solution to prepare nanofibers and fiber mats. The effects of parameters (such as flow rate, receiving distance and voltage) on the morphology and fibers diameter were also investigated. It was found that the effects of parameters on fibers accorded with a simple extensional creep model. In addition, there is a negative correlation between the content of CS and fibers diameter, which is because the CS is an ionic polyelectrolyte that could enhance the charge density of the surface of jet stream and the received electric field force, causing a decrease of fiber diameter.

2.2.2. Blending by Multiple-Jet Electrospinning

Traditional single-nozzle electrospinning method has restricted its industrial application because of its low output. After years of research and design, the combination of multiple nozzles with different specifications and quantities has been developed.Different nozzles are injected with various solutions, which are mixed and entangled into fibers, then deposited into mats during the electrospinning (as shown in Figure 3, [85]). For example, Ding et al. [86] prepared a series of biodegradable PVA/cellulose acetate (CA) nanofibrous mats via a multi-jet electrospinning method. The weight ratio of the PVA and CA in fiber mats can be controlled by changing the number ratio of PVA/CA jets. Moreover, this multiple-jet electrospinning process ensures a good dispersion of two polymers in the PVA/CA hybrid felts.

The method described below can also be used to prepare hybrid electrospun fibers. Wang et al. [87] utilized a special multi-jet electrospinning method to spin the melted polyethylene and PCL, which actually was an unconfined spinning geometry instead of a needle as performed in Figure 4. In this process, due to the influence of the applied electric field, numerous parallel jets of molten polymer are formed at the plate edge, and finally polymer films are obtained on the collector. Compared with traditional needle electrospinning, unconfined geometries [88–91] rely on electric-field induced spontaneous fluid perturbations to form jet sites, rather than mechanically pumping fluid through a

confining nozzle. As the nozzle blockage does not occur in this device, and nanofibers from parallel jets could be prepared synchronously in such an open configuration, so that the production rate has been greatly improved. It is a convenient and high-throughput method for industrial production of microfibers and nanofibers with thermoplastic or other high-viscosity fluids.

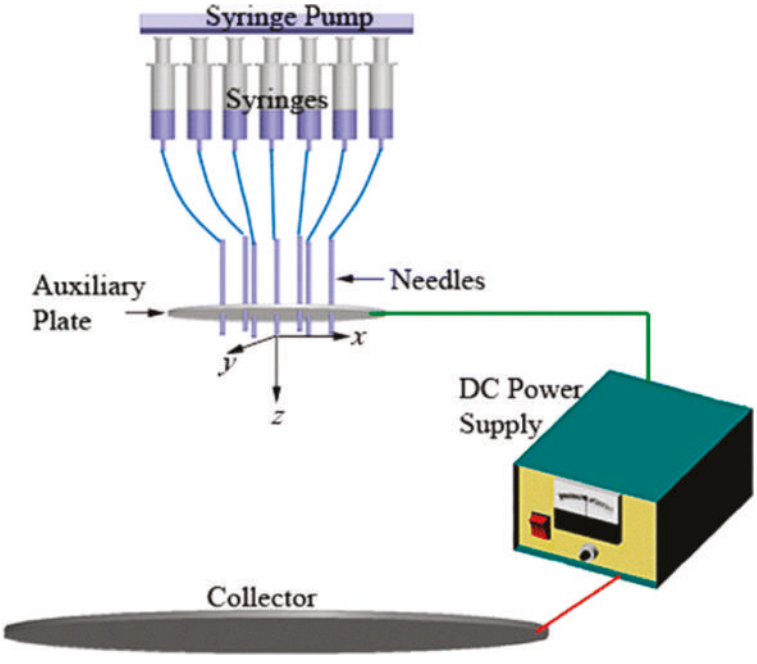

Figure 3. A schematic of the experimental setup used in the multi-jet electrospinning process [85]. © American Chemical Society 2014.

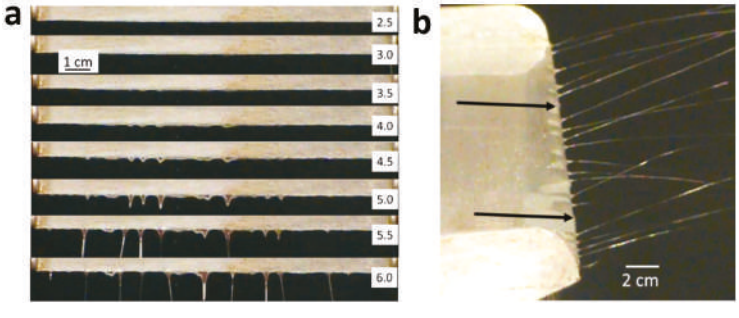

Figure 4. (**a**) Sequential images of the polymer-melt coated plate edge showing the progression of the fluid with time (in minutes, right side) at 180 °C at an applied voltage of −45 kV. The plate is oriented horizontally and being viewed from above. (**b**) Image of electrospinning from a polymer melt coated source plate (PE at 170 °C, −45 kV) in steady state (i.e., after 30 min). The black arrows indicate non-jetting perturbations. This figure is adapted from [87]. © 2014 IOP Publishing Ltd.

2.2.3. Blending by Coaxial Electrospinning

Coaxial electrospinning could produce a new type of nanofibers with a core-shell structure. In the coaxial electrospinning [57], the syringe is designed as two chambers, the outside chamber is generally

filled with the polymer solution, and another polymer solution or powders in the inside chamber. During the electrospinning, a core-shell droplet firstly appears at the outlet of the core-shell needle, and then forms the core-shell structure fibers under the force of electric field.

Yao et al. utilized coaxial electrospinning technology to successfully prepare a novel antibacterial composite through encapsulating orange essential oil (OEO) in zein prolamine. The obtained fine fibers ranging in diameter from 0.7 to 2.3 µm depending on the zein prolamine solution concentration and process parameters. Fiber composites exhibit an antibacterial activity against *Escherichia coli* and can be used as food packaging materials for bioactive food preservation, such as extending the shelf life of fruits [92].

It is common that the shell and core are different polymers. Komur et al. [93] fabricated starch and PCL composite nanofibers by coaxial needle electrospinning technique as shown in Figure 5. In this paper, the PCL solution was fed through the inner needle, and the starch solution was located at the outer medium. It was found that processing parameters have a significant influence on the fibers diameter, including polymer concentration, flow rate and voltage. The effect of starch ratio on the physical properties and morphological structures of fiber was also studied. That is, the higher the proportion of starch, the greater of the electrical conductivity, viscosity and density, while the beads would more likely appear in the fibers due to the starch tends to prefer to form beads rather than fibers. When the ratio of the starch increases, the volume of beads would become larger, which will cause the average fibers diameter becomes larger and the fibers strength gets higher. Park et al. [94] prepared levofloxacin-loaded CS and PCL nanofibers by coaxial electrospinning to control the release of antibiotics. They employed CS containing levofloxacin as a core, and PCL as a shell. PCL with different concentrations (8, 12, 16 and 20 wt.%) were set up to explore the effects of nozzle shapes on the sustained release of levofloxacin. As expected, the CS-PCL nanofiber scaffolds with coaxial nozzles had better performance on the sustained release of levofloxacin. Alharbi et al. [95] prepared PLA/PVA and PVA/PLA nanofibers with core/shell-structure to study the mechanical properties of PLA and PVA composite. According to the mechanical test results under static loading, the tensile strength and plasticity of core/shell PLA/PVA nanofibers increased by nearly 233% and 150% respectively compared with the original value. Dynamic loading and creep loading experiments show that there is a strong physical interaction between PLA layer and PVA layer, which could improve the mechanical properties.

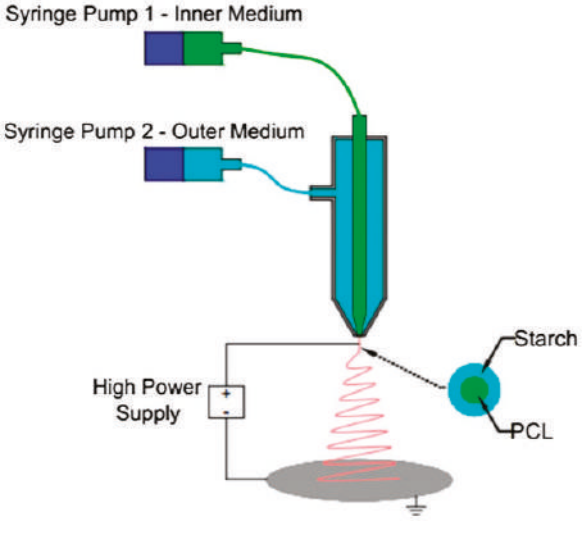

Figure 5. Schematic representation of the coaxial needle electrospinning set-up [94]. © The Korean Society of Pharmaceutical Sciences and Technology 2012.

Sometimes, functional substances such as antibacterial substances are loaded into the core of the coaxial electrospun fiber, which would release later so as to be effective. Korehei et al. [96] directly incorporated the T4 bacteriophage into the fiber core to prepare a core/shell fiber structure via a coaxial electrospinning method. The electrospun fibers were produced using a PEO/chloroform solution as the shell and a T4 bacteriophage/buffer suspension as the core. Coaxial electrospinning could produce continuous core/shell fibers with bead-free morphology, and the T4 bacteriophage was uniformly incorporated in the core of fibers. The core/shell fiber encapsulated bacteriophage exhibits full bacteriophage viability after storing for several weeks at +4 °C, which can be applied in meat packaging. He et al. [97] employed coaxial electrospinning technology to prepare anti-infective drug delivery carriers (Figure 6), i.e., poly (e-caprolactone)/zein uniform beadless core/shell nanofibers loaded with metronidazole (MNA). The prepared fiber membranes were hydrophobic and could inhibit the growth of anaerobic bacteria by releasing MNA.

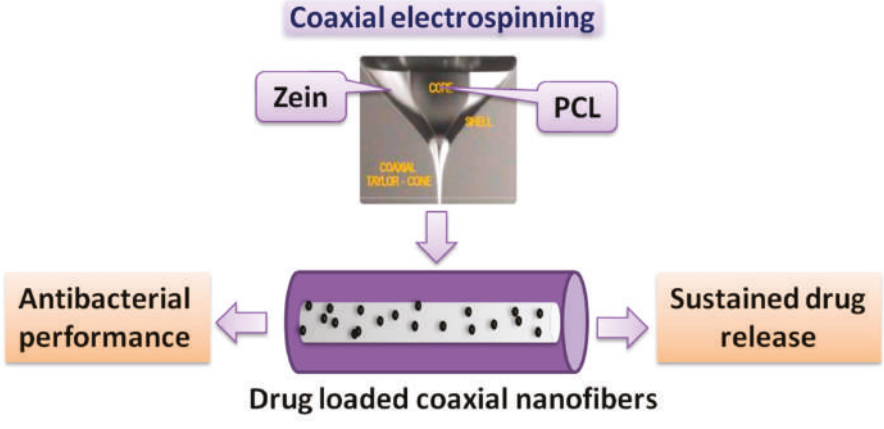

Figure 6. Structure diagram of coaxial fiber [97]. © Elsevier Inc. All rights reserved 2016.

2.3. Addition of Inorganic Fillers

In order to achieve multi-function for nanofiber-based food packaging materials, various fillers have been added into polymer substance, especially inorganic fillers that possess conductivity, magnetism, antibacterial property, etc. [98–101]. Then, a nanofiber-based food packaging material could be prepared through the electrospinning technique.

2.3.1. Conductive Fillers

Electrostatic hazard is a common problem in the packaging industry. Some severe accidents and impacts, such as fire, explosion and dust absorption are related to the electrostatic effect. Generally speaking, the insulating material is easy to produce static electricity. Adding conductive fillers is an efficient way to solve the problem and enhance the antistatic performance. Moreover, conductive packaging materials have a great potential for application in smart packaging due to their combination with some electronic devices.

Carbon-based conductive materials are often used as conductive additives to prepare conductive/anti-static packaging materials with wide application and large usage [102]. Carbon black has been widely adopted, but it has a huge loss of mechanical properties for the composites. By comparison, carbon nanotubes (CNTs) exhibit the advantages of less filling amount and negligible mechanical properties effects, which are emerged as a new generation of carbon-based conductive materials. Yang et al. [103] prepared electrospun biodegradable PLA composites which using CNTs as conductive fillers. They found that the morphology of the fibers is related to the loading of

CNTs. At a low loading level, the CNTs can be well embedded in the PLA matrix to form a fiber axis-oriented nanowire structure. At a high loading level, the CNTs are mainly dispersed in the form of bundles along with the fiber axis, and the resulting fibers are tortuous or misshaped. Meng et al. [104] studied the effects of different multiwalled CNTs (MWCNTs) content (0.1%, 0.5%, 1%, 2% and 5%) on the properties of non-bead PCL-MWCNTs nanofiber membranes, which found that the diameter distribution, average diameter, crystallinity and tensile strength are increased with the addition of MWCNTs. Moreover, the electrospun PCL–MWCNTs nanofiber membranes also exhibited a good degradability. Giner et al. [105] obtained electrospun nanocomposite fibers mats by embedding graphene nanoplatelets (GNPs) in poly (ethylene-co-vinyl alcohol) (EVOH) fibers. The heat-treated fibers mats at 158 °C could produce continuous, contact and transparent films, which have a great potential to be applied in the intelligent packaging field. For instance, smart labels or tags can be anticipated.

2.3.2. Magnetic Fillers

For various electronic components, such as electronic precision instruments, medical devices, computers, automatic office equipment and other products, are sensitive to electromagnetic radiation, therefore, the anti-electromagnetic radiation packaging is urgently needed. Adding magnetic filler is an effective way to endow materials with anti-electromagnetic radiation performance. Recently, Iron oxides or compounds have been often employed as the magnetic fillers for electrospun nanofibers.

Song et al. [106] encapsulated self-assembled iron-platinum (FePt) magnetic nanoparticles in PCL nanofibers by coaxial electrospinning. The discrete FePt nanoparticles array can be arranged in a long-range order along the fiber axis at 3000 nm. Wang et al. [107] prepared Fe_3O_4/PVA composite nanofibers by combining in-situ polymerization and electrospinning technology. The Fe_3O_4 magnetic fluids were synthesized through chemical co-precipitation method in the presence of 6 wt% PVA aqueous solution, which avoids the agglomeration of magnetic nanoparticles due to the stabilizing effect of PVA. Wei et al. [108] prepared a porous magnetic biodegradable Fe_3O_4/CS/PVA nanofiber membranes, and explored the influence of electrospinning parameters (polymer concentration, Fe_3O_4 content and magnitude of applied voltage) on the morphology of fibers. When the polymer concentration was 4.5 wt.%, the applied voltage was 20 kV and the loading of Fe_3O_4 nanoparticles was less than 5 wt.%, the uniform, smooth and continuous Fe_3O_4/CS/PVA nanofiber membrane can be obtained. Stylios [109] reported the effect of processing parameters on the morphology of PVA/$FeCl_3$ magnetic composite fibers, such as applied voltage, receiving distance, flow rate and solution concentration. This research provides guidance for the subsequent manufacture of flexible magnetic composite membranes. Kumar et al. [110] electrospun the PLA, PEG and magnetic nanoparticles (Fe_3O_4@SiO_2 core-shell NPs) mixed solution at room temperature to prepare a series of fibers. With other parameters remaining unchanged, the fiber diameter was reduced from 6 to 3 micrometers after the PLA solution was added to PEG. When the PLA solution mixed with PEG + MNPs (magnetic nanoparticles), the fiber diameter was decreased from 3 to 1 μm.

2.3.3. Photocatalytic Fillers

Photocatalytic fillers have the ability to impart the self-cleaning properties to functional packaging materials. Many scholars demonstrate the self-cleaning ability of materials by testing the rate of dyes degradation with different colors.

TiO_2 is a non-toxic, low-cost and good photocatalytic filler, which is often used to treat pollutants. Bedford et al. [111] prepared a photocatalytic self-cleaning fiber membrane through a coaxial electrospinning device, which employed a CA solution as a core and the TiO_2 dispersion as a shell. The obtained self-cleaning fiber membrane had been tested to completely degrade the blue dye within 7–8 h when exposed to a halogen lamp (Figure 7). Nasikhudin et al. [112] prepared PVA/TiO_2 composite nanofibers by electrospinning method, and studied the photocatalytic activity for

the degradation of methylene blue under ultraviolet light. It was found that the PVA/TiO_2 composite nanofibers suspended in dye solution could degrade 70% of the dye within 5 h.

ZnO is often doped as the filler into photocatalytic composite fibers because of its simple synthesis, non-toxic and pollution-free. Liu et al. [113] electrospun precursor solution of zinc acetate (ZnAc)/CA in mixed-solvent of N, N-dimethylformamide/acetone, then calcined that to obtain photo-catalytically active ZnO nanofibers. According to experiments, they found that ZnO nanofiber mats could degrade nearly 60% of Rhodamine B within 2 h under visible light irradiation. Khan et al. [114] successfully manufactured ZnO/poly (1,4-cyclohexanedimethylene isosorbide terephthalate) (PICT) nanofibers by electrospinning technique. When the load concentration of ZnO is 9% and the concentration of PICT is 10%, the composite fiber can achieve 99% self-cleaning efficiency within three hours exposed to UV light (Figure 7a). Apart from endowing the composite electrospun fiber membrane with self-cleaning ability, some photocatalytic fillers can also remove some organic compounds in the package. For example, Zhu et al. [115] prepared the electrospun PP films, which can be potentially be used as packaging material for bananas, because TiO_2 loaded in the fiber membrane would catalyze the degradation of ethylene and delay the excessive ripeness and deterioration of banana fruits (Figure 7b).

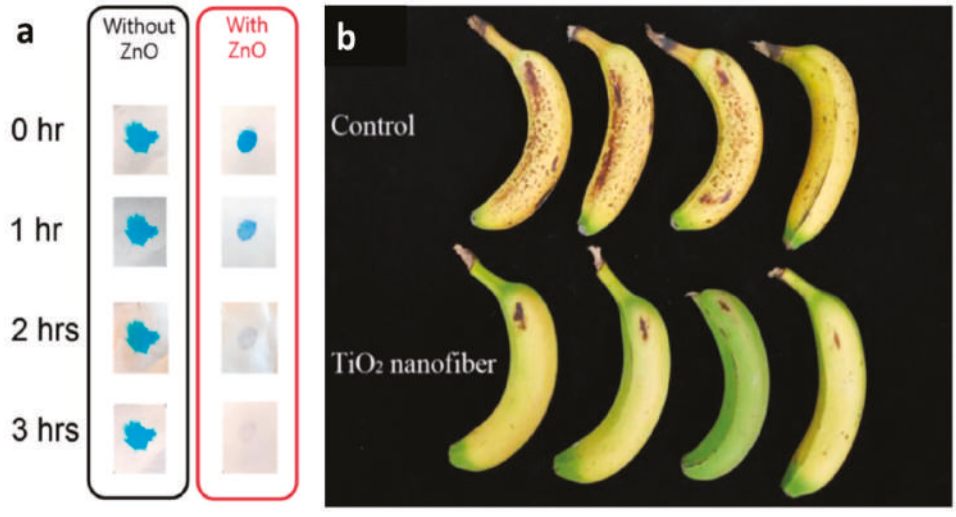

Figure 7. (**a**) Comparison of photocatalytic activity of fibers with and without ZnO [114], © 2018 SAGE Publications. (**b**) photographs of bananas stored for 10 days covered with PP film (control) or PP film and nanofiber containing 5 wt% TiO_2 [115]. © Springer Science+Business Media, LLC, part of Springer Nature 2018.

2.3.4. Antibacterial Fillers

Antimicrobial packaging materials has played a majority role in the field of food packaging, which could limit or prevent the growth of food spoilage bacteria or pathogens by prolonging the stagnation period of microorganisms, slowing down the growth rate or reducing the survival number of microorganisms, so as to ensure the quality and extend the shelf life of food. So far, there are three kinds of common antibacterial agents, which are the inorganic antibacterial agent, organic chemical antibacterial agent and natural biological antibacterial agent, respectively. Inorganic antibacterial agents mainly refer to some metal ions (such as Ag^+, Cu^{2+}, Zn^{2+}, etc.) or their compounds that would have antibacterial activity, and also the atomic oxygen sterilization, which is produced by a photochemical reaction. Among them, zinc oxide and titanium dioxide are the most investigated in previous reports.

The main characteristics of inorganic antibacterial agents are good heat resistance, wide antibacterial range, long effective antibacterial period and not easy to produce drug resistance [116].

Amna et al. [117] reported for the first time the fabrication of olive oil/polyurethane (PU) composite nanofibrous packaging mats decorated with ZnO nanoparticles by electrospinning. PU is thermoplastic polymer that demonstrates outstanding mechanical properties and water insolubility. Meanwhile, PU possesses good barrier properties, oxygen permeability and more like to the FDA (Food and Drug Administration) point. Olive oil, a natural material, is often loaded with various antibacterial ingredients, flavonoids and antioxidants. Likewise, zinc oxide nanoparticles (ZnO) possess antibacterial activity, which is low toxicity and biodegradability. These kinds of biodegradable packaging materials have displayed a potential antimicrobial activity against *S. aureus* and *S. typhimurium*. Therefore, it can be used for packaging fresh or processed meat and meat-based products (Figure 8). The synthesized nanofibers have the opportunity to replace non-degradable films and overcome the complexity of recycling.

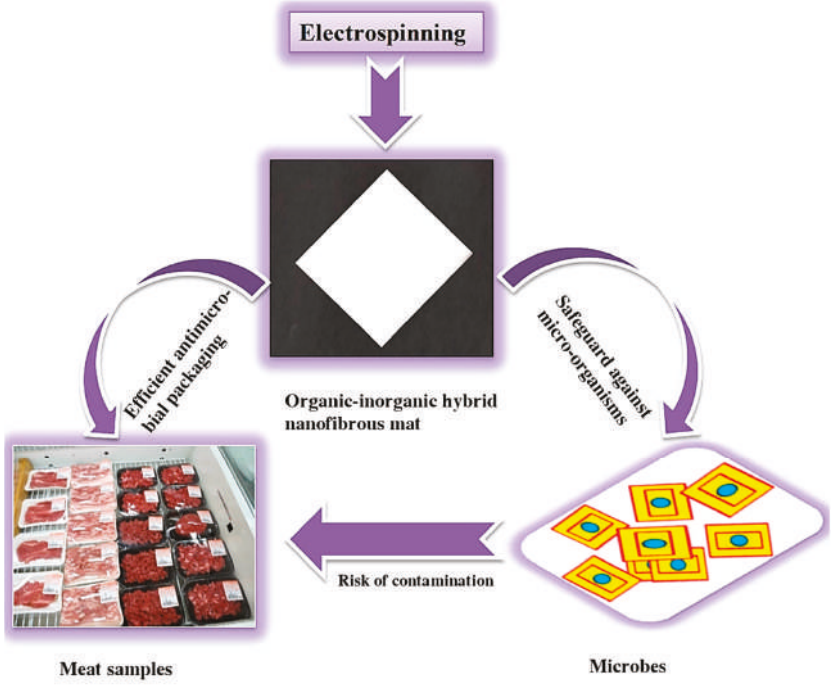

Figure 8. Electrospun hybrid mats; its antimicrobial concept and projected future applications as packaging material for meat and meat-based products [117]. © Association of Food Scientists & Technologists (India) 2014.

2.4. Post-Treatments of Electrospinning Membrane

Post-treatments, such as hot working, surface modification, dip coating, etc., could greatly enhance the performance of electrospun membranes, even expand the application range to meet the high requirements of designers.

2.4.1. Thermal Treatments

By heating the electrospun membrane, the nanofibers in the electrospun membrane can be crosslinked, and the properties such as mechanical properties can be further improved. For example,

Lee et al. [118] fabricated PVA nanofibers crosslinked with blocked isocyanate prepolymer (BIP) by the electrospinning process and subsequent thermal treatment. Their experiment showed that a chemical cross-linking reaction occurs between the hydroxyl group of PVA and the isocyanate group of BIP during the thermal treatment. After the chemical cross-linking finished, PVA/BIP nanofibers not only have a significant improvement in mechanical properties and water resistance, but also have an increased thermal stability. In addition, the fibers membrane has the general advantages of electrospun nanofibers, which is owing to a large surface area and high porosity, resulting in a wider application potential. Lee et al. [119] employed an electrospinning technology to prepare PCL fibers. In order to improve the mechanical properties, the fibers were placed in Pluronic F127 solution and heated at a various temperature ranging from 54 to 60 °C for 30 min. After the heat treatment, bonding occurs between fibers, and the biomechanical properties are improved significantly. Thus, these fibers possess adequate tensile properties, suture retention strength and burst pressure strength.

Theoretically, the solvent needs to volatilize in the electrospinning process, but there is always a little solvent remains in the fiber. As an effective strategy, thermal treatments could promote the volatilization of residual solvent. D'Amato et al. [120] have developed a new method for removing residual solvents to prolong the release time of small molecules in electrospun fibers (Figure 9). Firstly, degradable poly(L-lactic acid) (PLLA) composite nanofibers containing hydrophobic drug 6-aminonicotinamide (6AN) were prepared by using electrospinning technology. Then the composite nanofibers were placed in laboratory environment for 28 days, and heat-treated at fixed temperature and environment in incubator that was maintained at 37 °C, 5% CO_2, and 90–95% relative humidity. Compared with the untreated blank sample releasing 6AN over 9 days, the drug release time of PLLA composite nanofibers with heat-treatment can be extended to over 44 days.

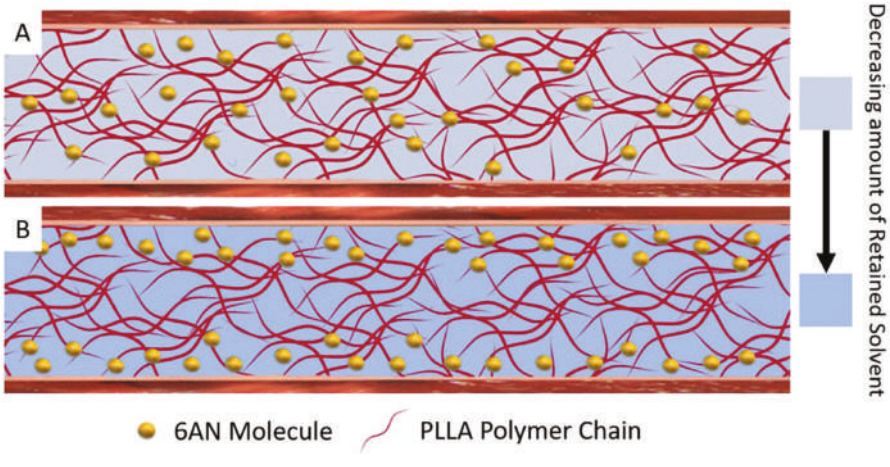

Figure 9. Schematic of the effects of solvent removal on the 6AN distribution inside of an individual electrospun nanofiber. (**A**) A single PLLA fiber immediately after electrospinning with uniformly distributed 6AN. (**B**) A single PLLA fiber after solvent removal shuttled 6AN from inaccessible fiber core towards the fiber surface [120]. © Elsevier Ltd. All rights reserved 2017.

2.4.2. Surface Modifications

The surface properties of nanofibers play an important role in packaging materials. Although electrospinning technology can produce fiber membranes with special internal structure, the surface properties of fiber membranes still cannot meet the application in food packaging fields, such as wettability, adsorption, etc. Thus, the subsequent modification is needed to change or modify surface of electrospun nanofibers in order to meet the packaging field characteristics and special application

requirements [121]. There are two usual strategies to modify the surface of electrospun film, one is grafting on the surface and the other is plasma treatment on the surface.

In the field of food packaging, the surface modifications for electrospun fiber membrane are often used to endow the membrane with antibacterial properties. For example, Li et al. [122] prepared the surface of electrospun poly(D,L-lactide) (PDLLA) membrane by plasma pretreatment, UV initiated graft copolymerization of 4-vinylpyridine (4VP) and quaternization of the grafted pyridine groups with hexylbromide. The antibacterial rate of the surface modified electrospun fiber membrane against gram-positive *Staphylococcus aureus* and gram-negative *Staphylococcus* was 99.999%.

Additionally, surface modifications can also improve the physical properties of electrospun fiber membrane, such as mechanical properties. Surucu et al. [123] reported a dielectric barrier discharge (DBD) Ar + O_2 and Ar + N_2 method to modify the surface of PCL/chitosan/PCL nanofibers. The plasma modifications based on Ar + O_2 had improved the mechanical properties and oxygen functionality.

2.4.3. Dip-Coating of Electrospinning Membrane

The dip coating method is to immerse the electrospun fiber membrane in a container for a period of time and take it out, so that the coating is attached to the electrospun fiber. The advantages of dip coating are high production efficiency and simple operation.

Some researchers coated electrospun fibers by the solution or suspension of antibacterial substances to make the composite fibers antibacterial properties. Ignatova et al. [124] combined electrospinning and impregnation techniques to prepare new materials of caffeic acid phenethyl ester (CAPE)/PVP-n-poly (3-hydroxybutyrate) (PHB). The prepared new CAPE-containing material has good antioxidant activity, suggesting that addition or coating of CAPE to the fiber can completely kill Gram-positive *S. aureus* and inhibit the growth of Gram-negative *E. coli*, which is expected to be used in the field of antimicrobial packaging.

Goha et al. [125] prepared beadless, smooth surface PLA/CS nanofibers by electrospinning, and then coated PLA nanofibers with cerium-doped bioactive glass (CeBG), copper-doped bioactive glass (CuBG) and silver-doped bioactive glass (AgBG). Then they tested the bacteriostatic activity against *Escherichia coli* (ATCC 25,922 strains) by the disk diffusion method, and found that the CeBG and CuBG modified PLA/CS nanofibers did not produce bacteriostatic areas against *E. coli* in three samples.

Yakub et al. [126] also combined electrospinning technology with the impregnation method to prepare PCL/CS composite nanofiber by using the natural phenolic acid ferulic acid (FA) as raw materials. The experimental results showed that a combination of FA and CS in the fibers is more effective for killing *Staphylococcus aureus* than FA-containing mats or CS-coated mats, and all the composite fibers containing CS and FA have a good antimicrobial activity.

This method can also modify the electrospun fiber membranes from hydrophobicity to hydrophilicity. Hu et al. [127] fabricated PLA/beta-tricalcium phosphate (b-TCP) composite fiber membranes, after that, the membrane was immersed in 5.0% (w/v) polyethylene oxide solution at room temperature for 5 minutes. After the dried, hot pressed and other steps, the surface modified composite fiber membranes were obtained, which exhibited an enhanced degradation rate, and a change of surface characteristic from hydrophobic to hydrophilic.

3. Functional Materials for Food Packaging Applications

The purpose of food packaging is to ensure the quality and safety of food, provide convenience for users, highlight the appearance and mark of commodity packaging and improve the value of merchandise. Most importantly, food packaging can prevent food deterioration and ensure food quality. With the progress of science and technology and the improvement of people's consumption level, functional food packaging is more and more crucial in people's daily life.

Fresh keeping, environmental protection and convenience are the new development direction of food packaging. Choosing proper packaging materials should not only consider the requirements of consumers and the needs of producers, but also consider the coordination and influence with

the environment. In principle, the electrospun nanofibers used in food packaging must have biocompatibility and low toxicity, even non-toxic. Based on these above considerations, functional food packaging materials gradually require some special characteristics like degradable, super-hydrophobic, self-cleaning, edible, antibacterial and high barrier.

3.1. Degradable Electrospun Packaging Membrane

At present, most of the packaging materials are polymers, such as polyethylene, polypropylene, polystyrene, polyvinyl chloride and so on, which are very stable in nature and difficult to degrade. The employment of these materials in packaging industry has caused a serious white pollution due to numerous consumptions of disposable goods, such as disposable tableware and plastic bags. Therefore, in the field of functional packaging, many scholars began to study polymers that could be able to degrade in the natural environment.

The degradable packaging materials generally refer to degradable plastics. According to the traditional classification, degradable plastics can be divided into two categories: photodegradable plastics and biodegradable plastics. So far, biodegradable polymers are very popular in the functional packaging field. Some chemically synthesized polymers, such as PCL, PPC, PLA and PVA are often used in food packaging materials through electrospinning. The presence of these polymers with good biocompatibility can provide a basic comprehension for functional modifications of packaging materials.

Biodegradable polymer materials synthesized by chemical method are similar to natural polymers or polymers with easily degradable functional groups, which can be designed and adjusted to meet the actual needs.

PCL possesses high biocompatibility and biodegradability, which always is applied as degradable packaging. Katsube et al. [128] prepared electrospun PCL nanofibers by using a solution of 12 wt. % PCL in acetone with a capillary flow rate of 24 mL/h, and an electric field of 1.005 kV/cm. Furthermore, the mechanical behavior of electrospun PCL under tensile loading was investigated. Subramanian et al. [129] studied the formation of nanofibers during electrospinning process by using melting PCL as spinning solution, and explored the effects of process parameters such as applied voltage, electrode spacing and molecular weight on fibers diameter. In this work, the diameter distribution was 5–20 microns. By controlling process parameters, the proportion of fine fibers in melt-electrospun PCL mesh was increased. Gaudio et al. [130] used 14% w/v solutions in mixture 1:1 of tetrahydrofuran and N, N-dimethylformamide and chloroform to fabricate micrometric and submicrometric fibrous PCL. The experiments have proved that PCL was nontoxic. Additionally, Bhullar et al. [131] used environmentally friendly and non-toxic melt spinning to obtain PCL micro-fibrous structure, followed by impregnation of bioactive rosemary extract. As expected, the rosemary extract was uniformly dispersed in the PCL microfiber structure. Finally, the bioactive packaging materials with satisfactory antimicrobial, structural and thermal properties can be obtained. The active bio-composite is biodegradable and biocompatible, which is able to replace traditional packaging materials.

CO_2 can be copolymerized with epoxy monomers to obtain a series of biodegradable polycarbonates, among which PPC is an alternating copolymer of carbon dioxide and propylene oxide (PO). Using CO_2 as monomer to synthesize PPC can not only overcome the shortage of petroleum resources, but also help to reduce carbon dioxide pollution. Generally speaking, PPC has good tensile toughness, transparency, biocompatibility and biodegradability. Park et al. [132] used sol–gel electrospinning to prepare pure PPC nanofibers, and found that the mechanical properties of pure PPC were significantly improved after the heat treatment at 60 °C due to the highly bonded structure of nanofibers, which was further interpreted by SEM diagram. Nagiah et al. [133] obtained PPC ultrathin fibers with 10% w/v polymer solution, which have good thermal stability, mechanical properties and high porosity.

PLA is defined as the most promising new packaging material in the new century by the industry, which has a series of advantages such as complete biodegradation, environmental friendliness and recyclability. PLA can be made into film products with high transparency, excellent processability and

mechanical properties, which are often used in food packaging. Li et al. [134] studied the morphology, structure and tensile properties of electrospun PLA porous nanofibers with different crystallinity. It was reported that rigid porous PLA nanofibers with high tensile modulus, high strength and small strain can be obtained by the denser structure and enhanced molecular orientation during electrospinning. The study from Casasola et al. [135] demonstrated that the effects of solution properties on the morphology and diameter of PLA nanofibers. It was found that there was the highest fiber productivity in the solvent system of acetone/dimethylformamide, which could prepare the defect-free nanofibers. In this system, the effect of polymer concentration on the formation of PLA nanofibers was also studied. The structure of PLA nanofibers obtained from the critical chain entanglement concentration (CE) was beaded and the defect-free nanofibers were obtained by increasing the concentration about twice higher than that of the entanglement concentration. Critical chain entanglement concentration has positive correlation with its elastic modulus and plastic modulus. In addition, the higher the conductivity of the solvent, the finer the diameter of the fiber.

Tang et al. [136] obtained a kind of electrospun PLA nanofibers with remarkable nano-porous surface and super high specific surface area. The formation mechanism of nanopores on the surface of fibers is solvent phase separation. Huang et al. [137] further studied the effect of different solvents on the surface morphology and internal porous structure of electrospun PLA fibers. Both surface and internal pore can be achieved through different mechanisms. It could be clearly found in Figure 10 that by choosing different solvent systems, electrospun PLA nanofibers with porous surface or inner surface and their combination can be obtained under suitable humidity and environment conditions.

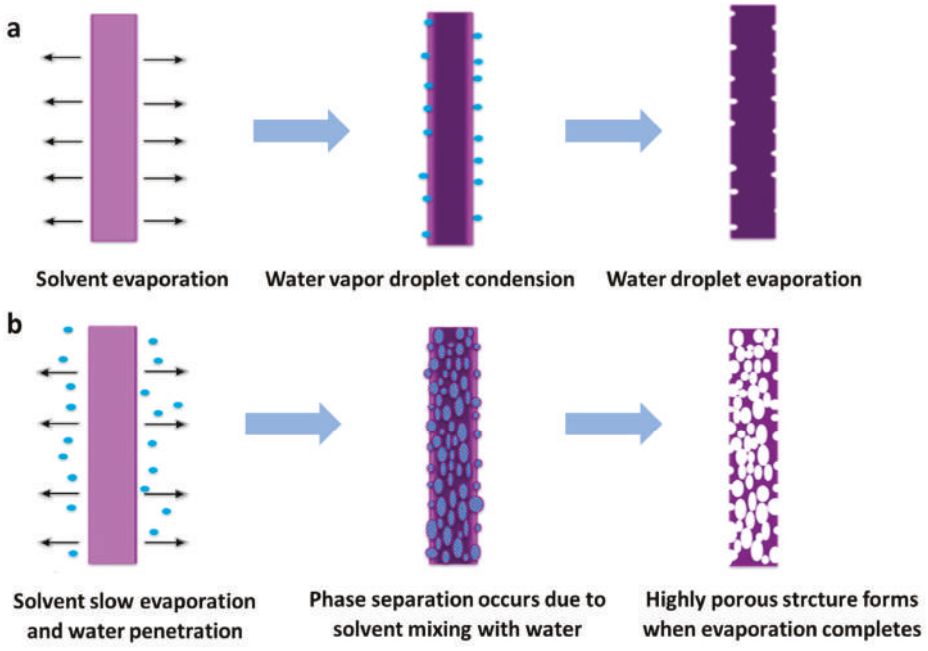

Figure 10. (**a**) Schematic diagram of surface pore formation induced by breath figures mechanism. (**b**) Schematic diagram of porosity induced by a vapor induced phase separation (VIPS) mechanism [137].

Tomaszewski et al. [138] studied the effects of molecular weight of PLA and spinning solution viscosity on the thickness and quality of fiber felt. In addition, the thermal and tensile properties of fiber felt were also studied. Li et al. [139] came to a similar but more detailed conclusion, which are

the uniform fibers that can only be obtained when the concentration of low molecular weight PLA solution is above the entanglement concentration. On the contrary, when the concentration of high molecular weight PLA solution is below entanglement concentration, uniform fibers cannot be obtained. Meanwhile, due to the low viscosity and deformation resistance of precursor solution, the PLA nanofiber has remarkable molecular alignment, which also leads to a rapid cold crystallization and high modulus in the nanofibers.

In the field of food packaging, biodegradable PVA is often combined with other substances to achieve the target functionality owing to some simple electrospinning conditions. Kayaci et al. [140] successfully produced PVA nanowebs incorporating vanillin/cyclodextrin inclusion complex (vanillin/CD–IC) via an electrospinning technique with the goal to obtain functional nanowebs containing flavor/fragrance molecules with enhanced thermal stability and durability. Therefore, PVA/vanillin/CD–IC nanowebs can be quite applicable in active food packaging. Wen et al. [141] fabricated electrospun PVA/cinnamon essential oil/b-cyclodextrin (PVA/CEO/b-CD) antimicrobial nanofibrous film, which can effectively prolong the shelf-life of strawberry, indicating it is potential for the application in active food packaging (Figure 11).

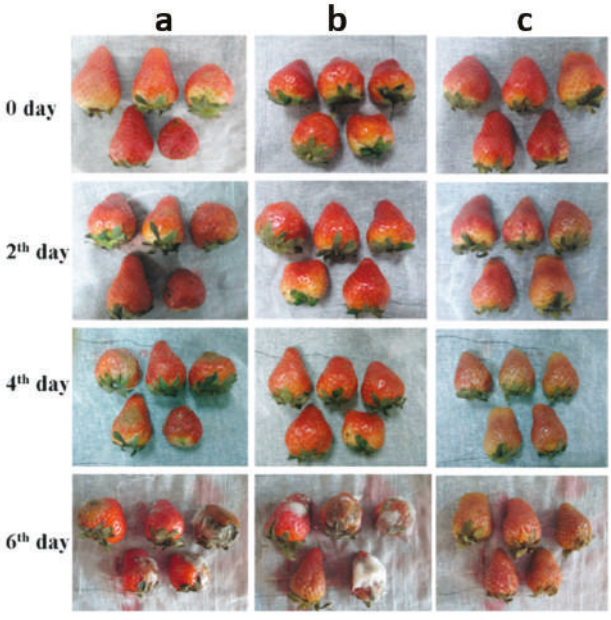

Figure 11. Appearance changes of strawberries stored at 21 °C. (**a**) Control; (**b**) packed with fresh-keeping film and (**c**) packed with PVA/cinnamon essential oil /b-CD nanofilm [141]. © Elsevier Ltd. All rights reserved 2015.

3.2. Superhydrophobic Electrospun Packaging Membrane

The superhydrophobic surface has the advantages of self-cleaning and anti-adhesion, which could delay the deterioration of food and prevent the propagation of microorganisms in food packaging, so the superhydrophobic packaging membrane is very popular in this field.

Ding et al. [142] obtained superhydrophobic fibrous PVA/ZnO composite films by electrospinning and surface treatment with fluoroalkylsilane (FAS). First, ZnO with nanostructured surface was formed by calcining the electrospun composite nanofiber membranes, and then the surface was modified by fluoroalkylsilane coating to obtain the superhydrophobic surface, and the contact angle of the rest with water has changed from 0 to 165 degrees, which means that the surface of composite was also

changed from superhydrophilic to superhydrophobic. The comparative experiments showed that the superhydrophobic surface of the composite fiber membrane is the result of combination of high surface roughness and hydrophobic FAS modification.

Actually, the rough surface has played an important role on the superhydrophobic surface, which involves a principle denoted as lotus leaf effect that is an important part for the superhydrophobic surface because there are many micron scale protrusions on the lotus leaf surface. The rough structure increases the air fraction in the space–time contact between the surface and water, and greatly reduces the actual contact area between water and lotus leaf [143]. Therefore, many research groups use the so-called nano plate making technology to prepare the surface with artificial lotus leaf. For instance, Kang et al. [144] utilized the volatility of solvent during electrospinning to prepare PS films with unique protuberances, which the structure is similar to the surface of the lotus leaf, so the electrospun fiber membrane has a superhydrophobic property, the water contact angle is 154.2 ± 0.7° (Figure 12).

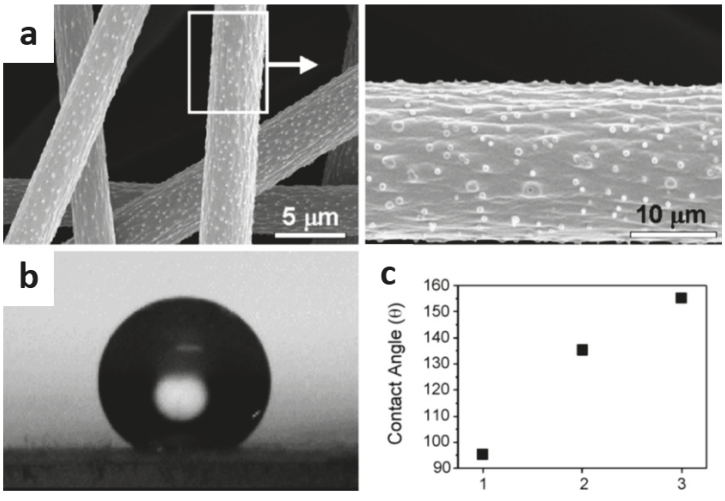

Figure 12. (**a**) FESEM images of electrospun PS fibers from 35 wt.% solution in DMF, (**b**) water droplet on electrospun PS fibers from 35 wt.% solution in DMF and (**c**) variation of water contact angles depending on surface structures (1: PS film; 2: electrospun PS fibers using THF; 3: electrospun PS fibers from DMF) [144]. © Elsevier B.V. All rights reserved 2007.

3.3. Edible Electrospun Packaging Membrane

The application of edible packaging in food packaging has a long history. For decades, the familiar glutinous rice paper used in candy packaging and the corn baking packaging cup used in ice cream packaging were typical edible packaging. With the improvement of people's requirements for food quality and preservation period, as well as the enhancement of people's awareness of environmental protection, edible films consisted of natural biological materials are becoming a research hotspot in the field of food packaging. Generally, edible packaging membranes have different kinds of ingredients according to their compositions. The first one is polysaccharide membranes, such as starch, cellulose derivative, pectin, chitosan, etc. the second one is protein membranes, such as collagen, gel, and the third one is lipid membranes, such as beeswax, paraffin, the fourth kinds is compound membranes, which are obtained through the combination of three above substances.

Tang et al. [145] prepared edible gelatin based composite fibers by electrospinning. The combination of gelatin nanofibers with peppermint essential oil (PO) and chamomile essential oil (CO) could enhance the hydrophobicity of membrane surface, and all the gelatin nanofibers containing PO, CO or PO/CO had better antibacterial properties against *Escherichia coli* and *Staphylococcus aureus*, and had certain

antioxidant properties (Figure 13). In particular, the addition of PO leads to a better antibacterial activity of the fiber membrane, while the oxidation resistance of fiber membrane containing CO is better.

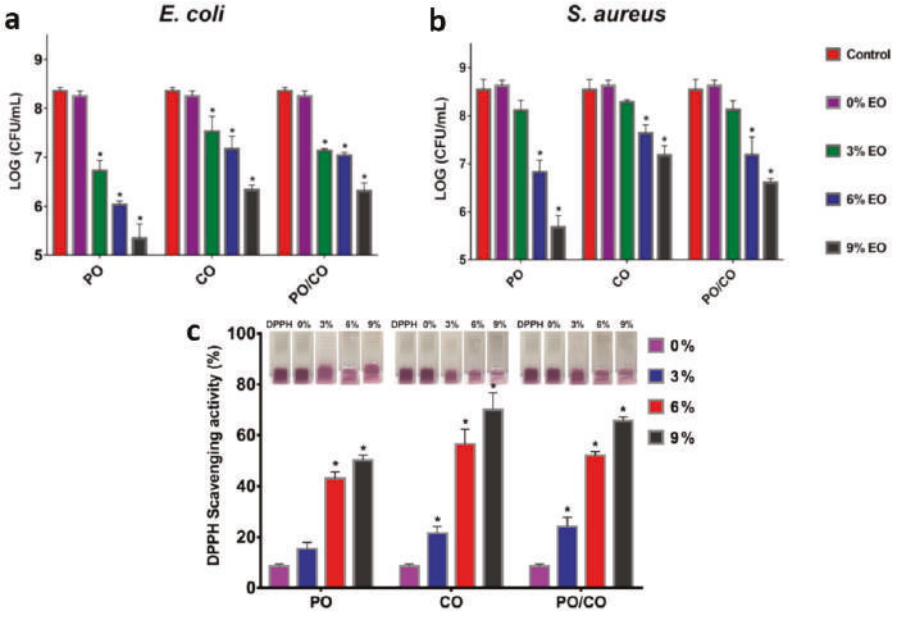

Figure 13. (**a**,**b**) The results of dynamic contact assays against *Escherichia coli* and *Staphylococcus aureus*. (**c**) The antioxidant performance of gelatin/EOs nanofibers was determined using the DPPH radical scavenging method, (∗) p (in Tukey's post hoc test) < 0.05 versus the control group [145]. © American Chemical Society 2019.

Based on one-step electrospinning technology, Mascheronia et al. [146] proposed an edible polysaccharide system that can be applied to food packaging. In this system, the cyclodextrin crystal is surrounded by aromatic compounds and fixed on the Prussian nanofiber mesh. The composite, combined with the membrane's pullulan nanofibers, is stable for several months without loss of volatiles when it was stored in ambient relative humidity and at different temperatures. Due to the ability of encapsulation and release of antibacterial aromatic compounds, the system has potential applicability for improving microbial safety, especially for fresh food.

3.4. Antibacterial Electrospun Packaging Membrane

According to the previous description, there are three kinds of antibacterial substances, including natural biological antibacterial agents (essential oil, etc.), organic chemical antibacterial agents (organic acid, etc.) and inorganic antibacterial agents.

Cristina et al. [147] successfully encapsulated a naturally occurring antimicrobial compound, allyl isothiocyanate (AITC) into soy protein isolate (SPI) and PLA fibers by electrospinning technology, and studied its effect on the fiber properties. By elaborately manipulating the formulation of solution, the morphology of composite nanofibers can be adjusted. Most of all, it was found that AITC released from SPI and PLA electrospun fibers could be controlled by changing relative humidity, and the increase of relative humidity of air can triggers the release of AITC in fibers.

Neo et al. [148] evaluated the applicability of gallic acid loaded zein (Ze-GA) electrospun fiber mats towards potential active food packaging. As expected, the Ze-GA fiber mats demonstrated

outstanding antibacterial activity and properties consistent with those considered desirable for active packaging material in the food industry.

As a natural mineral, montmorillonite (MMT) can also be applied in food packaging industry. Agarwal et al. [149] coated PP membranes with MMT and nylon 6 nanofibers by electrospinning. The effect of these membranes in the packaging of popular foods such as crisps and bread were investigated (Figure 14). When the membranes were used in the packaging of potato chips, the oxygen barrier property was significantly reduced, which was attributed to the MMT-N6 coating that slightly improves the water vapor barrier. The reason for decrease in microbial spoilage of bread was similar. Therefore, the coated MMT composite membranes can be applied in the packaging industry due to its non-toxic, which can realize the extension of shelf life of packed food.

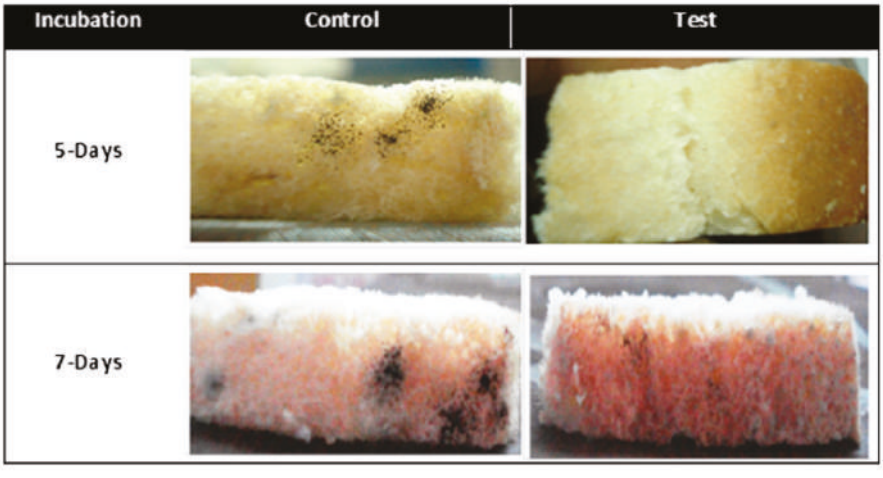

Figure 14. Effect of MMT-N6 nanofibrous membrane coating on PP packets on the natural flora of bread [149]. © Elsevier Ltd. All rights reserved 2014.

As mentioned above, chitosan is a natural antibacterial polymer, so it has attracted numerous attentions for the food packaging industry. Arkoun et al. [150] firstly studied the antibacterial potential of electrospun chitosan-based nanofibers (CNF) by storing with the actual foods, and further investigated its ability to reduce spoilage and food loss. They successfully obtained highly antibacterial CNF-based packaging (CNFP) materials by direct electrospinning. It was found that an advantageous potential for antimicrobial packaging materials is that the quality and freshness of unprocessed or minimally processed and perishable foods could be perfectly preserved along with the extension of meat shelf life to 1 week (Figure 15).

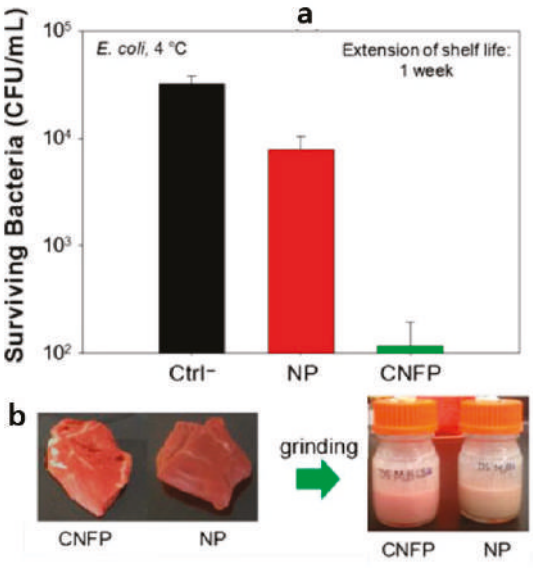

Figure 15. (**a**) In situ antibacterial activity of CNFP against *E. coli* after 7-day storage at 4 °C. (**b**) Appearance of packed red meat with and without CNFP, before and after grinding [150]. © John Wiley & Sons, Ltd 2018.

3.5. Barrier Electrospun Packaging Membrane

The barrier property of packaging materials refers to polymer materials with certain shielding ability for small molecule gas, liquid, water vapor, fragrance and drug taste. It can effectively prevent oxygen and water vapor from seeping into the environment, keep the specific gas composition in the package, and significantly improve the shelf life. At present, in order to meet the market demands, many countries have developed multi-functional high barrier packaging materials and multi-functional packaging materials in recent years.

Fabra et al. [151] developed a fully biodegradable multi-layer system based on a high barrier adhesive sandwich of electrospun zein nanofibers between poly hydroxybutyrate-co-valerate 5% (PHBV5) and poly-(3-hydroxybutyrate) (PHB) homopolymers with low valerate content. By adding zein nanofibers, the water and oxygen barrier in the multi-layer system of PHA was improved, and the flexibility was also enhanced. After that, electrospinning technology was employed to improve the barrier performance of packaging materials [152]. The effects of PCL, PHA and PLA on the oxygen and water resistance of TPCS membrane were compared. The result revealed that the PHB was the most effective in reducing the water and oxygen permeability.

The previous chapter has shown that zein can be prepared as an edible packaging film. In recent years, many scholars have also used electrospun zein film as the interlayer to enhance the barrier properties of food packaging. Fabra et al. [153] employed the electrospun zein as the middle layer and cast PHBV12 as the outer layer to prepare a multilayer structure food packaging films, which can significantly improve the oxygen barrier performance. They also compared the enhancement of the oxygen and water barrier properties of multi-layer packaging films with PHBV3 as the outer layers and different electrospun hydrocolloid films as the interlayers [153]. The result showed that oxygen and water vapor permeability values were significantly improved by employing electrospun zein film as the interlayer.

4. Conclusions and Challenges

In summary, the electrospinning technology is an effective method to prepare nanofibers with various nanostructure and surface characteristics, which can meet the functional requirements for packaging materials in the food fields depends on the different design of device and wide range of raw materials for selection, especially polymers. This article reviews the potential use of electrospinning technology in the food packaging field, not only to prepare pure degradable polymer packaging membranes, but also to obtain mixed polymer mats by designing the spinneret, such as multiple-jet and coaxial electrospinning. In addition, different inorganic fillers and other bioactive particles can be incorporated into the fibers to enhance the functionality and intend to be used in broader applications. The properties of common polymers and fillers mentioned above are summarized in Table 1. Alternatively, the resulting electrospun films are post-treated by the thermal treatments, surface modifications or dip-coating to obtain superior satisfactory performance. In the field of food packaging, based on some special requirements, it is possible to prepare packaging materials that own functions of degradable, superhydrophobic, edible, antibacterial and high barrier by electrospinning technology.

Table 1. Summary of promising properties related to packaging using electrospinning.

Categories	Materials	Properties or Function
Polymer	Chitosan (CS)	biodegradation, biocompatibility, anti-microbial, antifungal activities, and non-toxicity.
	Zein	good film-forming property, biocompatibility, biodegradation, renewable, edible
	Polyvinyl alcohol (PVA)	transparency, gantistatic property, biodegradation, biocompatibility
	Gelatin (GT)	biodegradation, biocompatibility, edible, good toughness
	Polycaprolactone (PCL)	biocompatibility, biodegradability, good mechanical properties, better solvent solubility
	Polyethylene terephthalate (PET)	non-toxic, good mechanical properties, high transparency, good toughness
	Cellulose acetate (CA)	non-toxic, biodegradable, low price, good transparency, high impact resistance
	Polylactic acid (PLA)	biodegradation, biocompatibility, easy to process, good mechanical properties and transparency
	Poly (propylene carbonate) (PPC)	good tensile toughness, transparency, biocompatibility and biodegradability
	Polystyrene (PS)	High transparency, non-toxic, easy to process
Inorganic fillers	Metronidazole (MNA)	hydrophobic, antibacterial
	Carbon nanotubes (CNTs)	conductive, antistatic, smart packaging
	FePt, Fe_3O_4, $FeCl_3$ nanoparticles	radiation protection
	TiO_2	photocatalytic, self-cleaning, photocatalytic degradation of ethylene
	ZnO	photocatalytic, self-cleaning, antibacterial
	Cerium-doped bioactive glass (CeBG), copper-doped bioactive glass (CuBG), silver-doped bioactive glass (AgBG)	antibacterial
	Montmorillonite (MMT)	antibacterial
Active substance	Orange essential oil (OEO)	antibacterial
	Metronidazole (MNA)	antibacterial
	Peppermint essential oil (PO), chamomile essential oil (CO)	antibacterial
	Vanillin/cyclodextrin inclusion complex (vanillin/CD-IC)	containing flavor/fragrance, enhancing thermal stability and durability
	Cinnamon essential oil/b-cyclodextrin (PVA/CEO/b-CD)	prolonging the shelf-life

Although the application of electrospinning technology in functional packaging has a wide range of development prospects, there are still some challenges that need to be faced and require more attention and studies. The biggest challenge is the choice of solvent. Some polymers are insoluble in non-toxic solvents, which would cause environmental damage and pollution. Furthermore, some organic solvents are harmful to human beings. Therefore, it is necessary to find more suitable and non-toxic solvents to prepare electrospun fibers, especially green electrospinning, a novel and aqueous strategy to overcome the disadvantages of organic solvents. Up to now, some commercially available polymers in packaging industry can only be dissolved in toxic solvents. Therefore, water or other non-toxic solvents with environment friendly property would be applied to prepare food packaging films in the future. In fact, during the electrospinning process, the solvents are mostly evaporated. Unfortunately, the above organic solvents are toxic and harmful to the environment, so it is crucial to replace the conventional toxic solvents with non-toxic or low-toxic solvents, such as emulsion electrospinning method [154,155], that will minimize the presence of toxic solvents in the final packaging material. Another challenge is some natural polymers cannot be directly electrospun into nanofibers, so it is crucial to select a suitable polymer, which is also a problem of electrospun material in food packaging. Most of all, the majority of research is still in the laboratories. So, as for the real food packaging industry, it is important to produce electrospun fibers on a large scale, and the subsequent development must be focused on high yields and industrialization. Ordinary multi-nozzle electrospinning or needless electrospinning is suitable for industrial production. There are already some manufacturers that can provide large-scale devices for producing electrospinning fibers or membranes. For example, Elmarco has developed needleless electrospinning device, which they claim is suitable for industrial applications (https://www.elmarco.com). Some factories already have begun large-scale production of nanofiber membranes, such as Jiangxi Xiancai Nanofibers Technology Co., Ltd. in China for the large scale production of electrospun polyimide fibrous membranes, yarns and short nanofibers (http://www.hinanofiber.com/english/). All of these have laid some foundation for the future electrospinning production of food packaging materials, and the focus of electrospinning food packaging materials also need to be transferred from laboratory research to industrial production in the future.

Funding: This research received no external funding.

Acknowledgments: The work was financially supported by National Natural Science Foundation of China (51803093, and 51903123), Natural Science Foundation of Jiangsu Province (BK20180770, and BK20190760), Priority Academic Program Development of Jiangsu Higher Education Institutions (PAPD), Opening Project of Division of Chemistry from Qingdao University of Science and Technology (QUSTHX201921).

Conflicts of Interest: The authors declare no conflict of interest.

References

1. Jayakumar, R.; Prabaharan, M.; Shalumon, K.T.; Chennazhi, K.P.; Nair, S.V. *Biomedical Applications of Polymer/Silver Composite Nanofibers*; Springer: Berlin/Heidelberg, Germany, 2011; Volume 246, pp. 263–282. [CrossRef]
2. Hou, H.; Xu, W.; Ding, Y. The recent progress on high-performance polymer nanofibers by electrospinning. *J. Jiangxi Norm. Univ. (Nat. Sci.)* **2018**, *42*, 551–564. [CrossRef]
3. Jiang, S.; Chen, Y.; Duan, G.; Mei, C.; Greiner, A.; Agarwal, S. Electrospun nanofiber reinforced composites: A review. *Polym. Chem.* **2018**, *9*, 2685–2720. [CrossRef]
4. Yao, K.; Chen, J.; Li, P.; Duan, G.; Hou, H. Robust strong electrospun polyimide composite nanofibers from a ternary polyamic acid blend. *Compos. Commun.* **2019**, *15*, 92–95. [CrossRef]
5. Liao, X.; Dulle, M.; de Souza e Silva, J.M.; Wehrspohn, R.B.; Agarwal, S.; Förster, S.; Hou, H.; Smith, P.; Greiner, A. High strength in combination with high toughness in robust and sustainable polymeric materials. *Science* **2019**, *366*, 1376–1379. [CrossRef] [PubMed]
6. Sundaramurthi, D.; Krishnan, U.M.; Sethuraman, S. Electrospun Nanofibers as Scaffolds for Skin Tissue Engineering. *Polym. Rev.* **2014**, *54*, 348–376. [CrossRef]

7. Yang, F.; Murugan, R.; Wang, S.; Ramakrishna, S. Electrospinning of nano/micro scale poly (l-lactic acid) aligned fibers and their potential in neural tissue engineering. *Biomaterials* **2005**, *26*, 2603–2610. [CrossRef]
8. Wu, T.; Ding, M.; Shi, C.; Qiao, Y.; Wang, P.; Qiao, R.; Wang, X.; Zhong, J. Resorbable polymer electrospun nanofibers: History, shapes and application for tissue engineering. *Chin. Chem. Lett.* **2019**. [CrossRef]
9. Buttafoco, L.; Kolkman, N.G.; Engbers-Buijtenhuijs, P.; Poot, A.A.; Dijkstra, P.J.; Vermes, I.; Feijen, J. Electrospinning of collagen and elastin for tissue engineering applications. *Biomaterials* **2006**, *27*, 724–734. [CrossRef]
10. Gao, S.; Tang, G.; Hua, D.; Xiong, R.; Han, J.; Jiang, S.; Zhang, Q.; Huang, C. Stimuli-responsive bio-based polymeric systems and their applications. *J. Mater. Chem. B* **2019**, *7*, 709–729. [CrossRef]
11. Ajalloueian, F.; Tavanai, H.; Hilborn, J.; Donzel-Gargand, O.; Leifer, K.; Wickham, A.; Arpanaei, A. Emulsion electrospinning as an approach to fabricate PLGA/chitosan nanofibers for biomedical applications. *BioMed Res. Int.* **2014**, *2014*, 475280. [CrossRef]
12. Dong, Z.; Kennedy, S.J.; Wu, Y. Electrospinning materials for energy-related applications and devices. *J. Power Sources* **2011**, *196*, 4886–4904. [CrossRef]
13. Han, J.; Wang, S.; Zhu, S.; Huang, C.; Yue, Y.; Mei, C.; Xu, X.; Xia, C. Electrospun Core–Shell Nanofibrous Membranes with Nanocellulose-Stabilized Carbon Nanotubes for Use as High-Performance Flexible Supercapacitor Electrodes with Enhanced Water Resistance, Thermal Stability, and Mechanical Toughness. *ACS Appl. Mater. Interfaces* **2019**. [CrossRef] [PubMed]
14. Sun, G.; Sun, L.; Xie, H.; Liu, J. Electrospinning of Nanofibers for Energy Applications. *Nanomaterials* **2016**, *6*, 129. [CrossRef] [PubMed]
15. Li, S.; Cui, Z.; Li, D.; Yue, G.; Liu, J.; Ding, H.; Gao, S.; Zhao, Y.; Wang, N.; Zhao, Y. Hierarchically structured electrospinning nanofibers for catalysis and energy storage. *Compos. Commun.* **2019**, *13*, 1–11. [CrossRef]
16. Hwang, T.H.; Lee, Y.M.; Kong, B.S.; Seo, J.S.; Choi, J.W. Electrospun core-shell fibers for robust silicon nanoparticle-based lithium ion battery anodes. *Nano Lett.* **2012**, *12*, 802–807. [CrossRef] [PubMed]
17. Drosou, C.G.; Krokida, M.K.; Biliaderis, C.G. Encapsulation of bioactive compounds through electrospinning/electrospraying and spray drying: A comparative assessment of food-related applications. *Dry. Technol.* **2016**, *35*, 139–162. [CrossRef]
18. Anu Bhushani, J.; Anandharamakrishnan, C. Electrospinning and electrospraying techniques: Potential food based applications. *Trends Food Sci. Technol.* **2014**, *38*, 21–33. [CrossRef]
19. Rezaei, A.; Nasirpour, A.; Fathi, M. Application of Cellulosic Nanofibers in Food Science Using Electrospinning and Its Potential Risk. *Compr. Rev. Food Sci. Food Saf.* **2015**, *14*, 269–284. [CrossRef]
20. Venugopal, J.; Prabhakaran, M.; Low, S.; Aw, T.; Gupta, D.; Venugopa, R.; Deepika, G. Continuous Nanostructures for the Controlled Release of Drugs. *Curr. Pharm. Des.* **2009**, *15*, 1799–1808. [CrossRef]
21. Duan, G.; Bagheri, A.R.; Jiang, S.; Golenser, J.; Agarwal, S.; Greiner, A. Exploration of Macroporous Polymeric Sponges As Drug Carriers. *Biomacromolecules* **2017**, *18*, 3215–3221. [CrossRef]
22. Ouyang, W.; Liu, S.; yao, K.; Zhao, L.; Cao, L.; Jiang, S.; Hou, H. Ultrafine hollow TiO2 nanofibers from core-shell composite fibers and their photocatalytic properties. *Compos. Commun.* **2018**, *9*, 76–80. [CrossRef]
23. Choi, S.J.; Chattopadhyay, S.; Kim, J.J.; Kim, S.J.; Tuller, H.L.; Rutledge, G.C.; Kim, I.D. Coaxial electrospinning of WO3 nanotubes functionalized with bio-inspired Pd catalysts and their superior hydrogen sensing performance. *Nanoscale* **2016**, *8*, 9159–9166. [CrossRef] [PubMed]
24. Li, Z.; Liu, S.; Song, S.; Xu, W.; Sun, Y.; Dai, Y. Porous ceramic nanofibers as new catalysts toward heterogeneous reactions. *Compos. Commun.* **2019**, *15*, 168–178. [CrossRef]
25. Han, C.; Wang, Y.; Lei, Y.; Wang, B.; Wu, N.; Shi, Q.; Li, Q. In situ synthesis of graphitic-C3N4 nanosheet hybridized N-doped TiO2 nanofibers for efficient photocatalytic H2 production and degradation. *Nano Res.* **2015**, *8*, 1199–1209. [CrossRef]
26. Qiao, Y.; Shi, C.; Wang, X.; Wang, P.; Zhang, Y.; Wang, D.; Qiao, R.; Wang, X.; Zhong, J. Electrospun Nanobelt-Shaped Polymer Membranes for Fast and High-Sensitivity Detection of Metal Ions. *ACS Appl. Mater. Interfaces* **2019**, *11*, 5401–5413. [CrossRef]
27. Chen, Y.; Lu, K.; Song, Y.; Han, J.; Yue, Y.; Biswas, S.K.; Wu, Q.; Xiao, H. A Skin-Inspired Stretchable, Self-Healing and Electro-Conductive Hydrogel with a Synergistic Triple Network for Wearable Strain Sensors Applied in Human-Motion Detection. *Nanomaterials* **2019**, *9*, 1737. [CrossRef]

28. Zheng, C.; Yue, Y.; Gan, L.; Xu, X.; Mei, C.; Han, J. Highly Stretchable and Self-Healing Strain Sensors Based on Nanocellulose-Supported Graphene Dispersed in Electro-Conductive Hydrogels. *Nanomaterials* **2019**, *9*, 937. [CrossRef]
29. Zhang, N.; Qiao, R.; Su, J.; Yan, J.; Xie, Z.; Qiao, Y.; Wang, X.; Zhong, J. Recent Advances of Electrospun Nanofibrous Membranes in the Development of Chemosensors for Heavy Metal Detection. *Small* **2017**, *13*, 1604293. [CrossRef]
30. Sun, B.; Long, Y.-Z.; Chen, Z.-J.; Liu, S.-L.; Zhang, H.-D.; Zhang, J.-C.; Han, W.-P. Recent advances in flexible and stretchable electronic devices via electrospinning. *J. Mater. Chem. C* **2014**, *2*, 1209–1219. [CrossRef]
31. Han, J.; Lu, K.; Yue, Y.; Mei, C.; Huang, C.; Wu, Q.; Xu, X. Nanocellulose-templated assembly of polyaniline in natural rubber-based hybrid elastomers toward flexible electronic conductors. *Ind. Crops Prod.* **2019**, *128*, 94–107. [CrossRef]
32. Yan, J.; Jeong, Y.G. High Performance Flexible Piezoelectric Nanogenerators based on BaTiO3 Nanofibers in Different Alignment Modes. *ACS Appl. Mater. Interfaces* **2016**, *8*, 15700–15709. [CrossRef] [PubMed]
33. Zhang, L.; Li, Y.; Zhang, Q.; Wang, H. Formation of the modified ultrafine anatase TiO2 nanoparticles using the nanofiber as a microsized reactor. *CrystEngComm* **2013**, *15*, 1607. [CrossRef]
34. Jiang, S.; Gruen, V.; Rosenfeldt, S.; Schenk, A.S.; Agarwal, S.; Xu, Z.-K.; Greiner, A. Virtually Wall-Less Tubular Sponges as Compartmentalized Reaction Containers. *Research* **2019**, *2019*, 4152536. [CrossRef] [PubMed]
35. Lv, D.; Zhu, M.; Jiang, Z.; Jiang, S.; Zhang, Q.; Xiong, R.; Huang, C. Green Electrospun Nanofibers and Their Application in Air Filtration. *Macromol. Mater. Eng.* **2018**, *303*, 1800336. [CrossRef]
36. Zhu, M.; Han, J.; Wang, F.; Shao, W.; Xiong, R.; Zhang, Q.; Pan, H.; Yang, Y.; Samal, S.K.; Zhang, F.; et al. Electrospun Nanofibers Membranes for Effective Air Filtration. *Macromol. Mater. Eng.* **2017**, *302*, 1600353. [CrossRef]
37. Lv, D.; Wang, R.; Tang, G.; Mou, Z.; Lei, J.; Han, J.; De Smedt, S.; Xiong, R.; Huang, C. Ecofriendly Electrospun Membranes Loaded with Visible-Light-Responding Nanoparticles for Multifunctional Usages: Highly Efficient Air Filtration, Dye Scavenging, and Bactericidal Activity. *ACS Appl. Mater. Interfaces* **2019**, *11*, 12880–12889. [CrossRef]
38. Huang, Z.-M.; Zhang, Y.Z.; Kotaki, M.; Ramakrishna, S. A review on polymer nanofibers by electrospinning and their applications in nanocomposites. *Compos. Sci. Technol.* **2003**, *63*, 2223–2253. [CrossRef]
39. Yang, H.; Jiang, S.; Fang, H.; Hu, X.; Duan, G.; Hou, H. Molecular orientation in aligned electrospun polyimide nanofibers by polarized FT-IR spectroscopy. *Spectrochim. Acta Part. A Mol. Biomol. Spectrosc.* **2018**, *200*, 339–344. [CrossRef]
40. Chen, C.-W.; Xie, J.; Yang, F.-X.; Zhang, H.-L.; Xu, Z.-W.; Liu, J.-L.; Chen, Y.-J. Development of moisture-absorbing and antioxidant active packaging film based on poly (vinyl alcohol) incorporated with green tea extract and its effect on the quality of dried eel. *J. Food Process. Preserv.* **2018**, *42*, e13374. [CrossRef]
41. Kim, J.-K.; Cho, B.-G.; Han, Y.-K.; Kim, Y.B. Modification of a crosslinked poly (acrylic acid) based new dehumidifying agent and its moisture absorbing characteristics. *Macromol. Res.* **2009**, *17*, 544–548. [CrossRef]
42. Ashwar, B.A.; Shah, A.; Gani, A.; Shah, U.; Gani, A.; Wani, I.A.; Wani, S.M.; Masoodi, F.A. Rice starch active packaging films loaded with antioxidants-development and characterization. *Starch Stärke* **2015**, *67*, 294–302. [CrossRef]
43. López de Dicastillo, C.; Bustos, F.; Guarda, A.; Galotto, M.J. Cross-linked methyl cellulose films with murta fruit extract for antioxidant and antimicrobial active food packaging. *Food Hydrocoll.* **2016**, *60*, 335–344. [CrossRef]
44. Soto-Cantu, C.D.; Graciano-Verdugo, A.Z.; Peralta, E.; Islas-Rubio, A.R.; Gonzalez-Cordova, A.; Gonzalez-Leon, A.; Soto-Valdez, H. Release of butylated hydroxytoluene from an active film packaging to Asadero cheese and its effect on oxidation and odor stability. *J. Dairy Sci.* **2008**, *91*, 11–19. [CrossRef] [PubMed]
45. Li, D.; Xia, Y.N. Electrospinning of Nanofibers: Reinventing the Wheel? *Adv. Mater.* **2004**, *16*, 1151–1170. [CrossRef]
46. Liu, Y.I.; Tan, J.; Yu, S.A.; Yousefzadeh, M.; Ramakrishna, S. High-fficiency preparation of polypropylene nanofiber by melt differential centrifugal electrospinning. *J. Appl. Polym. Sci.* **2019**, *137*, 48299.

47. Abdal-hay, A.; Abbasi, N.; Gwiazda, M.; Hamlet, S.; Ivanovski, S. Novel polycaprolactone/hydroxyapatite nanocomposite fibrous scaffolds by direct melt-electrospinning writing. *Eur. Polym. J.* **2018**, *105*, 257–264. [CrossRef]
48. Zeng, J.; Wang, H.; Lin, Y.; Zhang, J.; Liang, F.; Fang, F.; Yang, F.; Wang, P.; Zhu, Z.; Chen, X.; et al. Fabrication of microfluidic channels based on melt-electrospinning direct writing. *Microfluid. Nanofluid.* **2018**, *22*. [CrossRef]
49. Acik, G.; Altinkok, C. Polypropylene microfibers via solution electrospinning under ambient conditions. *J. Appl. Polym. Sci.* **2019**, *136*, 48199. [CrossRef]
50. Surip, S.N.; Abdul Aziz, F.M.; Bonnia, N.N.; Sekak, K.A. Effect of Pineapple Leaf Fibers (PALF) concentration on nanofibers formation by electrospinning. *IOP Conf. Ser. Mater. Sci. Eng.* **2018**, *290*, 012003. [CrossRef]
51. Wang, G.; Sun, X.; Bai, J.; Han, L. Preparation of Fe–C nanofiber composites by metal organic complex and potential application in supercapacitors. *J. Mater. Sci. Mater. Electron.* **2019**, *30*, 4665–4675. [CrossRef]
52. Han, J.; Branford-White, C.J.; Zhu, L.-M. Preparation of poly (ε-caprolactone)/poly (trimethylene carbonate) blend nanofibers by electrospinning. *Carbohydr. Polym.* **2010**, *79*, 214–218. [CrossRef]
53. Liu, S.; Song, Y.; Ma, C.; Shi, J.-l.; Guo, Q.-g.; Liu, L. The electrochemical performance of porous carbon nanofibers produced by electrospinning. *Carbon* **2012**, *50*, 3963. [CrossRef]
54. Jegina, S.; Kukle, S.; Gravitis, J. Evaluation of aloe vera extract loaded polyvinyl alcohol nanofiber webs obtained via needleless electrospinning. *IOP Conf. Ser. Mater. Sci. Eng.* **2018**, *459*, 012016. [CrossRef]
55. Wortmann, M.; Frese, N.; Sabantina, L.; Petkau, R.; Kinzel, F.; Gölzhäuser, A.; Moritzer, E.; Hüsgen, B.; Ehrmann, A. New Polymers for Needleless Electrospinning from Low-Toxic Solvents. *Nanomaterials* **2019**, *9*, 52. [CrossRef] [PubMed]
56. Sriyanti, I.; Jauhari, J. Synthesis of polyvinyl acetate (PVAc) fibers using needleless electrospinning technique with straight wire electrode. *J. Phys. Conf. Ser.* **2019**, *1166*, 012012. [CrossRef]
57. Yarin, A.L. Coaxial electrospinning and emulsion electrospinning of core-shell fibers. *Polym. Adv. Technol.* **2011**, *22*, 310–317. [CrossRef]
58. Lallave, M.; Bedia, J.; Ruiz-Rosas, R.; Rodríguez-Mirasol, J.; Loscertales, I.G. Filled and Hollow Carbon Nanofibers by Coaxial Electrospinning of Alcell Lignin without Binder Polymers. *Adv. Mater.* **2010**, *19*, 4292–4296. [CrossRef]
59. Han, D.; Steckl, A.J. Superhydrophobic and oleophobic fibers by coaxial electrospinning. *Langmuir ACS J. Surf. Colloids* **2009**, *25*, 9454–9462. [CrossRef]
60. Han, D.; Sherman, S.; Filocamo, S.; Steckl, A.J. Long-term antimicrobial effect of nisin released from electrospun triaxial fiber membranes. *Acta Biomater.* **2017**, *53*, 242–249. [CrossRef]
61. Jiang, S.; Duan, G.; Zussman, E.; Greiner, A.; Agarwal, S. Highly flexible and tough concentric triaxial polystyrene fibers. *ACS Appl. Mater. Interfaces* **2014**, *6*, 5918–5923. [CrossRef]
62. Yu, D.G.; Li, X.Y.; Wang, X.; Yang, J.H.; Bligh, S.W.; Williams, G.R. Nanofibers Fabricated Using Triaxial Electrospinning as Zero Order Drug Delivery Systems. *ACS Appl. Mater. Interfaces* **2015**, *7*, 18891–18897. [CrossRef]
63. Yoon, J.W.; Park, Y.; Kim, J.; Park, C.H. Multi-jet electrospinning of polystyrene/polyamide 6 blend: Thermal and mechanical properties. *Fash. Text.* **2017**, *4*. [CrossRef]
64. Zhang, Y.; Cheng, Z.; Han, Z.; Zhao, S.; Zhao, X.; Kang, L. Stable multi-jet electrospinning with high throughput using the bead structure nozzle. *RSC Adv.* **2018**, *8*, 6069–6074. [CrossRef]
65. Varesano, A.; Rombaldoni, F.; Mazzuchetti, G.; Tonin, C.; Comotto, R. Multi-jet nozzle electrospinning on textile substrates: Observations on process and nanofibre mat deposition. *Polym. Int.* **2010**, *59*, 1606–1615. [CrossRef]
66. Aider, M. Chitosan application for active bio-based films production and potential in the food industry: Review. *LWT Food Sci. Technol.* **2010**, *43*, 837–842. [CrossRef]
67. Ignatova, M.; Manolova, N.; Rashkov, I. Electrospun Antibacterial Chitosan-B ased Fibers. *Macromol. Biosci.* **2013**, *13*, 860–872. [CrossRef]
68. Ohkawa, K.; Cha, D.; Kim, H.; Nishida, A.; Yamamoto, H. Electrospinning of Chitosan. *Macromol. Rapid Commun.* **2004**, *25*, 1600–1605. [CrossRef]
69. Geng, X.; Kwon, O.H.; Jang, J. Electrospinning of chitosan dissolved in concentrated acetic acid solution. *Biomaterials* **2005**, *26*, 5427–5432. [CrossRef]

70. Sencadas, V.; Correia, D.M.; Areias, A.; Botelho, G.; Fonseca, A.M.; Neves, I.C.; Gomez Ribelles, J.L.; Lanceros Mendez, S. Determination of the parameters affecting electrospun chitosan fiber size distribution and morphology. *Carbohydr. Polym.* **2012**, *87*, 1295–1301. [CrossRef]
71. Torres-Giner, S.; Gimenez, E.; Lagaron, J.M. Characterization of the morphology and thermal properties of Zein Prolamine nanostructures obtained by electrospinning. *Food Hydrocoll.* **2008**, *22*, 601–614. [CrossRef]
72. Miyoshi, T.; Toyohara, K.; Minematsu, H. Preparation of ultrafine fibrous zein membranes via electrospinning. *Polym. Int.* **2005**, *54*, 1187–1190. [CrossRef]
73. Neo, Y.P.; Ray, S.; Easteal, A.J.; Nikolaidis, M.G.; Quek, S.Y. Influence of solution and processing parameters towards the fabrication of electrospun zein fibers with sub-micron diameter. *J. Food Eng.* **2012**, *109*, 645–651. [CrossRef]
74. Ding, Q.; Xu, X.; Yue, Y.; Mei, C.; Huang, C.; Jiang, S.; Wu, Q.; Han, J. Nanocellulose-Mediated Electroconductive Self-Healing Hydrogels with High Strength, Plasticity, Viscoelasticity, Stretchability, and Biocompatibility toward Multifunctional Applications. *ACS Appl. Mater. Interfaces* **2018**, *10*, 27987–28002. [CrossRef] [PubMed]
75. Han, J.; Ding, Q.; Mei, C.; Wu, Q.; Yue, Y.; Xu, X. An intrinsically self-healing and biocompatible electroconductive hydrogel based on nanostructured nanocellulose-polyaniline complexes embedded in a viscoelastic polymer network towards flexible conductors and electrodes. *Electrochim. Acta* **2019**, *318*, 660–672. [CrossRef]
76. Han, J.; Yue, Y.; Wu, Q.; Huang, C.; Pan, H.; Zhan, X.; Mei, C.; Xu, X. Effects of nanocellulose on the structure and properties of poly (vinyl alcohol)-borax hybrid foams. *Cellulose* **2017**, *24*, 4433–4448. [CrossRef]
77. Tao, J.; Shivkumar, S. Molecular weight dependent structural regimes during the electrospinning of PVA. *Mater. Lett.* **2007**, *61*, 2325–2328. [CrossRef]
78. Supaphol, P.; Chuangchote, S. On the electrospinning of poly (vinyl alcohol) nanofiber mats: A revisit. *J. Appl. Polym. Sci.* **2008**, *108*, 969–978. [CrossRef]
79. Yang, R.R.; He, J.H.; Xu, L.; Yu, J.Y. Effect of solution concentration on diameter and morphology of PVA nanofibres in bubble electrospinning process. *Mater. Sci. Technol.* **2013**, *26*, 1313–1316. [CrossRef]
80. Wang, X.; Niu, H.; Lin, T.; Wang, X. Needleless electrospinning of nanofibers with a conical wire coil. *Polym. Eng. Sci.* **2009**, *49*, 1582–1586. [CrossRef]
81. Niu, H.; Lin, T.; Wang, X. Needleless electrospinning. I. A comparison of cylinder and disk nozzles. *J. Appl. Polym. Sci.* **2009**, *114*, 3524–3530. [CrossRef]
82. Feng, B.; Tu, H.; Yuan, H.; Peng, H.; Zhang, Y. Acetic-acid-mediated miscibility toward electrospinning homogeneous composite nanofibers of GT/PCL. *Biomacromolecules* **2012**, *13*, 3917–3925. [CrossRef]
83. Espindola-Gonzalez, A.; Martinez-Hernandez, A.L.; Fernandez-Escobar, F.; Castano, V.M.; Brostow, W.; Datashvili, T.; Velasco-Santos, C. Natural-synthetic hybrid polymers developed via electrospinning: The effect of PET in chitosan/starch system. *Int. J. Mol. Sci.* **2011**, *12*, 1908–1920. [CrossRef]
84. Sajeev, U.S.; Anoop Anand, K.; Menon, D.; Nair, S. Control of nanostructures in PVA, PVA/chitosan blends and PCL through electrospinning. *Bull. Mater. Sci.* **2008**, *31*, 343–351. [CrossRef]
85. Zheng, Y.; Zhuang, C.; Gong, R.H.; Zeng, Y. Electric Field Design for Multijet Electropsinning with Uniform Electric Field. *Industrial & Engineering Chemistry Research* **2014**, *53*, 14876–14884. [CrossRef]
86. Ding, B.; Kimura, E.; Sato, T.; Fujita, S.; Shiratori, S. Fabrication of blend biodegradable nanofibrous nonwoven mats via multi-jet electrospinning. *Polymer* **2004**, *45*, 1895–1902. [CrossRef]
87. Wang, Q.; Curtis, C.K.; Thoppey, N.M.; Bochinski, J.R.; Gorga, R.E.; Clarke, L.I. Unconfined, melt edge electrospinning from multiple, spontaneous, self-organized polymer jets. *Mater. Res. Express* **2014**, *1*, 045304. [CrossRef]
88. Thoppey, N.M.; Bochinski, J.R.; Clarke, L.I.; Gorga, R.E. Edge electrospinning for high throughput production of quality nanofibers. *Nanotechnology* **2011**, *22*, 345301. [CrossRef]
89. Thoppey, N.M.; Gorga, R.E.; Bochinski, J.R.; Clarke, L.I. Effect of Solution Parameters on Spontaneous Jet Formation and Throughput in Edge Electrospinning from a Fluid-Filled Bowl. *Macromolecules* **2012**, *45*, 6527–6537. [CrossRef]
90. Roman, M.P.; Thoppey, N.M.; Gorga, R.E.; Bochinski, J.R.; Clarke, L.I. Maximizing Spontaneous Jet Density and Nanofiber Quality in Unconfined Electrospinning: The Role of Interjet Interactions. *Macromolecules* **2013**, *46*, 7352–7362. [CrossRef]

91. Thoppey, N.M.; Bochinski, J.R.; Clarke, L.I.; Gorga, R.E. Unconfined fluid electrospun into high quality nanofibers from a plate edge. *Polymer* **2010**, *51*, 4928–4936. [CrossRef]
92. Yao, Z.C.; Chen, S.C.; Ahmad, Z.; Huang, J.; Chang, M.W.; Li, J.S. Essential Oil Bioactive Fibrous Membranes Prepared via Coaxial Electrospinning. *J. Food Sci.* **2017**, *82*, 1412–1422. [CrossRef] [PubMed]
93. Komur, B.; Bayrak, F.; Ekren, N.; Eroglu, M.S.; Oktar, F.N.; Sinirlioglu, Z.A.; Yucel, S.; Guler, O.; Gunduz, O. Starch/PCL composite nanofibers by co-axial electrospinning technique for biomedical applications. *Biomed. Eng. Online* **2017**, *16*, 40. [CrossRef] [PubMed]
94. Park, H.; Yoo, H.; Hwang, T.; Park, T.-J.; Paik, D.-H.; Choi, S.-W.; Kim, J.H. Fabrication of levofloxacin-loaded nanofibrous scaffolds using coaxial electrospinning. *J. Pharm. Investig.* **2012**, *42*, 89–93. [CrossRef]
95. Alharbi, H.F.; Luqman, M.; Fouad, H.; Khalil, K.A.; Alharthi, N.H. Viscoelastic behavior of core-shell structured nanofibers of PLA and PVA produced by coaxial electrospinning. *Polym. Test.* **2018**, *67*, 136–143. [CrossRef]
96. Korehei, R.; Kadla, J. Incorporation of T4 bacteriophage in electrospun fibres. *J. Appl. Microbiol.* **2013**, *114*, 1425–1434. [CrossRef]
97. He, M.; Jiang, H.; Wang, R.; Xie, Y.; Zhao, C. Fabrication of metronidazole loaded poly (epsilon-caprolactone)/zein core/shell nanofiber membranes via coaxial electrospinning for guided tissue regeneration. *J. Colloid Interface Sci.* **2017**, *490*, 270–278. [CrossRef]
98. George, J.; Ishida, H. A review on the very high nanofiller-content nanocomposites: Their preparation methods and properties with high aspect ratio fillers. *Prog. Polym. Sci.* **2018**, *86*, 1–39. [CrossRef]
99. Yue, Y.; Wang, X.; Wu, Q.; Han, J.; Jiang, J. Assembly of Polyacrylamide-Sodium Alginate-Based Organic-Inorganic Hydrogel with Mechanical and Adsorption Properties. *Polymers* **2019**, *11*, 1239. [CrossRef]
100. Wolf, C.; Angellier-Coussy, H.; Gontard, N.; Doghieri, F.; Guillard, V. How the shape of fillers affects the barrier properties of polymer/non-porous particles nanocomposites: A review. *J. Membr. Sci.* **2018**, *556*, 393–418. [CrossRef]
101. Yue, Y.; Wang, X.; Han, J.; Yu, L.; Chen, J.; Wu, Q.; Jiang, J. Effects of nanocellulose on sodium alginate/polyacrylamide hydrogel: Mechanical properties and adsorption-desorption capacities. *Carbohydr. Polym.* **2019**, *206*, 289–301. [CrossRef]
102. Han, J.; Wang, H.; Yue, Y.; Mei, C.; Chen, J.; Huang, C.; Wu, Q.; Xu, X. A self-healable and highly flexible supercapacitor integrated by dynamically cross-linked electro-conductive hydrogels based on nanocellulose-templated carbon nanotubes embedded in a viscoelastic polymer network. *Carbon* **2019**, *149*, 1–18. [CrossRef]
103. Yang, T.; Wu, D.; Lu, L.; Zhou, W.; Zhang, M. Electrospinning of polylactide and its composites with carbon nanotubes. *Polym. Compos.* **2011**, *32*, 1280–1288. [CrossRef]
104. Meng, Z.X.; Zheng, W.; Li, L.; Zheng, Y.F. Fabrication and characterization of three-dimensional nanofiber membrance of PCL–MWCNTs by electrospinning. *Mater. Sci. Eng. C* **2010**, *30*, 1014–1021. [CrossRef]
105. Torres-Giner, S.; Echegoyen, Y.; Teruel-Juanes, R.; Badia, J.D.; Ribes-Greus, A.; Lagaron, J.M. Electrospun Poly (ethylene-co-vinyl alcohol)/Graphene Nanoplatelets Composites of Interest in Intelligent Food Packaging Applications. *Nanomaterials* **2018**, *8*, 745. [CrossRef]
106. Song, T.; Zhang, Y.; Zhou, T.; Lim, C.T.; Ramakrishna, S.; Liu, B. Encapsulation of self-assembled FePt magnetic nanoparticles in PCL nanofibers by coaxial electrospinning. *Chem. Phys. Lett.* **2005**, *415*, 317–322. [CrossRef]
107. Wang, S.; Wang, C.; Zhang, B.; Sun, Z.; Li, Z.; Jiang, X.; Bai, X. Preparation of Fe3O4/PVA nanofibers via combining in-situ composite with electrospinning. *Mater. Lett.* **2010**, *64*, 9–11. [CrossRef]
108. Wei, Y.; Zhang, X.; Song, Y.; Han, B.; Hu, X.; Wang, X.; Lin, Y.; Deng, X. Magnetic biodegradable Fe3O4/CS/PVA nanofibrous membranes for bone regeneration. *Biomed. Mater.* **2011**, *6*, 055008. [CrossRef]
109. Chowdhury, M.; Stylios, G. Process optimization and alignment of PVA/FeCl3 nano composite fibres by electrospinning. *J. Mater. Sci.* **2011**, *46*, 3378–3386. [CrossRef]
110. Kumar, M.; Unruh, D.; Sindelar, R.; Renz, F. Preparation of Magnetic Polylactic Acid Fiber Mats by Electrospinning. *Nano Hybrids Compos.* **2017**, *14*, 39–47. [CrossRef]
111. Bedford, N.; Steckl, A. Photocatalytic Self Cleaning Textile Fibers by Coaxial Electrospinning. *ACS Appl. Mater. Interfaces* **2010**, *2*. [CrossRef]

112. Nasikhudin; Ismaya, E.P.; Diantoro, M.; Kusumaatmaja, A.; Triyana, K. Preparation of PVA/TiO2 Composites Nanofibers by using Electrospinning Method for Photocatalytic Degradation. *IOP Conf. Ser. Mater. Sci. Eng.* **2017**, *202*, 012011. [CrossRef]
113. Liu, H.; Yang, J.; Liang, J.; Huang, Y.; Tang, C. ZnO Nanofiber and Nanoparticle Synthesized Through Electrospinning and Their Photocatalytic Activity Under Visible Light. *J. Am. Ceram. Soc.* **2008**, *91*, 1287–1291. [CrossRef]
114. Khan, M.Q.; Lee, H.; Koo, J.M.; Khatri, Z.; Sui, J.; Im, S.S.; Zhu, C.; Kim, I.S. Self-cleaning effect of electrospun poly (1,4-cyclohexanedimethylene isosorbide terephthalate) nanofibers embedded with zinc oxide nanoparticles. *Text. Res. J.* **2017**, *88*, 2493–2498. [CrossRef]
115. Zhu, Z.; Zhang, Y.; Shang, Y.; Wen, Y. Electrospun Nanofibers Containing TiO2 for the Photocatalytic Degradation of Ethylene and Delaying Postharvest Ripening of Bananas. *Food Bioprocess Technol.* **2018**, *12*, 281–287. [CrossRef]
116. Sawai, J.; Igarashi, H.; Hashimoto, A.; Kokugan, T.; Shimizu, M. Evaluation of Growth Inhibitory Effect of Ceramics Powder Slurry on Bacteria by Conductance Method. *J. Chem. Eng. Jpn.* **1995**, *28*, 288–293. [CrossRef]
117. Amna, T.; Yang, J.; Ryu, K.S.; Hwang, I.H. Electrospun antimicrobial hybrid mats: Innovative packaging material for meat and meat-products. *J. Food Sci. Technol.* **2015**, *52*, 4600–4606. [CrossRef]
118. Lee, J.-H.; Lee, U.-S.; Jeong, K.-U.; Seo, Y.-A.; Park, S.-J.; Kim, H.-Y. Preparation and characterization of poly(vinyl alcohol) nanofiber mats crosslinked with blocked isocyanate prepolymer. *Polym. Int.* **2010**, *59*, 1683–1689. [CrossRef]
119. Lee, S.J.; Oh, S.H.; Liu, J.; Soker, S.; Atala, A.; Yoo, J.J. The use of thermal treatments to enhance the mechanical properties of electrospun poly (epsilon-caprolactone) scaffolds. *Biomaterials* **2008**, *29*, 1422–1430. [CrossRef]
120. D'Amato, A.R.; Schaub, N.J.; Cardenas, J.M.; Fiumara, A.S.; Troiano, P.M.; Fischetti, A.; Gilbert, R.J. Removal of Retained Electrospinning Solvent Prolongs Drug Release from Electrospun PLLA Fibers. *Polymer (Guildf.)* **2017**, *123*, 121–127. [CrossRef]
121. Wang, H.-S.; Fu, G.-D.; Li, X.-S. Functional Polymeric Nanofibers from Electrospinning. *Recent Pat. Nanotechnol.* **2009**, *3*, 21–31. [CrossRef]
122. Yao, C.; Li, X.-s.; Neoh, K.G.; Shi, Z.-l.; Kang, E.T. Antibacterial poly (D,L-lactide) (PDLLA) fibrous membranes modified with quaternary ammonium moieties. *Chin. J. Polym. Sci.* **2010**, *28*, 581–588. [CrossRef]
123. Surucu, S.; Turkoglu Sasmazel, H. DBD atmospheric plasma-modified, electrospun, layer-by-layer polymeric scaffolds for L929 fibroblast cell cultivation. *J. Biomater. Sci. Polym. Ed.* **2016**, *27*, 111–132. [CrossRef] [PubMed]
124. Ignatova, M.; Manolova, N.; Rashkov, I.; Markova, N. Antibacterial and antioxidant electrospun materials from poly (3-hydroxybutyrate) and polyvinylpyrrolidone containing caffeic acid phenethyl ester—"in" and "on" strategies for enhanced solubility. *Int. J. Pharm.* **2018**, *545*, 342–356. [CrossRef] [PubMed]
125. Goh, Y.-f.; Akram, M.; Alshemary, A.; Hussain, R. Antibacterial polylactic acid/chitosan nanofibers decorated with bioactive glass. *Appl. Surf. Sci.* **2016**, *387*, 1–7. [CrossRef]
126. Yakub, G.; Ignatova, M.; Manolova, N.; Rashkov, I.; Toshkova, R.; Georgieva, A.; Markova, N. Chitosan/ferulic acid-coated poly (epsilon-caprolactone) electrospun materials with antioxidant, antibacterial and antitumor properties. *Int. J. Biol. Macromol.* **2018**, *107*, 689–702. [CrossRef]
127. Hu, H.-T.; Lee, S.-Y.; Chen, C.-C.; Yang, Y.-C.; Yang, J.-C. Processing and properties of hydrophilic electrospun polylactic acid/beta-tricalcium phosphate membrane for dental applications. *Polym. Eng. Sci.* **2013**, *53*, 833–842. [CrossRef]
128. Duling, R.R.; Dupaix, R.B.; Katsube, N.; Lannutti, J. Mechanical characterization of electrospun polycaprolactone (PCL): A potential scaffold for tissue engineering. *J. Biomech. Eng.* **2008**, *130*, 011006. [CrossRef]
129. Subramanian, C.; Ugbolue, S.C.; Warner, S.B.; Patra, P. *The Melt Electrospinning of Polycaprolactone (PCL) Ultrafine Fibers*; MRS Online Proceedings Library Archive: Warrendale, PA, USA, 2008; Volume 1134, p. 1134-BB1108.
130. Del Gaudio, C.; Bianco, A.; Folin, M.; Baiguera, S.; Grigioni, M. Structural characterization and cell response evaluation of electrospun PCL membranes: Micrometric versus submicrometric fibers. *J. Biomed. Mater. Res. Part A* **2009**, *89*, 1028–1039. [CrossRef]

131. Bhullar, S.K.; Kaya, B.; Jun, M.B.-G. Development of Bioactive Packaging Structure Using Melt Electrospinning. *J. Polym. Environ.* **2015**, *23*, 416–423. [CrossRef]
132. Park, J.-y.; Lee, E.-S.; Amna, T.; Jang, Y.; Park, D.H.; Kim, B.-S. Effects of heat-treatment on surface morphologies, mechanical properties of nanofibrous poly (propylene carbonate) biocomposites and its cell culture. *Colloids Surf. A Physicochem. Eng. Asp.* **2016**, *492*, 138–143. [CrossRef]
133. Nagiah, N.; Sivagnanam, U.T.; Mohan, R.; Srinivasan, N.T.; Sehgal, P.K. Development and Characterization of Electropsun Poly (propylene carbonate) Ultrathin Fibers as Tissue Engineering Scaffolds. *Adv. Eng. Mater.* **2012**, *14*, B138–B148. [CrossRef]
134. Li, Y.; Lim, C.T.; Kotaki, M. Study on structural and mechanical properties of porous PLA nanofibers electrospun by channel-based electrospinning system. *Polymer* **2015**, *56*, 572–580. [CrossRef]
135. Casasola, R.; Thomas, N.L.; Trybala, A.; Georgiadou, S. Electrospun poly lactic acid (PLA) fibres: Effect of different solvent systems on fibre morphology and diameter. *Polymer* **2014**, *55*, 4728–4737. [CrossRef]
136. Tang, X.P.; Xu, L.; Liu, H.Y.; Si, N. Fabrication of PLA Nanoporous Fibers by DMF/CF Mixed Solvent via Electrospinning. *Adv. Mater. Res.* **2014**, *941–944*, 400–403. [CrossRef]
137. Huang, C.; Thomas, N.L. Fabricating porous poly (lactic acid) fibres via electrospinning. *Eur. Polym. J.* **2018**, *99*, 464–476. [CrossRef]
138. Tomaszewski, W.; Duda, A.; Szadkowski, M.; Libiszowski, J.; Ciechanska, D. Poly (L-lactide) Nano- and Microfibers by Electrospinning: Influence of Poly (L-lactide) Molecular Weight. *Macromol. Symp.* **2008**, *272*, 70–74. [CrossRef]
139. Li, S.; Lv, R.; Liu, H.; Na, B.; Zhou, H.; Ge, L. Uniform high-molecular-weight polylactide nanofibers electrospun from a solution below its entanglement concentration. *J. Appl. Polym. Sci.* **2017**, *134*. [CrossRef]
140. Kayaci, F.; Uyar, T. Encapsulation of vanillin/cyclodextrin inclusion complex in electrospun polyvinyl alcohol (PVA) nanowebs: Prolonged shelf-life and high temperature stability of vanillin. *Food Chem.* **2012**, *133*, 641–649. [CrossRef]
141. Wen, P.; Zhu, D.-H.; Wu, H.; Zong, M.-H.; Jing, Y.-R.; Han, S.-Y. Encapsulation of cinnamon essential oil in electrospun nanofibrous film for active food packaging. *Food Control* **2016**, *59*, 366–376. [CrossRef]
142. Ding, B.; Ogawa, T.; Kim, J.; Fujimoto, K.; Shiratori, S. Fabrication of a super-hydrophobic nanofibrous zinc oxide film surface by electrospinning. *Thin Solid Films* **2008**, *516*, 2495–2501. [CrossRef]
143. Barthlott, W.; Neinhuis, C. Purity of the sacred lotus, or escape from contamination in biological surfaces. *Planta* **1997**, *202*, 1–8. [CrossRef]
144. Kang, M.; Jung, R.; Kim, H.-S.; Jin, H.-J. Preparation of superhydrophobic polystyrene membranes by electrospinning. *Colloids Surf. A Physicochem. Eng. Asp.* **2008**, *313–314*, 411–414. [CrossRef]
145. Tang, Y.; Zhou, Y.; Xingzi, L.; Huang, D.; Luo, T.; Ji, J.; Mafang, Z.; Miao, X.; Wang, H.; Wang, W. Electrospun Gelatin Nanofibers Encapsulated with Peppermint and Chamomile Essential Oils as Potential Edible Packaging. *J. Agric. Food Chem.* **2019**, *67*. [CrossRef]
146. Mascheroni, E.; Fuenmayor, C.A.; Cosio, M.S.; Di Silvestro, G.; Piergiovanni, L.; Mannino, S.; Schiraldi, A. Encapsulation of volatiles in nanofibrous polysaccharide membranes for humidity-triggered release. *Carbohydr. Polym* **2013**, *98*, 17–25. [CrossRef]
147. Vega-Lugo, A.-C.; Lim, L.-T. Controlled release of allyl isothiocyanate using soy protein and poly (lactic acid) electrospun fibers. *Food Res. Int.* **2009**, *42*, 933–940. [CrossRef]
148. Neo, Y.P.; Swift, S.; Ray, S.; Gizdavic-Nikolaidis, M.; Jin, J.; Perera, C.O. Evaluation of gallic acid loaded zein sub-micron electrospun fibre mats as novel active packaging materials. *Food Chem.* **2013**, *141*, 3192–3200. [CrossRef]
149. Agarwal, A.; Raheja, A.; Natarajan, T.S.; Chandra, T.S. Effect of electrospun montmorillonite-nylon 6 nanofibrous membrane coated packaging on potato chips and bread. *Innov. Food Sci. Emerg. Technol.* **2014**, *26*, 424–430. [CrossRef]
150. Arkoun, M.; Daigle, F.; Holley, R.A.; Heuzey, M.C.; Ajji, A. Chitosan-based nanofibers as bioactive meat packaging materials. *Packag. Technol. Sci.* **2018**, *31*, 185–195. [CrossRef]
151. Fabra, M.J.; Lopez-Rubio, A.; Lagaron, J.M. Nanostructured interlayers of zein to improve the barrier properties of high barrier polyhydroxyalkanoates and other polyesters. *J. Food Eng.* **2014**, *127*, 1–9. [CrossRef]
152. Fabra, M.J.; Lopez-Rubio, A.; Cabedo, L.; Lagaron, J.M. Tailoring barrier properties of thermoplastic corn starch-based films (TPCS) by means of a multilayer design. *J. Colloid Interface Sci.* **2016**, *483*, 84–92. [CrossRef]

153. Fabra, M.J.; Lopez-Rubio, A.; Lagaron, J.M. High barrier polyhydroxyalcanoate food packaging film by means of nanostructured electrospun interlayers of zein. *Food Hydrocoll.* **2013**, *32*, 106–114. [CrossRef]
154. Fabra, M.J.; López-Rubio, A.; Lagaron, J.M. On the use of different hydrocolloids as electrospun adhesive interlayers to enhance the barrier properties of polyhydroxyalkanoates of interest in fully renewable food packaging concepts. *Food Hydrocoll.* **2014**, *39*, 77–84. [CrossRef]
155. Klimov, E.; Raman, V.; Venkatesh, R.; Heckmann, W.; Stark, R. Designing Nanofibers via Electrospinning from Aqueous Colloidal Dispersions: Effect of Cross-Linking and Template Polymer. *Macromolecules* **2010**, *43*, 6152–6155. [CrossRef]

nanomaterials

MDPI

Article

Electrospun Nanofibers: from Food to Energy by Engineered Electrodes in Microbial Fuel Cells

Giulia Massaglia [1,2,*], Francesca Frascella [1], Alessandro Chiadò [1], Adriano Sacco [2], Simone Luigi Marasso [1,3], Matteo Cocuzza [1,3], Candido F. Pirri [1,2] and Marzia Quaglio [1,*]

[1] Department of Applied Science and Technology (DISAT), Politecnico di Torino, Corso Duca degli Abruzzi 24, 10129 Torino, Italy; francesca.frascella@polito.it (F.F.); alessandro.chiado@polito.it (A.C.); simone.marasso@polito.it (S.L.M.); matteo.cocuzza@infm.polito.it (M.C.); fabrizio.pirri@polito.it (C.F.P.)

[2] Center for Sustainable Future Technologies (CSFT)@Polito, Istituto Italiano di Tecnologia, Environment Park, Building B2 Via Livorno 60, 10144 Torino, Italy; adriano.sacco@iit.it

[3] IMEM-CNR, Parco Area delle Scienze 37, 43124 Parma, Italy

* Correspondence: giulia.massaglia@polito.it (G.M.); marzia.quaglio@polito.it (M.Q.)

Received: 31 January 2020; Accepted: 10 March 2020; Published: 14 March 2020

Abstract: Microbial fuel cells (MFCs) are bio-electrochemical devices able to directly transduce chemical energy, entrapped in an organic mass named fuel, into electrical energy through the metabolic activity of specific bacteria. During the last years, the employment of bio-electrochemical devices to study the wastewater derived from the food industry has attracted great interest from the scientific community. In the present work, we demonstrate the capability of exoelectrogenic bacteria used in MFCs to catalyze the oxidation reaction of honey, employed as a fuel. With the main aim to increase the proliferation of microorganisms onto the anode, engineered electrodes are proposed. Polymeric nanofibers, based on polyethylene oxide (PEO-NFs), were directly electrospun onto carbon-based material (carbon paper, CP) to obtain an optimized composite anode. The crucial role played by the CP/PEO-NFs anodes was confirmed by the increased proliferation of microorganisms compared to that reached on bare CP anodes, used as a reference material. A parameter named recovered energy (Erec) was introduced to determine the capability of bacteria to oxidize honey and was compared with the Erec obtained when sodium acetate was used as a fuel. CP/PEO-NFs anodes allowed achieving an Erec three times higher than the one reached with a bare carbon-based anode.

Keywords: electrospun nanofibers; polyethylene oxide nanofibers PEO-NFs; microbial fuel cells; honey; food industry; recovered energy (Erec)

1. Introduction

Microbial fuel cells (MFCs) are bio-electrochemical devices that directly convert the chemical energy embedded in an organic compound (i.e., the fuel) into electrical energy by the metabolic action of a particular class of microorganisms, named exo-electrogens.

Basically, the process is based on the ability of exo-electrogens to oxidize organic matter, acting as carbon energy sources [1], and to directly transfer the produced electrons outside their cells exogenously [2]. In an MFC, electrons are firstly released to the anode by the microorganisms arranged in a biofilm in intimate contact with the anode surface and successively they flow through an external circuit to reach the cathode side, where the terminal electron acceptor (TEA), usually oxygen, is finally reduced. Potential applications of MFCs have been foreseen in several areas [3,4], ranging from energy harvesting [5,6] to wastewater treatment [7] and sensing [8–12]. Since MFCs can operate their energy recovery and conversion processes starting from a wide range of molecules, even quite complex, during the last decades, they have attracted an ever-increasing interest for application in the food industry [13]. In this perspective, MFCs can contribute to the overall energetic efficiency of the process

by combining the treatment of wastewater streams to energy production. Interesting examples exist, concerning applications in the treatment of brewery wastewater [14,15], olive mill wastewater [16], winery wastes [17,18], and dairy wastewater [19].

The use of MFC for wastewater treatment plays a crucial role as an alternative to traditional treatment processes, such as anaerobic digestion with methane fermentation, which include indirect energy recovery from wastes [20]. Knowledge in this area has grown significantly, and information about the amount of energy than can be recovered from many substrates, such as urban wastewaters [21], short-chain volatile fatty acid [22], as well as fermentable and non-fermentable reference substrates, such as sodium acetate and glucose, respectively, is now available [23].

Nonetheless, further improvements are necessary to increase power production [24], which is currently hindering the marketability of MFCs. In this view, the anodic electrode and its interface with the bacteria biofilm play a crucial role, since they are responsible for energy conversion and the electron transfer process.

In the present work, a new nanofiber-based interface between a carbon paper (CP) anode and a bacterial biofilm is investigated with the aim to optimize the adhesion of the biofilm to the anode. Furthermore, optimized adhesion of the biofilm to the anode plays a crucial role in improving the biofilm–anode electrochemical interaction, thus effectively ameliorating the overall MFC performance in terms of energy production. The idea is based on the hypothesis that the larger is the number of bacteria on the anode, the higher is the resulting electron transfer rate, which is true only if the interface is designed in such a way to keep electrical resistance low. Therefore, in the present work, new nanostructured polymeric mats with high specific area were designed to modify the surface of carbon-based materials in order to improve their ability to create effective interfaces with bacterial biofilms.

During the last decades, some works in the literature [25–27] investigated the modification of carbon-based electrodes by the application of a polymeric matrix on their surfaces to increase the contact between bacteria and anodes in MFCs. Several polymeric matrices have been developed, using both natural polymers, such as agar, alginate, or agarose, and synthetic polymers [28–30]. Despite being interesting because of their sustainable origin and biocompatibility, natural polymers suffer from poor mechanical strength and durability, while synthetic polymers show an opposite behavior, since they combine higher mechanical strength and durability with a higher risk of toxicity for bacteria proliferation. Among the synthetic polymers proposed up to now in the literature, a promising one is poly(vinyl) alcohol (PVA) [25–27]. It has been investigated in different arrangements, as foams, nanofibers, and film, with the aim to reach a high density of immobilized microorganisms while ensuring good mass transfer properties. Currently, the best performing PVA anode-to-biofilm interface system is the one proposed by Bai et al. [27]. They developed a highly porous foam that showed good results in terms of immobilization of microorganisms, but the fabrication process required the use of boric acid, which caused side problems, such as agglomeration of PVA beads and residuals of toxic boric acid and enhanced swelling of the polymer foam. In order to overcome the limits of such technological approach, in the present work, polyethylene oxide nanofibers mats (PEO-NFs) are proposed as a biomass carrier. Electrospinning is selected as the process to obtain the highly porous matrix, and PEO works as the reference polymer. PEO shows a wide range of intriguing properties: (1) it is not cytotoxic, therefore it allows bacteria proliferation, (2) it is a sustainable and environmentally friendly material that can be processed using water as the only solvent, and (3) it is an important solid polymer electrolyte in electrochemical applications [28,29].

PEO-NFs were directly deposited onto CP-based electrodes, according to the electrospinning-on-electrode process, a binder-free method for nanofiber assembly onto an electrode that we introduced in our previous work [30].

The resulting anodes, named CP/PEO-NFs, were investigated in single-chamber MFCs (SCMFCs) and compared with reference devices using pure CP as anodes [30].

We demonstrate a huge improvement of microorganisms' proliferation toward the desired optical density (OD), thus confirming the possibility to use CP/PEO-NFs as a biomass carrier for bacteria entrapment. CP decorated by PEO-NFs interfaces were then tested in SCMFCs. A mixed bacterial consortium extracted from a marine sediment sample was used as the inoculum source [31]. A current density as high as 12 mA m^{-2} was reached when CP/PEO-NFs was used as the anode electrode. This value is higher than the one reached with CP anodes, indicating how the presence of PEO-NFs interfaces does not affect the electron transfer process, simultaneously inducing the proliferation of microorganisms.

Finally, we tested the potential of the newly designed anodic electrode to be used in MFCs for energy recovery in the agro-food industry. To demonstrate the robustness of our nanofiber-based interface, we selected honey as a new and more complex electron donor than those tested up to now in MFCs. The use of honey by humans traces back to ancient times, and today honey is a crucial ingredient in several products ranging from foods to beverages, as well as in medical products and cosmetics [32,33]. Honey can be classified as a natural sweetener with a complex composition [34]. In particular, honey is a saturated-sugar solution, where the carbohydrates amount to 95% of its chemical components. Moreover, other important compounds are naturally contained into honey, such as proteins, amino acids, enzymes, organic acids, minerals, and vitamins [34–36].

Given both its complex composition, that makes it a complete food from a nutritional point of view, and its natural antibiotic behavior, it is quite interesting to analyze the behavior of MFCs fed with water streams containing a limited amount of honey. Indeed, since MFCs' power production is based on the metabolic activity of exo-electrogenic microorganisms, all substances able to alter and/or modify the biofilm metabolism could alter the power output. Therefore, we tested the newly designed CP/PEO-NFs anodes in SCMFCs in which a honey-in-water solution at 0.02 wt % was used as the electrolyte. Given the aforementioned antibiotic behavior of honey, the first goal of this study was to demonstrate that MFCs can convert the organic matter of honey into electricity without damaging the biofilms, and the second goal was to demonstrate that new nanofiber-based anodes are more efficient than the commonly used CP references.

Results are analyzed in terms of recovered energy (E_{rec}) per unit volume [18,21,37]. E_{rec} was obtained by the integration of the measured power output over the batch treatment time. In particular, E_{rec} obtained for honey was compared with E_{rec} obtained when sodium acetate was used as a fuel in SCMFCs, demonstrating the microorganisms' capability to oxidize honey. A further comparison is then proposed to appreciate the different behavior of CP/PEO-NFs anodes in comparison to CP reference anodes.

Finally, we demonstrate that the SCMFCs' response, in terms of power output, changes with honey concentration. Different concentrations of honey (from 0.83 to 2 gL^{-1}) were tested and correlated with the corresponding energy recovery parameter.

2. Materials and Methods

2.1. Materials and Nanofibers Synthesis

A new nanofiber-based interface between a carbon paper-based anode and a bacteria biofilm was investigated. In particular, new nanostructured polymeric mats with high specific area were designed to modify the surface of carbon-based materials. Nanofibers mats based on PEO, were directly electrospun on a carbon-based material (named CP, Fuel Cell Earth, Woburn, Massachusetts, USA), used as reference material since it is the most employed anode in MFCs. As already demonstrated in our previous work [30], the morphology of CP, characterized by several conductive micro-protrusions, plays a crucial role in tuning a selective patterned deposition of PEO nanofibers (CP/PEO-NFs), thus leading to ensure a binder-free deposition of nanofibers. In particular, CP/PEO-NFs were obtained by electrospinning, starting from a polymeric solution containing PEO (purchased from Sigma Aldrich, with an average molecular weight Mw = 600 kDa) dissolved in deionized water. Electrospinning was

performed by the NANON 01A machine from MECC Co. Ltd. The polymeric solution was loaded into a syringe, and nanofiber were obtained by applying a high positive voltage equal to 20 kV and a flow rate of 0.5 mL h^{-1} at a working distance of 12 cm. The duration of the electrospinning process was close to 10 min to ensure at the same time an ordered distribution of nanofibers, which were directly collected onto CP without a binder, and a high surface area-to-volume ratio. As demonstrated in our previous work [30], the ordered distribution is mainly due to the conductive protrusions of CP that induce electric field enhancement. This ordered distribution can be optimized when the thickness of the nanofibers is close to few micrometers. Indeed, a higher thickness of nanofiber mats could induce an insulator effect onto a carbon-based surface, minimizing the electric field variations that rule the nanofibers' distribution onto a CP surface. Moreover, in the present work, the surface area was defined by implementing Brunauer–Emmett–Tell (BET) measurements. In order to establish the lack of cytotoxicity of PEO for microorganisms, optical density (OD) measurements were carried out by means of a LAMBDA 850+ UV/Vis spectrophotometer.

In particular, OD measurement estimated the growth and metabolic activity of bacteria. Both CP/PEO-NFs and bare CP pieces were put into a tube containing the inoculum source and the electrolyte solution. The electrolyte solution was based on sodium acetate ($C_2H_3NaO_2$), ammonium chloride (0.31 gL^{-1} of NH4Cl) used as a nitrogen source to aid bacteria growth, and phosphate-buffered solution (PBS) that maintained a neutral pH. Every day, total cell density (dead and alive cells) was established by measuring OD at 600 nm using the spectrophotometer.

2.2. MFC Architecture and Configuration

The MFCs used in the present work were squared single-chamber microbial fuel cells (SCMFCs) with an open-air cathode, fabricated by micro milling (Al.Tip srl). [38]. In particular, our devices were composed of 3 compartments: the anodic part, the intermediate compartment, and the cathodic compartment. The internal volume of SCMFCs was 12.5 mL, and both anode and cathode had a geometric area equal to 5.76 cm^2. Furthermore, in the present work, two different anodes were investigated and compared: (1) CP/PEO-NFs obtained by direct deposition of PEO nanofiber mats on a carbon-based electrode, employed as a carbon backbone to ensure the electron transfer generated and released by the microorganisms; (2) a carbon-based material (CP) used as a control. The cathode was based on CP, properly modified in order to present gas diffusion layers (DLs) based on polytetrafluoroethylene (PTFE) on its outer side and a catalyst layer based on Platinum (Pt/C 0.5 mg/cm^2, from Sigma Aldrich, St.Louis, Missouri, USA) and Nafion (5 wt % Nafion, from Sigma Aldrich) on its inner side. Titanium wires (Goodfellow Cambridge Limited) were fixed onto the anode and cathode through a conductive paste made of carbon cement (Leit-C Cement). Two different electrolyte solutions were used. The first was an electrolyte solution based on sodium acetate ($C_2H_3NaO_2$), used as a carbon energy source at a concentration of 2 gL^{-1} together with other compounds able to ensure the optimal operation of the SCMFCs. All these compounds were based on ammonium chloride (0.31 gL^{-1} of NH4Cl), used as a nitrogen source to support bacterial growth, and PBS, able to maintain a neutral pH (containing 0.13 gL^{-1} of potassium chloride, 4.28 gL^{-1} of sodium phosphate dibasic, and 2.45 gL^{-1} of sodium phosphate monobasic monohydrate). The second electrolyte contained honey in the same amount defined for sodium acetate, close to 2 gL^{-1}, dissolved in deionized water and PBS. In the second electrolyte, PBS was added to ensure a neutral pH of the solution; due to the complexity of honey, the second electrolyte did not require any further addition of nutritional compounds for the microorganisms. Both solutions were autoclaved prior to use. All experiments were conducted in duplicate for each tested electrolyte: 2 SCMFCs with CP/PEO-NFs anode and 2 SCMFCs with CP anodes were studied. All SCMFCs were inoculated with a mixed culture of bacteria from a seawater sediment. All SCMFCs worked under batch mode, meaning that all devices are filled with "*new electrolyte*" when the drop of power output reached its minimum value. Anodes and cathodes of the SCMFCs were connected to a multichannel data acquisition unit (Agilent 34972A), and two different values of external resistance were applied. At the beginning of the experiments, to ensure

the formation of biofilm on both anodes, i.e., CP/PEO-NFs and CP, an external load equal to 47 Ω was applied, and the electrolyte containing sodium acetate was used. Successively, to evaluate the overall SCMFCs' performance and to demonstrate that SCMFCs can convert honey organic matter into electricity without damaging the biofilms, an external load of 1000 Ω was applied. Furthermore, to establish and confirm the possibility to employ honey as a fuel in SCMFCs and demonstrate that its natural antibiotic behavior does not affect the overall SCMFCs' performance, we introduced a physical parameter, i.e., energy recovery (E_{rec}), calculated for both honey and sodium acetate [18,21,37]. The E_{rec} was defined according to Equation (1):

$$E_{rec} = \frac{\int Pdt}{V_{int}} \quad (1)$$

where E_{rec} $(J\ m^{-3})$ is energy recovery, V_{int}(m^3) is the internal volume of SCMFCs, and $\int Pdt$ (J) is the integral of the generated power over time. We were able to demonstrate the possibility of using honey as a fuel in SCMFCs. In order to simultaneously verify the SCMFCs' response in terms of power output as honey concentration changed, different honey concentrations (from 0.83gL^{-1} to 2 gL^{-1}) were tested and correlated with the values of power output.

Internal resistance of the SCMFCs was evaluated through Nyquist plots, using electrochemical impedance spectroscopy (EIS). EIS was performed in open-circuit voltage (OCV) over the range of frequency between 150 and 200 mHz, with a sinusoidal signal with an amplitude of 25 mV.

3. Results and Discussion

3.1. Electrospun Nanofibers Onto Carbon-Based Materials and Their Role as a Biomass Carrier

As already demonstrated in our previous work [30] and in order to optimize the deposition of nanofiber mats onto carbon-based materials, we selected CP as a carbon-based material. The morphology of bare CP is reported in Figure 1a. In particular, it is possible to appreciate that the morphology of CP shows many naturally occurring conductive protrusions, based on carbon fibers, whose diameter was over 10 μm. All these protrusions, as also demonstrated in our previous work [30], play a crucial role in modulating the electric field during the electrospinning process, inducing an intensity enhancement and granting an ordered distribution of PEO-NFs. As represented in the Figure 1b, CP/PEO-NFs nanofibers preferentially arranged themselves on top of the conductive protrusions of CP, thus optimizing the interface between the nanofibers mats and the carbon-based electrode without the presence of a binder, commonly used to fix the nanostructures onto the electrode.

Figure 1a,b shows that PEO-NFs were mostly deposited onto the CP surface in correspondence of the interconnections between the conductive protrusions, covering completely the CP surface. Moreover, the final CP/PEO-NFs anode resulted to be an engineered electrode with a high surface area-to-volume ratio. As indicated by the BET results, PEO-NFs showed a surface area close to 40 $m^2\ g^{-1}$.

As presented in Figure 1c, the OD measurements confirmed the capability of CP/PEO-NFs to create an effective interface with bacterial biofilms, thus ensuring bacterial proliferation onto the CP-based anode. This result also confirmed the possibility to apply CP/PEO-NFs as a biomass carrier. The high bacterial proliferation is due to the capability exhibited by CP/PEO-NFs to entrap the microorganisms into its nanostructures.

3.2. SCMFCs Performance

Thanks to CP/PEO-NFs biocompatibility, in terms of microorganisms' proliferation and their morphological properties, CP/PEO-NFs mats were produced and directly deposited onto the carbon-based material. During the first phase of the experiment, known as the acclimation phase, we applied an external resistance close to 47 Ω with the main aim to ensure biofilm formation onto the electrodes. The duration of this acclimation phase was 1 month. As shown in Figure 2, the overall performance reached by the CP/PEO-NFs composite anode was three times higher than the one

obtained with the bare carbon-based material. Since all the other features, i.e., the cathode, SCMFCs' configuration, and the electrolyte, were the same, it was possible to establish that the enhancement of the current density was related to the proliferation extent of the microorganisms, being higher onto PEO–NFs composite anodes. Moreover, by analyzing all peaks reported in Figure 2, it was possible to demonstrate a good electrical output produced by SCMFCs and, consequently, a stable and sustained bacteria proliferation on the anodes.

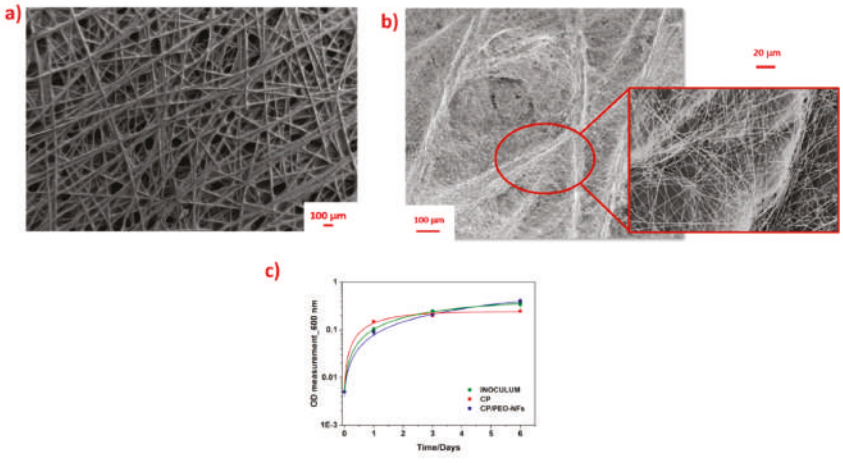

Figure 1. (**a**) FESEM images representing the bare carbon-based material (CP); (**b**) FESEM images representing the ordered distribution of CP/polyethylene oxide nanofibers (PEO-NFs) onto the carbon-based material. In the red box, the preferential distribution of CP/PEO-NFs onto the conductive protrusions of CP is highlighted; (**c**) logarithmic representation of OD measurements performed for all samples: bare inoculum (green), carbon-based material (CP, red), and CP/PEO-NFs (blue).

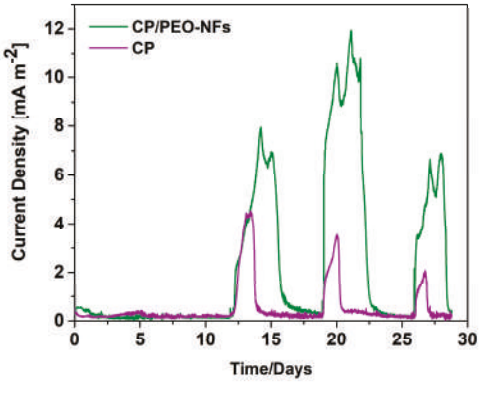

Figure 2. Current density produced in the acclimation phase, during which the biofilm formed onto the anodes: CP/PEO-NFs (green line) and carbon-based material used as a reference electrode (purple line). In this phase, the electrolyte contained sodium acetate; an external load of 47 Ω was applied.

The overall performance obtained with CP/PEO-NFS was compared with that of a reference material consisting of bare carbon-based anodes (CP). Moreover, given the complex composition of honey and its natural antibiotic behavior, a second experiment was implemented to demonstrate that SCMFCs can convert honey organic matter into electricity without damage to a biofilm and to confirm that the new nanofiber-based anodes (CP/PEO-NFs) perform better than the CP reference anodes.

In this experiment, an external load of 1kΩ was applied, and the overall performance, when both electrolytes were used, was analyzed. In this case, the concentration of sodium acetate and honey was 2 gL^{-1}. The current density trends, obtained from all tests in SCMFCs, were defined by normalizing with respect to the anode geometric area (5.76 cm^2) and are reported in Figure 3a,b. It is possible to appreciate that the maximum current densities reached when sodium acetate and honey were used as electrolytes were comparable, demonstrating the capability of bacteria to catalyze the oxidation reaction of honey. These results also suggest the possibility to apply SCMFCs to convert honey organic matter into electricity without damaging the biofilms. Moreover, since all these devices exploited formally identical cathodes and architectures, the current density trends were univocally correlated with the anodic reaction. Furthermore, as presented in Figure 3a,b, the maximum current density of total SCMFCs, reached when CP/PEO-NFs were used as the anode, was equal to (23.2 ± 0.1) mA m^{-2} and was comparable to the one obtained when CP was used as the reference anode. The presence of PEO-NFs, which basically showed insulating properties from an electrical point of view, not only did not affect the electron transfer rate but also simultaneously sustained the proliferation of microorganisms onto the anode. Moreover, all results are analyzed in terms of recovered energy ($E_{rec,}$ mJ m^{-3}). E_{rec} is calculated by integrating the electric power density over the batch treatment time and normalizing with respect to the electrolyte volume. Figure 3c shows that E_{rec} (equal to 100 mJ m^{-3}) obtained when using honey and CP material was close to E_{rec} reached when sodium acetate was employed as the electrolyte. Moreover, for both fuels, E_{rec} achieved when using CP/PEO-NFs was three times higher than the one reached when using the carbon-based material, confirming the crucial role of nanofibers, which ensure a better interface between the anode and the bacteria and enhance the overall performance of SCMFC. This latter result demonstrates that PEO-NFs can act as a biomass carrier. The interface between biofilm and CP/PEO-NFs anode was enhanced, as also confirmed by the OD measurements, underlying a more extensive bacterial proliferation onto CP/PEO-NFs anodes. Both features, the optimized interface between anode and biofilm and the role of PEO as a polymeric electrolyte in electrochemical devices, allowed reaching a higher E_{rec} in comparison with the one reached when using a bare carbon-based material (CP).

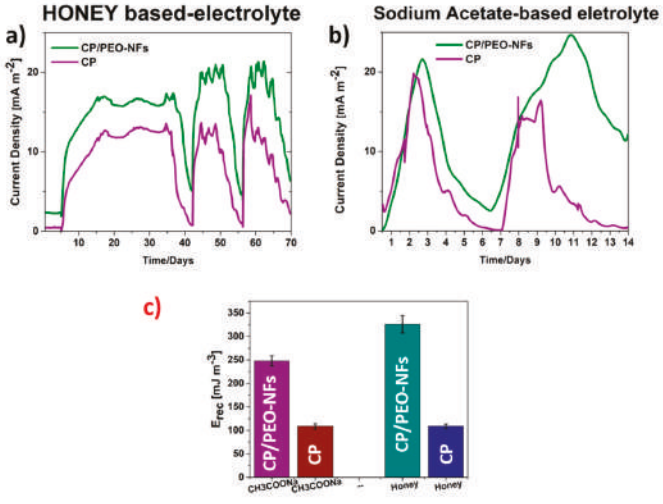

Figure 3. (**a**) Current density obtained when honey was used as a fuel and comparison of the current density values obtained for CP/PEO-NFs and CP; (**b**) current density reached using sodium acetate as a fuel and comparison of the values obtained for CP/PEO-NFs and CP; (**c**) recovered energy (E_{rec}) determined for CP/PEO-NFs and CP, using two different fuels.

Figure 4a,b show that the performance of all devices increased with increasing honey concentrations from 0.83 gL^{-1} to 2 gL^{-1}. The maximum value of recovered energy E_{rec} was reached at the highest honey concentration employed (2 gL^{-1}) for both CP/PEO-NFs and CP anodes. At all honey concentrations, CP/PEO-NFs showed a better performance in terms of E_{rec} than the CP anodes.

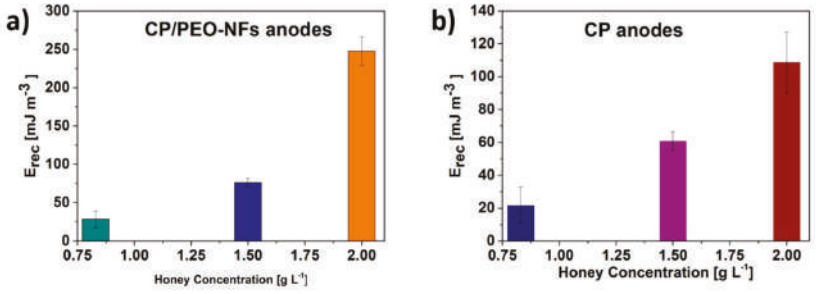

Figure 4. (**a**) Recovered energy defined for CP/PEO-NFs correlated with honey concentration; (**b**) Recovered energy defined for CP correlated with honey concentration.

3.3. Electrochemical Impedance Spectroscopy Results

EIS was performed to investigate the impedance behavior and, in particular, the internal resistance [39] when honey was employed as a fuel. By analyzing the Nyquist plot represented in Figure 5, it can be observed that MFCs exploiting CP/PEO-NFs as the anode were characterized by similar total impedance values with respect to carbon-based devices (982.2 Ω and 916.5 Ω, respectively). Moreover, the results allowed analyzing the resistance related to the charge transfer (R_{ct}) of both CP/PEO-NFs and CP anodes. The obtained results confirmed that SCMFCs exploiting CP/PEO-NFs as the anode presented impedance values close to those reached with a CP-based anode. The value of R_{ct} for CP/PEO-NFs, close to 761 Ω, was quite similar to that obtained for CP, equal to about 808 Ω. These results demonstrated that the presence of PEO-NFs, which basically has insulating properties from an electrical point of view, not only did not affect the electron transfer rate but also simultaneously sustained the proliferation of microorganisms onto the anode

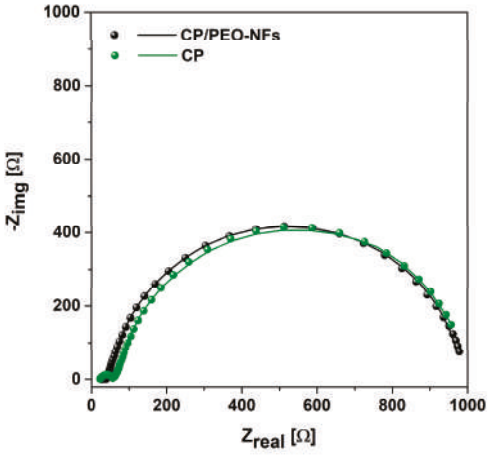

Figure 5. Impedance spectra of CP/PEO NFs (black dots and line, representing the experimental data and their fitting) and CP anode (green dots and line).

This result suggests the possibility to apply CP/PEO-NFs to achieve a large nanofiber-based interface between a CP anode and a bacterial biofilm, thus optimizing the adhesion of the biofilm to the anode.

4. Conclusions

In the present work, a CP/PEO-NFs composite anode, based on PEO-NFs directly electrospun onto a carbon-based material, was designed and optimized. CP/PEO-NFs showed a final ordered arrangement of PEO-NFs, able to grant a large surface area-to-volume ratio. We demonstrated that the resulting structure of PEO/NFs greatly promoted microorganisms' proliferation, thus suggesting the possibility to employ PEO-NFs as a biomass carrier for bacteria entrapment. Therefore, we investigated the behavior of a CP/PEO-NFs anode in SCMFCs, using a mixed bacterial consortium extracted from a marine sediment sample as the biofilm source. In particular, a high current density, close to 20 mA m^{-2}, was reached when CP/PEO-NFs were used as the anode. This value, higher than the one reached when bare CP was used as the anode, allowed us to demonstrate that the presence of PEO-NFs, with their insulating properties from an electrical point of view, did not affect the electron transfer rate and simultaneously sustained the proliferation of the microorganisms. Finally, the results concerning the evaluation of energy recovery confirmed the possibility to use a more complex substrate, such as honey, as a fuel in MFCs. Moreover, we evidenced that the new designed CP/PEO-NFs anodes are able to ensure a three-time higher recovered energy (i.e., 300 mJ m^{-3}) than that obtained when using a bare carbon-based anode.

The results show that nanostructured interfaces made of PEO-based nanofibers are advantageous for the fabrication of robust and efficient electrodes to be used in MFCs as energy conversion tools for the valorization of waste in the food industry.

Author Contributions: M.Q. and G.M. conceived the work. G.M. worked on electrospinning and MFCs. A.S. carried out the electrochemical characterization. M.Q., M.C., S.L.M. worked on the design and preparation of MFCs. F.F. and A.C. designed the experiments with honey. C.F.P. and M.Q. organized the research activity. All authors contributed to the final manuscript. All authors have read and agreed to the published version of the manuscript.

Funding: The present work was performed in the framework of the POLITO BIOMed LAB, an interdepartmental laboratory financed by Politecnico di Torino. The activity was partially financed by SMART3D ("Smart 3D Polymer Devices Production Chain") project, financed by MIUR and Piedmont Region agreement in the framework of "Smart Industry" and by Piedmont Region in the framework of the "FOOD-DRUG-FREE" Platform project. In the frame of the FOOD-DRUG-FREE project, the authors especially acknowledge support from Sebaste Srl for providing the honey samples used in the work.

Conflicts of Interest: The authors declare no conflict of interest

References

1. Slate, A.J.; Whiteland, K.A.; Brownson, D.A.C.; Banks, C.E. Microbial fuel cells: An overview of current technology. *Renew. Sustain. Energy Rev.* **2019**, *101*, 60–81. [CrossRef]
2. Logan, B.E. *Microbial Fuel Cells*; John Wiley & Sons Inc.: New York, NY, USA, 2008.
3. Santoro, C.; Arbizzani, C.; Erable, B.; Ieropoulos, I. Microbial fuel cells: From fundamentals to applications. *A review. J. Power Sources* **2017**, *356*, 225–244. [CrossRef] [PubMed]
4. Harnisch, F.; Aulenta, F.; Schroeder, U. Microbial Fuel Cells and Bioelectrochemical Systems: Industrial and Environmental Biotechnologies Based on Extracellular Electron Transfer. In *Comprehensive Biotechnology*, 2nd ed.; Elsevier: Amsterdam, The Netherlands, 2011; pp. 644–659.
5. Melhuish, C.; Ieropoulos, I.; Greenman, J.; Horsfield, I. Energetically autonomous robots: Food for thought. *Auton. Robots* **2006**, *21*, 187–198. [CrossRef]
6. Sanket, G. From waste to watts in micro-devices: Review on development of Membraned and Membraneless Microfluidic Microbial Fuel Cell. *Appl. Mater. Today* **2018**, *11*, 270–279.
7. Li, W.-W.; Yu, H.-Q.; He, Z. Towards sustainable wastewater treatment by using microbial fuel cells-centered technologies. *Energy Environ. Sci.* **2014**, *7*, 911–924. [CrossRef]

8. Chang, I.S.; Jang, J.K.; Gil, G.C.; Kim, M.; Kim, H.J.; Cho, B.W.; Kim, B.H. Continuous determination of biochemical oxygen demand using microbial fuel cell type biosensor. *Biosens. Bioelectron.* **2004**, *19*, 607–613. [CrossRef]
9. Shantaram, A.; Beyenal, H.; Raajan, R.; Veluchamy, A.; Lewandowski, Z. Wireless sensors powered by microbial fuel cells. *Environ. Sci. Technol.* **2005**, *39*, 5037–5042. [CrossRef]
10. Donovan, C.; Dewan, A.; Heo, D.; Beyenal, H. Batteryless, wireless sensor powered by a sediment microbial fuel cell. *Environ. Sci. Technol.* **2008**, *42*, 8591–8596. [CrossRef]
11. Tender, L.M.; Gray, S.A.; Groveman, E.; Lowy, D.A.; Kauffman, P.; Melhado, J.; Tyce, R.C.; Flynn, D.; Petrecca, R.; Dobarro, J. The first demonstration of a microbial fuel cell as a viable power supply: powering a meteorological buoy. *J. Power Sources* **2008**, *179*, 571–575. [CrossRef]
12. Venkata Mohan, S.; Raghavulu, V.S.; Sarma, P.N. Biochemical evaluation of bioelectricity production process from anaerobic wastewater treatment in a single chambered microbial fuel cell (MFC) employing glass wool membrane. *Biosens. Bioelectron.* **2008**, *23*, 1326–1332. [CrossRef]
13. Cecconet, D.; Molognoni, D.; Callegari, A.; Capodaglio, A.G. Agro-food industry wastewater treatment with microbial fuel cells: Energetic recovery issues. *Int. J. Hydrogen Energy* **2018**, *43*, 500–511. [CrossRef]
14. Feng, Y.; Wang, X.; Logan, B.E.; Lee, H. Brewery wastewater treatment using air-cathode microbial fuel cells. *Appl. Microbiol. Biotechnol.* **2008**, *78*, 873–880. [CrossRef] [PubMed]
15. Wang, X.; Feng, Y.J.; Lee, H. Electricity production from beer brewery wastewater using single chamber microbial fuel cell. *Water Sci. Technol.* **2008**, *57*, 1117–1121. [CrossRef] [PubMed]
16. Sciarra, T.P.; Tenca, A.; D'Epifanio, A.; Mecheri, B.; Merlino, G.; Barbato, M.; Borin, S.; Licoccia, S.; Garaviglia, V.; Adani, F. Using olive mill wastewater to improve performance in producing electricity from domestic wastewater by using single-chamber microbial fuel cell. *Bioresour. Technol.* **2013**, *147*, 246–253. [CrossRef]
17. Sciarra, T.P.; Merlino, G.; Scaglia, B.; D'Epifanio, A.; Mecheri, B.; Borin, S.; Licoccia, S.; Adani, F. Electricity generation using white and red wine lees in air cathode microbial fuel cells. *J. Power Sources* **2015**, *274*, 393–399. [CrossRef]
18. Penteado, E.D.; Fernandez-Marchante, C.M.; Zaiat, M.; Canizares, P.; Gonzales, E.R.; Rodrigo, M.A.R. Energy recovery from winery wastewater using a dual chamber microbial fuel cell. *J Chem. Technol. Biotechnol.* **2016**, *91*, 1802–1808. [CrossRef]
19. Mardanpour, M.M.; Esfahany, M.N.; Behzad, T.; Sedaqatvand, R. Single chamber microbial fuel cell with spiral anode for dairy wastewater treatment. *Biosens. Bioelectron.* **2012**, *38*, 264–269. [CrossRef]
20. Oh, S.T.; Kim, J.R.; Premier, G.C.; Lee, T.H.; Kim, C.; Sloan, W.T. Sustainable wastewater treatment: How might microbial fuel cells contribute. *Biotechnology Advances.* **2010**, *28*, 871–881. [CrossRef]
21. Yang, G.; Wang, J.; Zhang, H.; Jia, H.; Zhang, Y.; Cui, Z.; Gao, F. Maximizing energy recovery from homeostasis in microbial fuel cell by synergistic conversion of short-chain volatile fatty acid. *Bioresour. Technol. Rep.* **2019**, *7*, 100200. [CrossRef]
22. Lee, H.S.; Parameswaran, P.; Kato-Marcus, A.; Torres, C.I.; Rittmann, B.E. Evaluation of energy-conversion efficiencies in microbial fuel cells (MFCs) utilizing fermentable and non-fermentable substrates. *Water Res.* **2008**, *24*, 1501–1510. [CrossRef]
23. Ge, Z.; Ping, Q.; Xiao, L.; He, Z. Reducing effluent discharge and recovering bioenergy in an osmotic microbial fuel cell treating domestic wastewater. *Desalination.* **2013**, *312*, 52–59. [CrossRef]
24. Fornero, J.J.; Rosenbaum, M.; Angenent, L.T. Electric Power Generation from Municipal, Food, and Animal Wastewaters Using Microbial Fuel Cells. *Electroanalysis.* **2010**, *22*, 832–843. [CrossRef]
25. Zhang, L.S.; Wu, W.; Wang, J. Immobilization of activated sludge using improved polyvinyl alcohol (PVA) gel. *J. Environ. Sci.* **2007**, *19*, 1293–1297. [CrossRef]
26. Jiang, D.; Li, B. Novel electrode materials to enhance the bacterial adhesion and increase the power generation in microbial fuel cells (MFCs). *Water Sci. Technol.* **2009**, *59*, 557–563. [CrossRef] [PubMed]
27. Bai, X.; Ye, Z.F.; Li, Y.F.; Zhou, L.C.; Yang, L.Q. Preparation of crosslinked macroporous PVA foam carrier for immobilization of microorganisms. *Process Biochem.* **2010**, *45*, 60–66. [CrossRef]
28. Bruce, P.G. Structure and electrochemistry of polymer electrolytes. *Electrochim. Acta* **1995**, *40*, 2077–2086. [CrossRef]
29. Xie, J.; Duan, R.G.; Han, Y.; Kerr, J.B. Morphological, rheological and electrochemical studies of Poly(ethylene oxide) electrolytes containing fumed silica nanoparticles. *Solid State Ionics* **2004**, *175*, 755–758. [CrossRef]

30. Quaglio, M.; Chiodoni, A.; Massaglia, G.; Delmondo, L.; Sacco, A.; Garino, N.; Castellino, M.; Bianco, S.; Margaria, V.; Salvador, G.P.; et al. Electrospinning-on-Electrode Assembly for Air-Cathodes in Microbial Fuel Cells. *Adv. Mater. Interfaces* **2018**, *5*, 1801107. [CrossRef]
31. Massaglia, G.; Margaria, V.; Sacco, A.; Tommasi, T.; Pentassugli, S.; Ahmed, D.; Mo, R.; Pirri, C.F.; Quaglio, M. In situ continuous current production from marine floating microbial fuel cells. *Appl. Energy* **2018**, *230*, 78–85. [CrossRef]
32. Alvarez-Suarez, J.M.; Tulipani, S.; Romandini, S.; Bertoli, E.; Battino, M. Contribution of honey in nutrition and human health: A review. *Mediterr. J. Nutr. Metab.* **2010**, *3*, 15–23. [CrossRef]
33. Burlando, B.; Cornara, L. Honey in dermatology and skin care: A review. *J. Cosmet. Dermatol.* **2013**, *12*, 306–313. [CrossRef] [PubMed]
34. De-Melo, A.A.M.; Almeida-Muradina, L.B.; Sancho, M.T.; Pascual-Mate, A. Composition and properties of Apis mellifera honey: A review. *J. Apicult. Res.* **2018**, *57*, 5–37. [CrossRef]
35. Doner, L.W. Honey. In *Encyclopedia of Food Sciences and Nutrition*, 2nd ed.; Caballero, B., Finglas, P.M., Trugo, L.C., Eds.; Academic Press: London, UK, 2003; pp. 3125–3130.
36. Sabatini, A.G. Il miele: Origine, composizione e proprieta. In *Conscere il Miele*; Sabatini, A.G., Botolotti, L., Marcazzan, G.L., Eds.; Avenue Media: Bologna/Milano, Italy, 2007; pp. 3–37.
37. Capodaglio, A.G.; Molognoni, D.; Dallago, E.; Liberale, A.; Cella, R.; Longoni, P.; Pantaleoni, L. Microbial Fuel Cells for Direct Electrical Energy Recovery from Urban Wastewaters. *Sci. World J.* **2013**, *2013*, 634738. [CrossRef] [PubMed]
38. Massaglia, G.; Gerosa, M.; Agostino, V.; Cingolani, A.; Sacco, A.; Saracco, G.; Margaria, V.; Quaglio, M. Fluid Dynamic Modeling for Microbial Fuel Cell Based Biosensor Optimization. *Fuel Cells* **2017**, *17*, 627–634. [CrossRef]
39. Hidalgo, D.; Sacco, A.; Hernàndez, S.; Tommasi, T. Electrochemical and impedance characterization of Microbial Fuel Cells based on 2D and 3D anodic electrodes working with seawater microorganisms under continuous operation. *Bioresour. Technol.* **2015**, *195*, 139–146. [CrossRef] [PubMed]

nanomaterials

MDPI

Communication

Electrospun Cadmium Selenide Nanoparticles-Loaded Cellulose Acetate Fibers for Solar Thermal Application

Nicole Angel [1,†], S. N. Vijayaraghavan [2,†], Feng Yan [2,*] and Lingyan Kong [3,*]

[1] Department of Mechanical Engineering, The University of Alabama, Tuscaloosa, AL 35487, USA; nmangel@crimson.ua.edu
[2] Department of Metallurgical and Materials Engineering, The University of Alabama, Tuscaloosa, AL 35487, USA; vsankaranarayanannair@crimson.ua.edu
[3] Department of Human Nutrition and Hospitality Management, The University of Alabama, Tuscaloosa, AL 35487, USA
* Correspondence: fyan@eng.ua.edu (F.Y.); lkong@ches.ua.edu (L.K.)
† These authors contributed equally to this work.

Received: 28 June 2020; Accepted: 4 July 2020; Published: 8 July 2020

Abstract: Solar thermal techniques provide a promising method for the direct conversion of solar energy to thermal energy for applications, such as water desalination. To effectively realize the optimal potential of solar thermal conversion, it is desirable to construct an assembly with localized heating. Specifically, photoactive semiconducting nanoparticles, when utilized as independent light absorbers, have successfully demonstrated the ability to increase solar vapor efficiency. Additionally, bio-based fibers have shown low thermal conductive photocorrosion. In this work, cellulose acetate (CA) fibers were loaded with cadmium selenide (CdSe) nanoparticles to be employed for solar thermal conversion and then subsequently evaluated for both their resulting morphology and conversion potential and efficiency. Electrospinning was employed to fabricate the CdSe-loaded CA fibers by adjusting the CA/CdSe ratio for increased solar conversion efficiency. The microstructural and chemical composition of the CdSe-loaded CA fibers were characterized. Additionally, the optical sunlight absorption performance was evaluated, and it was demonstrated that the CdSe nanoparticles-loaded CA fibers have the potential to significantly improve solar energy absorption. The photothermal conversion under 1 sun (100 mW/cm^2) demonstrated that the CdSe nanoparticles could increase the temperature up to 43 °C. The CdSe-loaded CA fibers were shown as a feasible and promising hybrid material for achieving efficient solar thermal conversion.

Keywords: photoactive nanoparticles; cadmium selenide; cellulose acetate; electrospun fibers; solar thermal

1. Introduction

Currently, clean freshwater scarcity is a significant issue that is closely linked with social and economic development [1–3]. Already, billions of people worldwide lack access to safe drinking water, and millions die annually due to diseases relating to water-borne illnesses [2,4]. Some proposed solutions for addressing water scarcity work at the expense of aggravating present energy problems, while others suggest the implementation of large-scale infrastructure [1,4]. Therefore, developing a method to address water scarcity in a clean, affordable, and sustainable manner is of increasing importance. Solar thermal techniques provide an affordable way to convert solar energy to thermal energy; for instance, solar vapor generation for water desalination has been demonstrated as a potential technique to provide a sustainable solution to water scarcity [1,3,5,6].

One of the main drawbacks of this technique is low solar thermal conversion efficiency [1]. Both the low solar absorption of the water as well as heat loss due to the use of conventional water heating systems have significantly contributed to this low efficiency [1]. Therefore, shifting from a bulk water heating system to a nanoscaled solar absorber system with localized heating capability, specifically through the implementation of photosensitive nanoparticles (NPs), has demonstrated a noticeable increase in conversion efficiency [1,5,6]. To form a localized heating structure, it is desirable to couple high thermal conductive, photoactive NPs with a low thermal conductive polymer matrix (such as a bio-based polymer). The thermal energy generated from the photoexcited carriers in the NPs become localized heat that has difficulty diffusing into the surrounding polymer substrate; thus, the localized heating of water is enabled [7]. This advantage of localized heating can overcome the remarkable heat dissipation that occurs during bulk water heating via conventional semiconductor abosrbers. Beneficially, this process does not require the total surrounding liquid volume to reach its boiling point for successful vapor generation [6].

In this study, we investigate the implementation of electrospun cellulose acetate (CA) fibers carrying photosensitive cadmium selenide (CdSe) NPs as a nanoscaled solar conversion device for solar thermal conversion. CdSe, a Group II-VI compound semiconductor, exhibits extraordinary electronic and optoelectronic properties [8,9]. CdSe displays optimal sunlight absorption with a bandgap of 1.74 eV [10] and a high thermal conductivity (−0.53 W/cmK) [11]. Cellulose acetate is a low-cost cellulose derivative produced via the acetylation of cellulose [12,13] with low thermal conductivity (−0.10 W/cmK) [14]. It was chosen as the fiber material in this study due to its advantageous mechanical properties, excellent fiber-forming ability, biodegradability, stability in water, and cost-effectiveness [13,15]. Electrospinning has become a popular method for the synthesis of micro- and nanofibrous materials due to the use of relatively simple manufacturing equipment, low spinning cost, variety of spinnable materials, and highly controllable processes [16,17]. Moreover, micro- to nanoscale fibers display a high surface-area-to-volume ratio, good flexibility, high porosity, and superior stiffness and tensile strength than when compared to other forms of the spun material [15]. Note that, for the seawater desalination application, the heavy toxic metal element, i.e., Cd, may diffuse into the water via photocorrosion and lead to water contamination. Here, we use the CdSe as a model semiconductor with a suitable sunlight absorption band edge to explore the potential to load into CA fibers through electrospinning technique. Other low-toxic and nontoxic semiconductor particles with desired light absorption capability, such as Sb_2S_3, Fe_2O_3, and Fe_3O_4, will be explored in future studies. In particular, the diffusion behavior of the metal elements during the water desalination will also be investigated later.

2. Materials and Methods

2.1. Materials

Cellulose acetate (MW ~100,000 Da; acetyl content ~39.7 wt%) and acetone were purchased from VWR International (Radnor, PA, USA).

Based on the slow reaction between Cd^{2+} and Se^{2-} ions in an aqueous basic bath with pH > 10, the CdSe nanoparticles were synthesized using a chemical bath deposition process. Cadmium sulfate ($CdSO_4$) and sodium selenosulfite (Na_2SSeO_3) were used as the sources for Cd^{2+} and Se^{2-}, respectively. Na_2SSeO_3 was prepared by dissolving elemental Se in the form of fine powder in an aqueous solution of sodium sulfite heated to 60 °C. The solution was stirred well until the Se was completely dissolved. The pH of the solution was adjusted by adding excess NaOH. CdSe was formed in 2 h at a temperature of 70 °C. The obtained CdSe powder was washed using deionized water, centrifuged repeatedly, and subsequentially dried in a vacuum oven.

Because CdSe is considered toxic to human cells, it was handled with the utmost care during this study [18]. CdSe toxicity has been mainly attributed to the release of Cd^{2+} ions from the CdSe to surrounding cells [18]. The method of exposure by which this diffusion occurs highly alters how

significantly the affected cells react to CdSe [18]. Consequently, equipment in contact with CdSe was cleaned thoroughly, waste was properly disposed of, and the CdSe NPs were properly labeled and stored before and after use.

2.2. Methods

2.2.1. Electrospinning

In this study, the CA concentration in the spinning dope was held constant at 12% (w/v). To prepare the spinning solutions, CA and CdSe were mixed in pure acetone via magnetic stirring at room temperature (20 °C) and then ultrasonicated (VWR International, Radnor, PA, USA). The spinning dope was then loaded into a 10-mL syringe (Becton, Dickinson and Company, Franklin Lakes, NJ, USA) with a 22-gauge blunt needle (Hamilton Company, Reno, NV, USA) as the spinneret.

The electrospinning setup was comprised of a high voltage generator (ES30P, Gamma High Voltage Research, Inc., Ormond Beach, FL, USA), a syringe pump (NE-300, New Era Pump Systems, Inc., Farmingdale, NY, USA), and a grounded aluminum foil as the collector. In the present study, the optimal spinning parameters to spin CA fibers were determined from our previous study [15]. Specifically, the spinning distance was held at 8 cm, the feed rate at 3 mL/h, and the voltage at 12 kV. Electrospinning was conducted in a fume hood at 20 °C without airflow. Airflow was removed due to the high evaporation rate of acetone. Eliminating airflow helped to slow the buildup of viscous fluid at the spinneret tip that could directly cause the destabilization of the spinning jet. Periodically, fiber formation can be halted because the spinneret can become clogged and the jet will no longer be considered continuous. Consequently, despite the lack of airflow in this study, the spinneret required constant cleaning during the spinning process to successfully fabricate fibers [19]. After the spinning process, the formed fibers, which had deposited on the aluminum foil directly beneath the spinneret tip, were collected and stored away from light and moisture for further analysis.

2.2.2. Scanning Electron Microscopy (SEM)

The morphology of the electrospun fibers was studied using an Apreo field emission SEM (FE-SEM, Thermo Fisher Scientific, Waltham, MA, USA), equipped with energy-dispersive X-ray spectroscopy (EDS), at an accelerating voltage of 20 kV. Images were subsequently analyzed using ImageJ software (National Institute of Health, Bethesda, MD, USA). Three images were used for each fiber sample. Ten random segments on each image were taken and used to measure the fiber diameters. Through visual inspection, fiber morphology was evaluated as either good, fair, or poor [20]. Good fibers were defined as continuous, uniform, smooth, and defect-free. Fair fibers exhibited a fibrous shape with moderate defects. Poor fibers had significant defects, such as beads or sprayed particles. Notably, the CdSe NPs altered how smooth the fibers appeared, but were not considered to be fiber defects.

2.2.3. Wide-Angle X-ray Diffraction (XRD)

The wide-angle X-ray diffraction (XRD) patterns of the fibers were obtained using a Philips X'Pert Materials Research Diffractometer (Malvern Panalytical, Westborough, MA, USA) operated at 45 kV under 40 mA Cu Kα radiation (λ = 0.15405 nm).

2.2.4. Ultraviolet-Visible (UV-vis) Spectroscopy

The light absorbance of the fiber samples were measured using EnliTech QE measurement system (Kaohsiung City, Taiwan). The incident wavelength was swept from 300 to 1100 nm, and the absorbance of the fibers were recorded. The optical direct bandgap (Eg) of the fibers was determined by using Tauc plot relation to the plot $(\alpha h\nu)^{1/r}$ versus the energy of the photons, where α is the absorption coefficient of the materials, and r represents the nature of the transition of the charge carriers, and r = ½ for direct bandgap materials.

2.2.5. Solar Energy Conversion

Using a compact infrared (IR) camera (FLIR C2, FLIR Systems, Inc., Wilsonville, OR, USA), the fibers were tested for solar vapor generation under 1 sun (100 mW/cm^2) illumination. The thermal images were recorded after the nanofibers were exposed to the simulated sunlight for 30 min to stabilize in the air between heating and cooling.

3. Results and Discussion

3.1. Electrospinnability and Fiber Morphology

The CA fibers were fabricated by electrospinning, a simple, scalable, and versatile technique for nanofiber production [21]. Given the potential applications of this study, the ability for our resulting solar vapor generator to be mass scaled is of utmost importance. The basic lab-scale electrospinning setup only requires a high voltage source, a syringe with a blunt needle tip (i.e. the spinneret), and a grounded collector [15,21]. High voltage is applied to the spinneret where the spinning dope is pumped via a syringe pump at a constant rate. Once the applied voltage reaches the critical point, a Taylor cone will form at the spinneret tip. A continuous jet flows from the Taylor cone to the grounded collector. During this process, the electric field causes the jet to stretch and elongate as the solvent evaporates. Fibers form on the grounded collector, e.g. the aluminum foil, as used in this study [15].

The CA fibers were loaded with varying CdSe concentrations (CdSe:CA ratio of 1:4 and 1:1, w/w) to analyze the successful uptake of CdSe into the CA fibers and to observe the resulting photosensitive properties of the fibers as provided by the CdSe NPs. The overall electrospinnability of the CdSe-CA compositions was analyzed through both visual inspection during spinning and the obtained fiber images (Figure 1). All three CdSe-CA dispersions were able to successfully produce fibers in a relatively short amount of time. The time needed for the collector to become completely covered in fibers was about the same for all three runs, suggesting that CdSe did not have a drastic effect on the electrospinnability of CA in the single solvent acetone. The overall quality of the electrospun fibers was also independent of the addition of CdSe. As seen in Figure 1, the CdSe-CA fibers remain continuous and smooth, discounting the CdSe NPs, and display approximately the same amount of beading as the pure CA fibers. These fibers were thus rated as good fibers, albeit their size was on the microscale rather than the nanoscale.

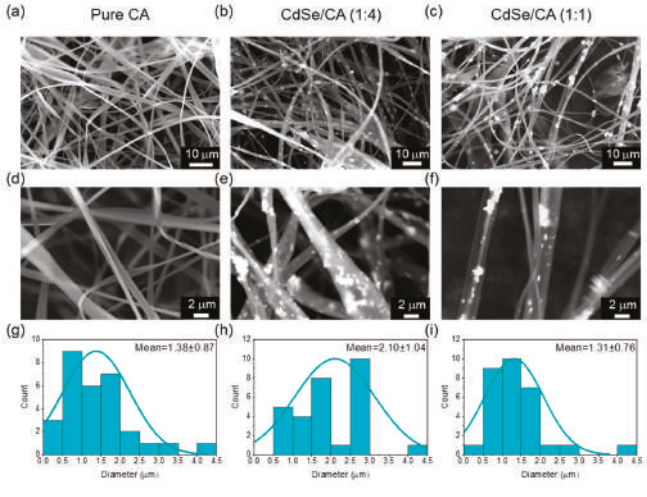

Figure 1. (**a**–**f**) Field emission scanning electron micrographs (FE-SEM) images and (**g**–**i**) fiber diameter distributions of CA, CdSe-CA (1:4), and CdSe-CA (1:1) fibers, respectively.

3.2. CdSe Incorporation

As shown in Figure 2, CdSe was successfully incorporated into the CA fibers. The white particles embedded in the fibers were confirmed to be comprised of elements Cd and Se, respectively (Figure 2c–f). As expected, CdSe-CA (1:1) fibers demonstrated a higher quantity of successful CdSe incorporation as compared with CdSe-CA (1:4) fibers. However, in both the (1:1) and (1:4) fibers, the CdSe particles were segregated in clusters rather than being evenly dispersed. This could be a result of the difficulty in achieving a homogeneous distribution and stable suspension of CdSe in the spinning dope. Additionally, during electrospinning, the CdSe particles may be charged and easily segregated together.

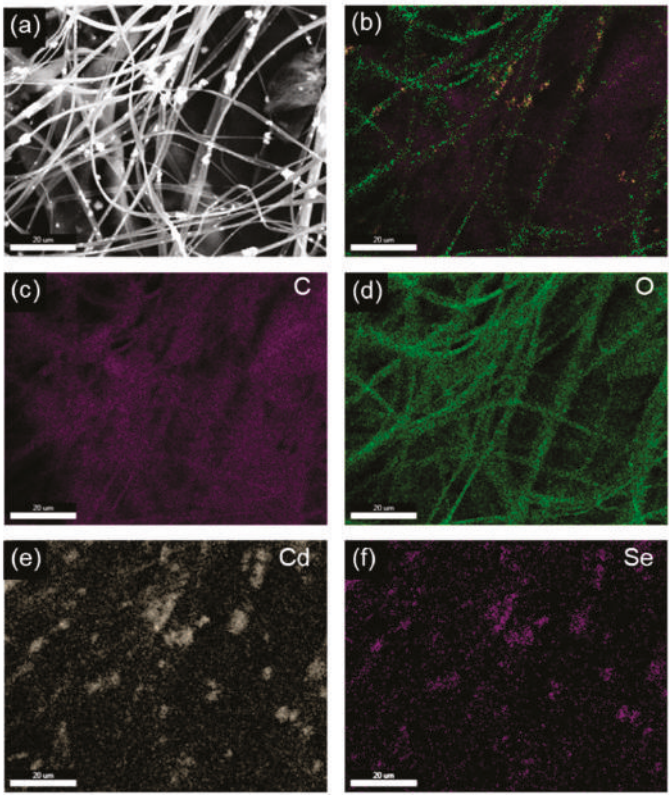

Figure 2. (**a**) FESEM, (**b**) overall elemental distribution, and (**c**–**f**) C, O, Cd, and Se elemental distribution of CdSe-CA (1:1) fibers obtained using energy dispersive X-ray spectrometry (EDS) mapping.

The structure of the CdSe loaded CA fibers was characterized using X-ray diffraction (XRD), as shown in Figure 3. The XRD peaks of CdSe at 2θ = 25.3°, 42°, and 50° were observed in the CdSe-loaded fibers, whereas these peaks did not exist in the pattern of the pure CA fibers. The (002), (110), and (201) peaks of CdSe, corresponding to 2θ ~ 25°, 41°, and 50°, respectively, can be indexed to the wurtzite phase. Similar to most other biopolymers, CA is semi-crystalline yet largely amorphous. The diffraction peaks around 10° and 20°, corresponding to the (101) and (020) planes, respectively, confirm the semi-crystalline nature of CA [22]. When the CdSe/CA ratio increased, the intensity of the CdSe peaks increased.

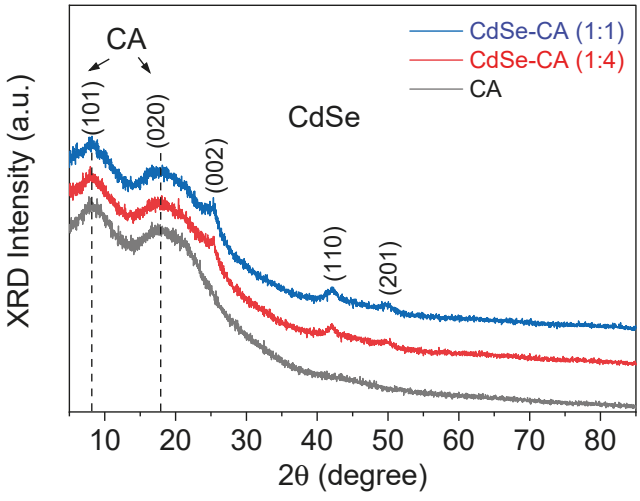

Figure 3. X-ray diffraction patterns of CA, CdSe-CA (1:4), and CdSe-CA (1:1) fibers.

3.3. Optical Properties

As shown in Figure 4a, the absorbance of the CA fibers increased as the CdSe content increased, with the light absorption edge around 700 nm for the CdSe-loaded CA fibers. These fibers have superior sunlight absorption than pure CA fibers which indicates increased solar thermal conversion [23]. From the extrapolation of the Tauc plot, as shown in Figure 4b, CA was determined to have a wide bandgap of ~3.4 eV which corresponds to the ultraviolet light range in the solar spectrum. When CdSe was introduced into CA fibers with varying concentrations, the CdSe-CA (1:4) fibers were found to have a bandgap of ~1.7 eV. When more CdSe was incorporated into CA in the CdSe-CA (1:1) fibers, the bandgap remained constant. Note that pure CdSe is estimated to have a bandgap of 1.74 eV according to previous works [10]. The fact that the bandwidth of the CdSe-loaded fibers is close to that of pure CdSe demonstrates that loading CdSe into CA fibers can significantly increase the sunlight absorption of CA fibers. Therefore, CA fibers show great potential in their ability to act as a supporting matrix for CdSe NPs-based solar thermal conversion for improved localized heating.

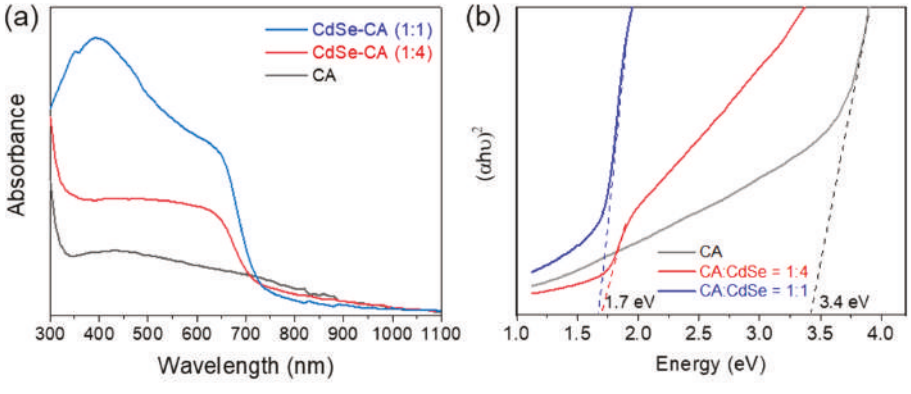

Figure 4. (**a**) UV-vis absorbance spectra (normalized at 1100 nm) and (**b**) Tauc plot of CA, CdSe-CA (1:4), and CdSe-CA (1:1) fibers.

3.4. Photothermal Conversion

To investigate the solar thermal properties of the CA and CA-CdSe fibers, both optical and IR thermal images were captured (Figure 5). As seen in the optical image, the CdSe-CA (1:4) fibers were dark due to the light absorption by CdSe, while the pure CA fibers were white, which is in agreement with the UV-Vis absorbance test above. The maximum temperature in the CdSe-CA (1:4) fibers can be over 40 °C under the 1 sun (100 mW/cm^2) illumination, while the pure CA fibers maintained a low temperature without photothermal conversion. This solar thermal conversion performance is similar to the carbonaceous membrane assisted by localized heating design [24]. It is suggested that the CA-CdSe fibers could effectively absorb sunlight and convert it into thermal energy.

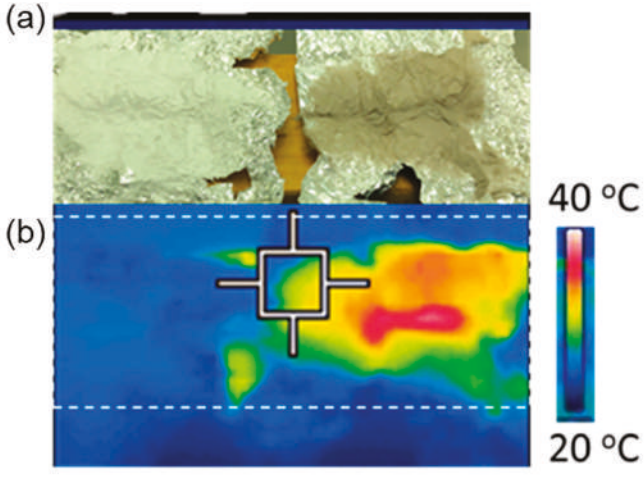

Figure 5. (**a**) Optical picture and (**b**) infrared thermal image of the CA and CA-CdSe fiber mats.

4. Conclusions

In conclusion, the loading of highly thermal conductive CdSe NPs into CA fibers of low thermal conductivity was successfully demonstrated in this study. Overall, fiber morphology, including quality and diameter, was relatively independent of the addition of CdSe. The solar energy absorption of CdSe NPs were virtually unaffected while in the fibers. Specifically, the bandwidth of CdSe NPs remained the same while in the CA fibers, and the final assemblies were highly absorbent in the visible light spectrum. It was demonstrated that electrospinning can effectively introduce photosensitive NPs into the bio-based CA fibers. This low-cost and scalable technique can be used to facilitate water desalination through solar thermal evaporation with localized heating that has the potential to help address the current concerns regarding water scarcity encountered across the globe.

Author Contributions: Conceptualization, F.Y. and L.K.; methodology, N.A., and S.N.V.; writing—original draft preparation, N.A., and S.N.V.; writing—review and editing, F.Y. and L.K.; project administration, F.Y. and L.K.; funding acquisition, F.Y. and L.K. All authors have read and agreed to the published version of the manuscript.

Funding: This research was funded by the USDA National Institute of Food and Agriculture (NIFA), AFRI project award # 2020-67022-31376, and the NSF Award #1944374.

Acknowledgments: The Alabama Water Institute and the College of Human Environmental Sciences at the University of Alabama are acknowledged for their support.

Conflicts of Interest: The authors declare no conflict of interest.

References

1. Gao, M.; Zhu, L.; Peh, C.K.; Ho, G.W. Solar absorber material and system designs for photothermal water vaporization towards clean water and energy production. *Energy Environ. Sci.* **2019**, *12*, 841–864. [CrossRef]
2. Shannon, M.A.; Bohn, P.W.; Elimelech, M.; Georgiadis, J.G.; Marinas, B.J.; Mayes, A.M. Science and technology for water purification in the coming decades. In *Nanoscience and Technology: A Collection of Reviews from Nature Journals*; World Scientific: Singapore, 2010; pp. 337–346.
3. Liu, C.; Huang, J.; Hsiung, C.E.; Tian, Y.; Wang, J.; Han, Y.; Fratalocchi, A. High-performance large-scale solar steam generation with nanolayers of reusable biomimetic nanoparticles. *Adv. Sustain. Syst.* **2017**, *1*, 1600013. [CrossRef]
4. Rijsberman, F.R. Water scarcity: Fact or fiction? *Agric. Water Manag.* **2006**, *80*, 5–22. [CrossRef]
5. Zhao, F.; Zhou, X.; Shi, Y.; Qian, X.; Alexander, M.; Zhao, X.; Mendez, S.; Yang, R.; Qu, L.; Yu, G. Highly efficient solar vapour generation via hierarchically nanostructured gels. *Nat. Nanotechnol.* **2018**, *13*, 489–495. [CrossRef]
6. Neumann, O.; Urban, A.S.; Day, J.; Lal, S.; Nordlander, P.; Halas, N.J. Solar vapor generation enabled by nanoparticles. *Acs Nano* **2013**, *7*, 42–49. [CrossRef] [PubMed]
7. Govorov, A.O.; Richardson, H.H. Generating heat with metal nanoparticles. *Nano Today* **2007**, *2*, 30–38. [CrossRef]
8. Jin, W.; Hu, L. Review on quasi one-dimensional cdse nanomaterials: Synthesis and application in photodetectors. *Nanomaterials* **2019**, *9*, 1359. [CrossRef] [PubMed]
9. Li, P.; Zhu, B.; Li, P.; Zhang, Z.; Li, L.; Gu, Y. A facile method to synthesize cdse-reduced graphene oxide composite with good dispersion and high nonlinear optical properties. *Nanomaterials* **2019**, *9*, 957. [CrossRef]
10. Mahato, S.; Kar, A.K. The effect of annealing on structural, optical and photosensitive properties of electrodeposited cadmium selenide thin films. *J. Sci. Adv. Mater. Devices* **2017**, *2*, 165–171. [CrossRef]
11. Ma, Y.; Liu, M.; Jaber, A.; Wang, R.Y. Solution-phase synthesis and thermal conductivity of nanostructured cdse, in 2 se 3, and composites thereof. *J. Mater. Chem. A* **2015**, *3*, 13483–13491. [CrossRef]
12. Fischer, S.; Thümmler, K.; Volkert, B.; Hettrich, K.; Schmidt, I.; Fischer, K. *Macromolecular Symposia: In Properties and Applications of Cellulose Acetate*; Wiley Online Library: Hoboken, NJ, USA, 2008; pp. 89–96.
13. Nosar, M.N.; Salehi, M.; Ghorbani, S.; Beiranvand, S.P.; Goodarzi, A.; Azami, M. Characterization of wet-electrospun cellulose acetate based 3-dimensional scaffolds for skin tissue engineering applications: Influence of cellulose acetate concentration. *Cellulose* **2016**, *23*, 3239–3248. [CrossRef]
14. Gutiérrez, M.C.; De Paoli, M.-A.; Felisberti, M.I. Cellulose acetate and short curauá fibers biocomposites prepared by large scale processing: Reinforcing and thermal insulating properties. *Ind. Crop. Prod.* **2014**, *52*, 363–372. [CrossRef]
15. Angel, N.; Guo, L.; Yan, F.; Wang, H.; Kong, L. Effect of processing parameters on the electrospinning of cellulose acetate studied by response surface methodology. *J. Agric. Food Res.* **2020**, *2*, 100015. [CrossRef]
16. Yu, J.; Zhao, Z.; Sun, J.; Geng, C.; Bu, Q.; Wu, D.; Xia, Y. Electrospinning highly concentrated sodium alginate nanofibres without surfactants by adding fluorescent carbon dots. *Nanomaterials* **2020**, *10*, 565. [CrossRef]
17. Odhiambo, V.O.; Ongarbayeva, A.; Kéri, O.; Simon, L.; Szilágyi, I.M. Synthesis of tio2/wo3 composite nanofibers by a water-based electrospinning process and their application in photocatalysis. *Nanomaterials* **2020**, *10*, 882. [CrossRef]
18. Wang, L.; Nagesha, D.K.; Selvarasah, S.; Dokmeci, M.R.; Carrier, R.L. Toxicity of cdse nanoparticles in caco-2 cell cultures. *J. Nanobiotechnol.* **2008**, *6*, 1–15. [CrossRef] [PubMed]
19. Rodríguez, K.; Gatenholm, P.; Renneckar, S. Electrospinning cellulosic nanofibers for biomedical applications: Structure and in vitro biocompatibility. *Cellulose* **2012**, *19*, 1583–1598. [CrossRef]
20. Wang, H.; Kong, L.; Ziegler, G.R. Fabrication of starch-nanocellulose composite fibers by electrospinning. *Food Hydrocoll.* **2019**, *90*, 90–98. [CrossRef]
21. Teo, W.E.; Ramakrishna, S. A review on electrospinning design and nanofibre assemblies. *Nanotechnology* **2006**, *17*, R89. [CrossRef] [PubMed]
22. Sanjay, P.; Deepa, K.; Madhavan, J.; Senthil, S. Synthesis and spectroscopic characterization of cdse nanoparticles for photovoltaic applications. *MsE* **2018**, *360*, 012010. [CrossRef]

23. López-Herraiz, M.; Fernández, A.B.; Martinez, N.; Gallas, M. Effect of the optical properties of the coating of a concentrated solar power central receiver on its thermal efficiency. *Sol. Energy Mater. Sol. Cells* **2017**, *159*, 66–72. [CrossRef]
24. Wu, D.; Liang, J.; Zhang, D.; Zhang, C.; Zhu, H. Solar evaporation and electricity generation of porous carbonaceous membrane prepared by electrospinning and carbonization. *Sol. Energy Mater. Sol. Cells* **2020**, *215*, 110591. [CrossRef]

nanomaterials

MDPI

Communication

Physico-Chemically Distinct Nanomaterials Synthesized from Derivates of a Poly(Anhydride) Diversify the Spectrum of Loadable Antibiotics

Amalia Mira [1], Carlos Sainz-Urruela [1], Helena Codina [1], Stuart I. Jenkins [2], Juan Carlos Rodriguez-Diaz [3], Ricardo Mallavia [1,*] and Alberto Falco [1,*]

[1] Institute of Research, Development and Innovation in Biotechnology of Elche (IDiBE), Miguel Hernández University (UMH), 03202 Elche, Alicante, Spain; a.mira@umh.es (A.M.); carlos.sainz@goumh.umh.es (C.S.-U.); helena.codina@goumh.umh.es (H.C.)

[2] Neural Tissue Engineering group: Keele (NTEK), School of Medicine, Keele University, Keele ST5 5BG, Staffordshire, UK; s.i.jenkins@keele.ac.uk

[3] Microbiology Section, University General Hospital of Alicante, Alicante Institute for Health and Biomedical Research (ISABIAL-FISABIO Foundation), Alicante 03010, Spain; rodriguez_juadia@gva.es

* Correspondence: r.mallavia@umh.es (R.M.); alber.falco@umh.es (A.F.)

Received: 17 February 2020; Accepted: 6 March 2020; Published: 8 March 2020

Abstract: Recent advances in the field of nanotechnology such as nanoencapsulation offer new biomedical applications, potentially increasing the scope and efficacy of therapeutic drug delivery. In addition, the discovery and development of novel biocompatible polymers increases the versatility of these encapsulating nanostructures, enabling chemical properties of the cargo and vehicle to be adapted to specific physiological requirements. Here, we evaluate the capacity of various polymeric nanostructures to encapsulate various antibiotics of different classes, with differing chemical structure. Polymers were sourced from two separate derivatives of poly(methyl vinyl ether-*alt*-maleic anhydride) (PMVE/MA): an acid (PMVE/MA-Ac) and a monoethyl ester (PMVE/MA-Es). Nanoencapsulation of antibiotics was attempted through electrospinning, and nanoparticle synthesis through solvent displacement, for both polymers. Solvent incompatibilities prevented the nanoencapsulation of amikacin, neomycin and ciprofloxacin in PMVE/MA-Es nanofibers. However, all compounds were successfully loaded into PMVE/MA-Es nanoparticles. Encapsulation efficiencies in nanofibers reached approximately 100% in all compatible systems; however, efficiencies varied substantially in nanoparticles systems, depending on the tested compound (14%–69%). Finally, it was confirmed that both these encapsulation processes did not alter the antimicrobial activity of any tested antibiotic against *Staphylococcus aureus* and *Escherichia coli*, supporting the viability of these approaches for nanoscale delivery of antibiotics.

Keywords: biomaterials; polymers; PMVE/MA; electrospinning; nanofibers; nanoparticles; nanoencapsulation; antibiotics

1. Introduction

So far, antibiotics are the most reliable weapon against infectious diseases of bacterial origin. However, the dramatic diminishment in the rate of discovery of new antibiotics limits our response to pathogens resistant to conventional antibiotics and to new emerging diseases. In response, the scientific community is developing alternative strategies to increase the effectiveness, and/or to overcome the limitations, of existing antibiotics [1,2]. In this context, recent advances in the field of nanotechnology offer new tools such as nanoencapsulation: the loading of pharmaceutical agents within nanomaterials [3,4].

From a commercial and clinical point of view, nanoencapsulation can protect pharmaceutical products, extending both shelf-life and biological half-life (e.g., in circulation). In addition, with the corresponding modifications, these nanostructured systems can facilitate targeted drug delivery and/or specific controlled-release kinetics, thereby increasing the effectiveness of the treatment and, thus, reducing necessary dosage and side effects [3,4].

In line with this, the continuing development of novel biocompatible polymers contributes to the potential versatility of these nanostructures, by enabling the delivery of compounds with solubility limitations. In addition, manipulation of synthesis or layering protocols can generate nanostructures with properties tailored to highly specific applications, for example injectable nanoparticles, or nanofibers for wound dressings [5–8].

Examples of such highly versatile materials include derivates of poly(methyl vinyl ether-*alt*-maleic anhydride) (PMVE/MA), an alternating copolymer of methyl-ether-vinyl and maleic anhydride. This material is marketed by Ashland Inc. as Gantrez® and presents suitable properties for biomedical applications (low toxicity, high biocompatibility, high mucoadhesivity and low cost). In particular, it is reported that PMVE/MA can be structured as loadable nanoparticles [9] and its derivates poly(methyl vinyl ether-alt-maleic acid) (PMVE/MA-Ac) and poly(methyl vinyl ether-alt-maleic monoethyl ester) (PMVE/MA-Es) as nanofibers [10,11]. In addition, these polymers have shown utility as matrix elements, allowing the combination with other materials to generate novel mixtures of chemical properties in the final nanostructures [11–13], such as with homemade fluorescent cationic fluorene-based polyelectrolytes [11,14–16].

In this work, both nanoparticles and nanofibers were synthesized using these polymers, and their relative capacities for encapsulation were compared. There are several possible procedures for the synthesis of each of these nanomaterials. For instance, solvent displacement, emulsion solvent diffusion, interfacial deposition and nanoprecipitation synthesis for nanoparticles [17] and electrospinning, self-assembly, phase separation and template synthesis for nanofibers [18]. The two nanostructuring methodologies utilized here (solvent displacement and electrospinning, for particle and fiber synthesis, respectively), although differing markedly in terms of the processes involved, were selected because of the high degree of uniformity in their products, as well as being scalable processes for industrial production. The range of compounds tested as cargo encompassed four antibiotics of three different classes, differing in their molecular weights, structures and modes of action, i.e., two aminoglycosides (amikacin and neomycin), a cephalosporin (cefotaxime) and a quinolone (ciprofloxacin). Finally, the antimicrobial activity of the encapsulated compounds, as well as their structural stability, were also assessed, to confirm that nanoencapsulation was not an impairment to their antimicrobial potency.

2. Materials and Methods

2.1. Materials

The polymers PMVE/MA-Es (CAS number: 25087-06-3; MW: 130 kg/mol), provided as 50% *w*/*w* solution in ethanol, and PMVE/MA-Ac (CAS number: 25153-40-6; MW: 216 kg/mol), in powder format, were purchased from Sigma-Aldrich (St. Louis, MO, USA). Amikacin (Mw: 585.6 g/mol; 250 mg/mL) and cefotaxime (MW: 455.5 g/mol; powder) were acquired from Laboratorios Normon (Tres Cantos, Spain). Neomycin (MW: 614.6 g/mol; 10 mg/mL) was obtained from Sigma-Aldrich and ciprofloxacin (MW: 331.3 g/mol; 2 mg/mL) from Genéricos Españoles laboratorios S.A. (Las Rozas, Spain). The chemical structure inputs of all these compounds are shown in Figure 1.

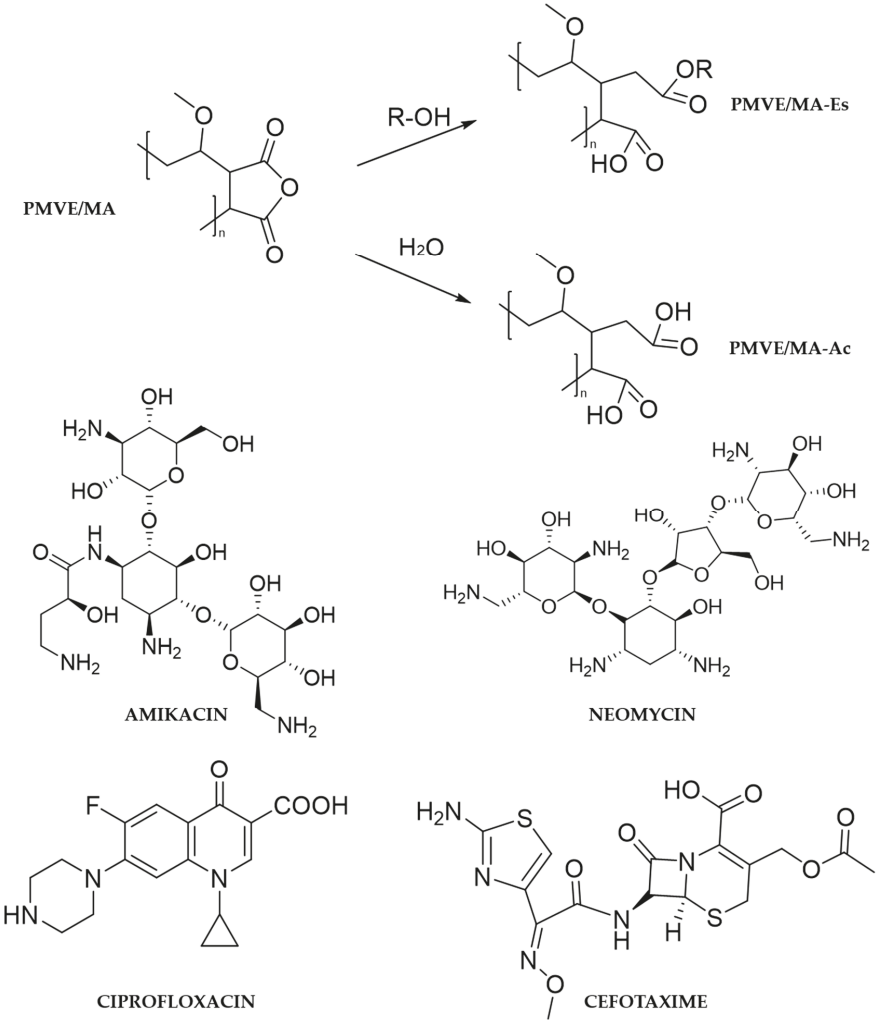

Figure 1. Structures of the principal compounds used. All structures were drawn using ChemBioDraw Ultra v14.0 (CambridgeSoft, Cambridge, MA, USA).

Phosphate buffered saline (PBS; pH 7.4), Mueller-Hinton broth (MHB; powder format), methanol, acetone, phosphoric acid and trifluoroacetic acid with HPLC grade purity, and dimethylsulfoxide (DMSO) and ethanol with purity >95%, were all from Sigma-Aldrich. The water used was double distilled and deionized (DDW) from a Milli-Q Synthesis A10 system (Millipore, Madrid, Spain).

2.2. Preparation of Nanofibers by Electrospinning

From our previous studies, either 20% *w*/*w* PMVE/MA-Ac in H_2O or 25% *w*/*w* PMVE/MA-Es in ethanol were selected as optimal polymeric solutions for the creation of electrospun nanofibers [10,11]. Antibiotics were added to the polymeric solutions to reach a final concentration of 1% *w*/*w* with respect to both PMVE/MA-Ac and PMVE/MA-Es. All solutions were stirred for 1 h and then bath-sonicated for 10 min prior to electrospinning.

As for the electrospinning system, the polymer solutions inside a 2-mL Discardit II syringe (Becton Dickinson, Franklin Lakes, NJ, USA) were pumped through a 20-Gauge blunt-end stainless steel hypodermic needle 316 (Sigma-Aldrich) at a constant flow rate by using a KDS 100 infusion pump (KD Scientific, Holliston, MA, USA). A Series FC high voltage supplier (Glassman High Voltage Inc., Whitehouse Station, NJ, USA) was responsible for the generation of the electrostatic field, which focused the jet onto a collector, made of aluminum foil and located in front of the syringe tip (vertical orientation). Any surface intended to be covered with a mat of electrospun nanofibers would be placed on the collector, for instance common glass slides for fluorescence/optical microscopy analysis or copper grids (diameter 3 mm) for transmission electron microscopy (TEM; Electron Microscopy Sciences, Hatfield, PA, USA). Operational parameters: 15 kV, flow rate 0.5 mL/h, needle-collector distance 15 cm, room temperature (RT) and relative humidity 40%–60%. Finally, in order to evaporate solvent excess, the obtained mats were kept in a fume hood overnight. Synthesized nanofibers were then stored protected from light at RT and dry atmosphere until used.

2.3. Preparation of Nanoparticles by Solvent Displacement

The PMVE/MA-Es nanoparticles were created using the solvent displacement procedure previously described by Arbós et al. (2002) [19] with some modifications. Briefly, different amounts of PMVE/MA-Es (12.5–200 mg) were dissolved in up to 5 g of ethanol by means of magnetic agitation for 10 min at RT. Subsequently, 2 μg of antibiotic in DDW were added (control nanoparticles were prepared only with DDW). After 10 min further magnetic stirring, gradual addition of DDW brought the final volume to 15 g. Then, the ethanol was evaporated under reduced pressure (BUCHI Rotavapor R-230, Flawil, Switzerland). Finally, obtained nanoparticles were purified twice by centrifugation (Sigma 3K30, Sigma Instruments, Osterode, Germany) at 20,000 g for 20 min at 4 °C. The pellet was then resuspended in up to 10 g of DDW and thus the final concentrations were 0.125%–2% *w*/*w* (or 1.25–20 mg/g) of PMVE/MA-Es and 200 ng/g of antibiotic. The supernatants were further centrifuged at 30,000 g for 30 min at 4 °C and collected again to quantify the amount of unloaded antibiotics. The purified nanoparticles and supernatants from all batches were stored at −20 °C until use.

2.4. Average Size and Zeta Potential Determination of Nanoparticles

Photon correlation spectroscopy (PCS), also known as dynamic light scattering (DLS), was used to determine the average hydrodynamic diameter (HDD) and polydispersity index (PDI) of each batch of nanoparticles (90 Plus Nanoparticle Size Analyzer; 35 mV red diode laser source, λ = 640 nm; Brookhaven Instruments Corporations, Holtsville, NY, USA). Each suspension sample was diluted with DDW to yield an appropriate scattering intensity of 100–400 kcps. All measurements were performed three times at 25 °C with angle detection fixed at 90° on 2 mL samples.

The zeta potential (ZP) of the synthesized nanoparticles was determined by electrophoretic laser Doppler anemometry with the 90 Plus Particle Size Analyzer (Brookhaven Instruments Corporation). Suspension samples were prepared as described before and analyzed in triplicate. All results are shown as the mean and standard deviation (s.d.) of the values obtained from three different batches.

2.5. Microscopy

For optical microscopy initial screenings, the nanofibers were electrospun on microscope slides (Deltalab, Barcelona, Spain) and observed by means of a Mycrosystems DMI3000B inverted fluorescence microscope equipped with an EL6000 compact light source and a DFC 3000G digital camera, all from Leica (Bensheim, Germany). All images were taken with a 63× objective in phase contrast and image processing performed manually using the software Leica Application SuiteAF6000 Module Systems.

Detailed observations of selected nanofiber samples were carried out by scanning electron microscopy (SEM), without metal coating, in a JSM-6360 LV device (Jeol, Tokyo, Japan). For size analysis, diameter measurements were performed on 100 nanofibers (minimum three micrographs)

per nanofiber synthesis condition using ImageJ software (National Institutes of Health, NIH, Bethesda, MD, USA).

Transmission electron microscopy (TEM) was used to confirm the size and describe the morphology of the synthesized nanoparticles (Jeol 1011 apparatus, at 120 kV). Samples were placed onto Formvar/carbon 300-Mesh, copper grids (Electron Microscopy Science, Hatfield, PA, USA) and then incubated with citrate lead solution (0.03% p/v) to generate contrast in images. Diameter measurements were performed on 50 nanoparticles (minimum three micrographs) per nanoparticle synthesis condition using ImageJ software (National Institutes of Health).

2.6. HPLC Analysis

The quantitation of antibiotics was performed by HPLC in order to determine their encapsulation efficiency (EE, percentage of encapsulated compound relative to the theoretically maximum one) in both nanostructures. For nanoparticles, non-loaded compound, i.e., free in supernatants obtained during synthesis prior to purification, was quantitated then subtracted from the total added antibiotics to determine the amount of loaded compound. Nanoparticle supernatants or 0.1% *w*/*w* nanofiber solutions in DDW were filtered through a 0.4 μm PTFE membrane (Chmlab group, Barcelona, Spain) prior to volume injections (10 μL for amikacin and neomycin, 20 μL for ciprofloxacin and 5 μL for cefotaxime).

A Merck-Hitachi D-7000 HPLC system (Hitachi Instruments, Tokyo, Japan) equipped with an Alltech 3300 evaporative light scattering detector (ELSD; Alltech Associates Inc., Lokeren, Belgium) was used to analyze amikacin and neomycin. Cefotaxime and ciprofloxacin were analyzed by means of an Agilent LC 214 1100 series HPLC system controlled by ChemStation software and equipped with a G1311A quaternary pump, a G1329A ALS automated sample injector, a G1316A thermostat column compartment and a G1316A diode array detector (Agilent Technologies, Inc., Palo Alto, CA, USA).

All methods used were isocratic and their particularities for each antibiotic were as follows. For amikacin and neomycin, the mobile phase was acetone:DDW with 0.15% *v*/*v* TFA at a 1:1 ratio, a flow rate at 1.0 mL/min. ELSD conditions were nitrogen pressure at 3.5 bar and temperature at 45 °C. For cefotaxime, the mobile phase was methanol:DDW at 30:70 *v*/*v* (adjusted to pH 4 with acetic acid), a flow rate at 0.8 mL/min and detection at 235 nm. For ciprofloxacin, the mobile phase was 0.25 M phosphoric acid:acetonitrile at 75:25 *v*/*v*, a flow rate at 0.8 mL/min and detection at 280 nm. Standard curves for each antibiotic were generated using the same concentration range (6.25–300 μg/mL). Within this range, a linear correlation was found between concentration and detected peak area with regression coefficient values (R^2) greater than 0.99 (Figure S1).

2.7. Antibacterial Assays

The antimicrobial activity of the experimental formulations was tested on antibiotic-sensitive strains of Gram-positive *Staphylococcus aureus* (CECT 59) and Gram-negative *Escherichia coli* (CECT 515) obtained from the Spanish Type Culture Collection (Colección Española de Cultivos Tipo, CECT, Universitat de Valencia, Spain). Prior to each assay, a colony of bacteria previously grown in MHB-agar plates was isolated and incubated in MHB for 12 h at 37 °C to prepare bacteria inocula.

Minimal inhibitory concentration (MIC) was determined by the two-fold broth microdilution method according to the Clinical and Laboratory Standards Institute (CLSI) guidelines [20], with some modifications. Briefly, two-fold dilutions in MHB of the experimental formulations and the control antibiotics at twice the final concentration were prepared and 50 μL/well were dispensed in each column (1 column per concentration) of round-bottom 96-well polystyrene plates (Deltalab S.L., Rubí, Spain). Then, bacteria suspension, after adjustment to 0.5 McFarland and then further diluted by 1:100 in MHB, was added to all wells (50 μL/well), except for sterile controls. Plates were then incubated for 24 h at 37 °C and finally MIC was defined as the lowest concentration of antibiotic that visibly inhibited the growth of the bacterium being investigated. All assays were performed in triplicate and results are shown as the mean and s.d.

2.8. Data Analysis and Graphics

Data were analyzed and graphs produced using GraphPad Prism v6 and Microsoft Excel software. Statistical analysis was performed with GraphPad Prism v6.

3. Results

3.1. Electrospinnability of Formulations and Characterization of Obtained Nanofibers

In our previous works [10,11], the optimal conditions for the electrospinning of the polymer solutions for both of these PMVE/MA derivates were determined, and hence taken as starting points for the present study (briefly, 15 kV, flow rate of 0.5 mL/h, needle-collector distance of 15 cm and polymer concentrations of 20% *w/w* PMVE/MA-Ac in H_2O or 25% *w/w* PMVE/MA-Es in ethanol). In this study, such conditions proved suitable for generating morphologically uniform nanofibers when initial polymeric solutions were homogenous. However, amikacin, neomycin and ciprofloxacin were found to be insoluble in ethanol, and therefore insoluble in PMVE/MA-Es solutions. Therefore, nanofibers were obtained from PMVE/MA-Ac solutions in combination with all antibiotics, but PMVE/MA-Es solution was only used with cefotaxime.

From both optical microscopy (data not shown) and SEM images (Figure 2), the morphology of all nanofibers was observed to be uniform (no shape anomalies), continuous (appropriate length, no breaks) and with a smooth surface appearance (no visible pores).

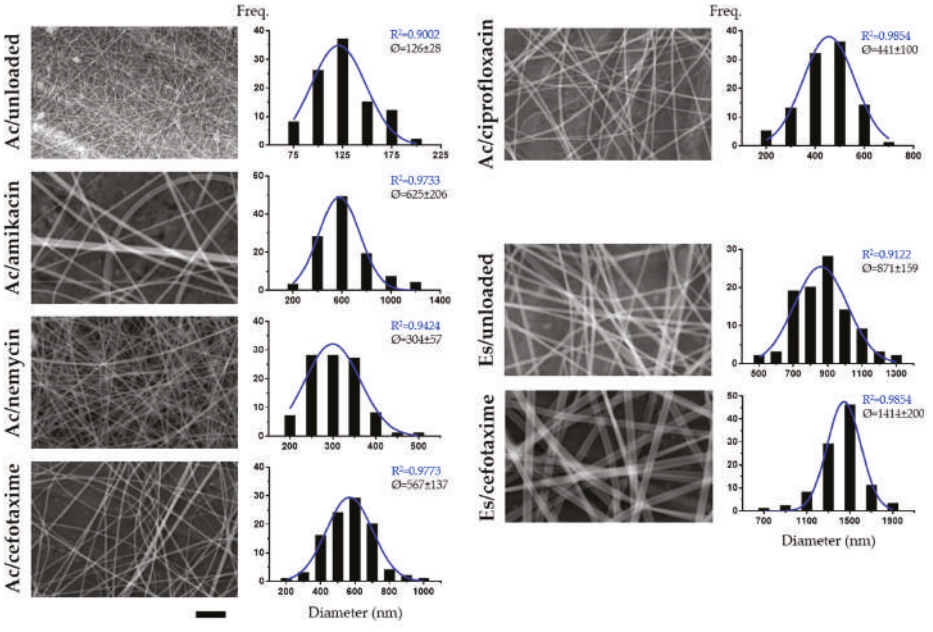

Figure 2. SEM analysis of antibiotic-loaded electrospun nanofibers. Representative SEM micrographs and corresponding diameter frequency histograms for PMVE/MA-Ac, PMVE/MA-Ac/amikacin, PMVE/MA-Ac/neomycin, PMVE/MA-Ac/cefotaxime, PMVE/MA-Ac/ciprofloxacin, PMVE/MA-Es and PMVE/MA-Es/cefotaxime. Histogram data were obtained from multiple micrographs (100 individual measurements). Best-fit adjustments (and their R^2) to a Gaussian distribution are indicated in blue. Average diameter (Ø) ± s.d. is also stated. Scale bar: 5 μm.

As SEM offers higher resolution and contrast imaging, as well as broader depth of field, these images were used for size analysis (Figure 2). All nanofiber types showed average diameter values < 1000 nm,

except PMVE/MA-Es/cefotaxime (1414 ± 200 nm). PMVE/MA-Ac nanofibers with no encapsulated compound were the narrowest in diameter (126 ± 28 nm), which contrasts starkly with non-loaded PMVE/MA-Es fibers (871 ± 159 nm). The encapsulation of compounds increased the diameter of both PMVE/MA-Es and PMVE/MA-Ac nanofibers by a minimum of 1.6-fold (PMVE/MA-Es/cefotaxime) and a maximum of 5.0-fold (PMVE/MA-Ac/amikacin). Among PMVE/MA-Ac nanofibers, the smallest diameter increase was found when loading neomycin (2.4-fold), then ciprofloxacin (3.5-fold), with cefotaxime increasing the most (4.5-fold). In terms of size variability, PMVE/MA-Ac/amikacin, PMVE/MA-Ac/cefotaxime, PMVE/MA-Ac/ciprofloxacin and PMVE/MA-Es/cefotaxime nanofibers most closely fitted a Gaussian distribution ($R^2 > 0.95$), although all formulations showed R^2 values higher than 0.9. Of note, EEs reached maximum levels (≥97%) with relatively low s.d. (±2%) in all cases.

3.2. Optimization of the Preparation of PMVE/MA-Es Nanoparticles and Their Characterization

The low solubility in ethanol of most of the antibiotics tested, and the low solubility in DDW of PMVE/MA-Es, severely limited their compatibility for encapsulation in electrospun PMVE/MA-Es nanofibers. In contrast, encapsulation of these antibiotics in PMVE/MA-Es nanoparticles would appear feasible, since their preparation by the solvent displacement method requires, initially, both much lower polymer and ethanol concentrations (32.33% *w*/*w*). This method continues with the selective evaporation of ethanol to reach final nanoparticle suspensions in just DDW.

Preliminarily, the process of preparation of PMVE/MA-Es nanoparticles was optimized. For this purpose, several concentrations of PMVE/MA-Es were tested, ranging from 0.125% to 2% *w*/*w* (thus, 1.25–20 mg/g) in the final formulation. The physico-chemical parameters analyzed for these nanoparticles are summarized in Table 1. Overall, within the concentration range tested, greater polymer concentration was associated with larger nanoparticle diameter. No associations were noted between polymer concentration and either PDI or ZP parameters. PDI values ranged 0.06-0.20, indicating suspensions with high quality dispersion in general. In contrast, ZP values were more variable (from −5 to −35 mV), but only nanoparticles made of 10 and 20 mg/g PMVE/MA-Es displayed values yielding fairly good physical stability (≥30 mV approximately). Given these results, nanoparticles made of 10 mg/g PMVE/MA-Es were selected for further studies.

Table 1. Physico-chemical characteristics of nanoparticles made with different PMVE/MA-Es concentrations.

Conc. (mg/g)	HDD (nm)	PDI (a.u.)	ZP (mV)
1.25	84 ± 5	0.11 ± 0.04	−26 ± 10
2.5	139 ± 26	0.19 ± 0.03	−5 ± 4
5	106 ± 4	0.10 ± 0.04	−5 ± 6
10	202 ± 11	0.20 ± 0.06	−35 ± 9
20	230 ± 1	0.06 ± 0.01	−32 ± 1

Conc., concentration in the final formulation. a.u., arbitrary units. Results shown as the mean ± s.d. (n = 3).

Such nanoparticle formulations were then analyzed by TEM (Figure 3), which revealed consistent spherical shapes and, in contrast to PCS results, not only a lower average size (114 ± 24 nm), but also a less homogeneous population, as can be observed from the frequency histogram of their diameters.

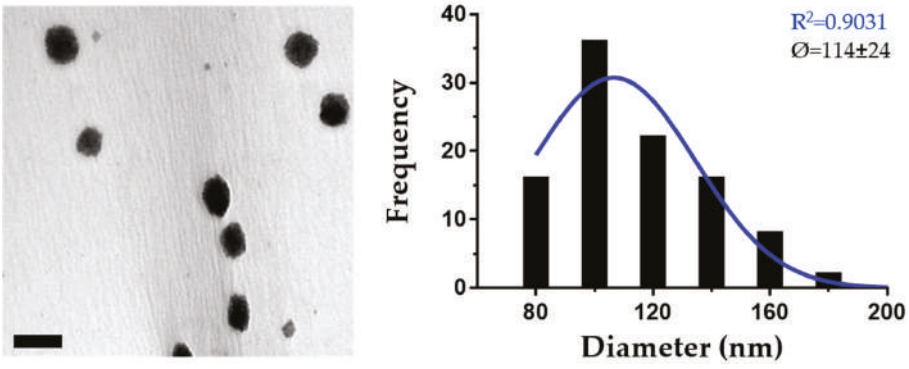

Figure 3. TEM analysis of optimized PMVE/MA-Es nanoparticles. Representative TEM image and diameter frequency histogram of PMVE/MA-Es nanoparticles synthesized by the solvent displacement method. The histogram was generated from data obtained from multiple images, until reaching 50 individual measurements. The best-fit adjustment (and R^2) to a Gaussian distribution is indicated in blue. Average diameter (Ø) and s.d. are also included in the inset. Scale bar: 200 nm.

3.3. Characterization of PMVE/MA-Es Nanoparticles Loaded with Antibiotics

By following the methodology described above, antibiotic-loaded PMVE/MA-Es nanoparticles were prepared containing 10 mg/g PMVE/MA-Es and 200 ng/g antibiotic (if 100% EE). The physico-chemical characteristics and EE displayed by these formulations are summarized in Table 2. Control (non-loaded) nanoparticles showed similar physico-chemical values as observed before (previous section), confirming the high reproducibility of the technique. As for loaded nanoparticles, there were significant compound-dependent variations in these parameters. For instance, both amikacin- and ciprofloxacin-loading was associated with greater particle size, but only the latter showed a notably change in ZP value (−16 ± 3 mV). Nanoparticles loaded with cefotaxime showed lower diameter (156 ± 6 nm) in comparison to control, and only neomycin-loaded particles showed no substantial differences compared to controls. Regarding their EE, only amikacin showed relatively low values (14% ± 4%), with the other antibiotics ranging from 40% to 69%.

Table 2. Physico-chemical characteristics and encapsulation efficiency (EE) of PMVE/MA-Es nanoparticles loaded with antibiotics.

Antibiotic	HDD (nm)	PDI (a.u.)	ZP (mV)	EE (%)
None	195 ± 7	0.15 ± 0.04	−38 ± 13	-
Amikacin	253 ± 5	0.17 ± 0.07	−39 ± 2	14 ± 4
Neomycin	209 ± 4	0.20 ± 0.07	−29 ± 7	40 ± 3
Cefotaxime	156 ± 6	0.29 ± 0.03	−31 ± 8	69 ± 7
Ciprofloxacin	256 ± 8	0.17 ± 0.01	−16 ± 3	59 ± 8

a.u., arbitrary units. Results shown as the mean and s.d. (n = 3).

3.4. Analysis of the Antibacterial Activity

The antibacterial activity of encapsulated antibiotics was assessed against Gram-positive (*S. aureus*) and Gram-negative (*E. coli*) bacteria by determining their MIC values and comparing to those obtained for the free drug. The MIC values displayed by the encapsulated and free antibiotics were not significantly different (data not shown). As free compounds, MIC values for amikacin, neomycin, ciprofloxacin and cefotaxime were 1.25, 0.31, 2.5 and 0.16 μg/mL against *S. aureus* and 2.5, 1.25, 0.06 and 0.004 μg/mL against *E. coli*, respectively.

4. Discussion

The present work provides evidence of the versatility of polymers for generating nanostructures adapted to the solubility properties of the compounds of interest, for successful encapsulation of these compounds. Our previous studies provided the first demonstration of electrospinning procedures optimized for creating nanofibers of the two PMVE/MA derivates used here [10,11]. These were used to encapsulate 5-aminolevulinic acid (5-ALA) into nanofibers made of each polymer [11], and a combination of salicylic acid, methyl salicylate and capsaicin into PMVE/MA-Es nanofibers [10]. Here, we demonstrated the encapsulation of four structurally different molecules (with a common application: antibiotics) into electrospun nanofibers of either PMVE/MA-Ac or PMVE/MA-Es. All the antibiotics tested were soluble in water, and thus encapsulate into PMVE/MA-Ac nanofibers, but only cefotaxime was also soluble in ethanol, and consequently the only one loadable into PMVE/MA-Es nanofibers. In this regard, as many drugs are hydrophobic, the description of electrospinnable polymers with properties compatible for encapsulating hydrophobic compounds, is of great importance in order to incorporate such molecules into electrospun nanofibers while maintaining their biological functionality. This issue has been revisited by several authors recently [21,22]. Furthermore, these polymers might also work as a shell phase in both co-axial and layer-by-layer electrospinning in order to either manipulate the delivery dynamics of high hydrophilic molecules to the particular requirements or to adapt the delivery system to the needs of the biological context [23,24].

Although the morphology of the nanofibers was not affected by the encapsulation of molecules, their diameter did undergo considerable changes in comparison to non-loaded fibers. The extent of these increases in diameter was related to the compound used (1.6-fold for PMVE/MA-Es/cefotaxime nanofibers and 2.4–5.0-fold for loaded PMVE/MA-Ac nanofibers). These increases were larger than expected, as only 1% *w*/*w* antibiotic was used in all cases and loading percentages for relatively similar compounds are usually much higher with no, or even reduced, diameter [10,25,26]. In general, within moderate encapsulation levels, the diameter of electrospun nanofibers commonly increases with viscosity and decreases with conductivity [25–29], and since the compounds used here are not salts or polyelectrolytes, they might be increasing the viscosity of the electrospinnable solution [25,26]. In any case, the current study employs the same synthesis parameters for all formulations in order to reliably determine any possible morphological or size changes between the different antibiotics incorporated, and if it is desirable to strictly limit any increase in size, it might be achievable by optimizing such parameters for each particular formulation, as shown in our previous studies [10,11].

This work has shown the flexibility of nanostructuration of some polymers and offers alternative encapsulating nanomaterials for compounds whose solubility limitations hinder their biological/therapeutic applications. Although amikacin, neomycin and ciprofloxacin could not be loaded into PMVE/MA-Es nanofibers by electrospinning, the solubility of all integrating molecules with water:ethanol solutions allowed their encapsulation into PMVE/MA-Es nanoparticles, synthesized by the solvent displacement method. This methodology has been widely reported to create PMVE/MA nanoparticles for drug delivery purposes because of the interesting mucoadhesive properties of this polymer [19,30]; however, to our knowledge, there are no publications describing nanoparticles made of PMVE/MA-Es apart from the patent with reference number US20140161892A1 [31].

The optimized methodology for encapsulating particles (10 mg/g PMVE/MA-Es) produced polymeric nanoparticles with size (200 nm), PDI (0.2) and ZP (−35 mV). Briefly, at the concentrations tested, the greater the polymer concentration used, the larger the nanoparticle diameter produced, while formulations with smaller nanoparticles showed less adequate PDI and ZP values than the selected one. The PDI, which ranges from 0 to 1, reflects the width of the particle size distribution and values lower than 0.3 are commonly considered as optimum [32]. Regarding the ZP, which reflects the level of surface electrostatic potential, values of approximately −30 mV are associated with physical stability and are considered at the limit for colloidal organizations (theoretically, about −60 mV minimum is considered optimal) [33,34]. Comparing to these results, loaded nanoparticles did not differ much in the PDI, ZP and size values obtained, which is in accordance with some studies [35–39].

In contrast, the size of PMVE/MA-Es nanoparticles did change notably (increased by about 25%) for some antibiotics, although not as dramatically as in loaded PMVE/MA-Ac nanofibers. Interestingly, the greatest size increases were found when encapsulating amikacin into both types of nanostructures; however, no further correlations could be established for the remaining antibiotics. These size changes do not appear to be related to their MWs, nor to their EEs. For instance, despite the two aminoglycosides tested, amikacin and neomycin, presenting similar MWs (585.6 and 614.6 g/mol, respectively) and chemical structures (see Figure 1), the size change of their encapsulating nanostructures (625 vs. 304 nm in nanofibers and 253 vs. 209 nm in nanoparticles) and their EEs (14% vs. 40%) are very different. In this regard, the scarcity of nanoencapsulation studies for amikacin, neomycin cefotaxime and, to a lesser extent, ciprofloxacin [40–43], hampers any meaningful assessment or comparison.

Nevertheless, all tested antibiotics, when encapsulated into either nanomaterial, showed similar antibacterial activity as their free forms, indicating that none of the synthesis methodologies used substantially modified their chemical structures. This observation encourages the performance of follow-up experiments focused on assessing any potential advantages conferred by the described encapsulating nanomaterials in terms of controlled release, targeted delivery or other therapeutic impact. Any such advantages may help to overcome the drawbacks restricting the clinical use of some therapeutics (such as toxicity, poor penetration of biological barriers and short circulating half-life) [44].

5. Conclusions

The compatibility in solubility of both the polymer source and the compound of interest is a critical factor limiting the production of loaded polymeric electrospun nanofibers. However, it has been demonstrated here that the high versatility with which some polymers can be assembled into nanomaterials, in this work PMVE/MA-Ac and PMVE/MA-Es, offers novel encapsulating strategies to overcome such constraints. In this context, it has also been shown that the encapsulation efficiency, nanostructuration settings and/or the morphology/size of the final nanostructures are highly dependent upon the chemical properties, rather than the molecular weight, of the compounds to be encapsulated. In contrast, it is confirmed that none of the nanostructuring procedures employed alters the activity of a set molecules with different chemical structures.

Supplementary Materials: The following are available online at http://www.mdpi.com/2079-4991/10/3/486/s1, Figure S1: Representative HPLC chromatograms and calibration curves of tested antibiotics.

Author Contributions: Conceptualization, R.M. and A.F.; methodology, A.M., C.S.-U. and H.C.; software, A.M., C.S.-U. and A.F.; validation, A.M.; formal analysis, S.I.J., R.M. and A.F.; investigation, A.M., R.M. and A.F.; resources, J.C.R.-D., R.M. and A.F.; data curation, A.F.; writing—original draft preparation, A.F.; writing—review and editing, S.I.J.; visualization, A.F.; supervision, R.M. and A.F.; project administration, R.M.; funding acquisition, R.M. and A.F. All authors have read and agreed to the published version of the manuscript.

Funding: This research was funded by the Spanish Ministerio de Economía y Competitividad, grant numbers MAT-2017-86805-R and MAT-2014-53282-R, and Spanish Ministerio de Ciencia e Innovación (MCI)—Agencia Estatal de Investigación (AEI)/Fondo Europeo de Desarrollo Regional (FEDER), grant number RTI2018-101969-J-I00.

Acknowledgments: We thank Elisa Pérez for technical assistance.

Conflicts of Interest: The authors declare no conflict of interest.

References

1. Coates, A.R.; Halls, G.; Hu, Y. Novel classes of antibiotics or more of the same? *Br. J. Pharmacol.* **2011**, *163*, 184–194. [CrossRef] [PubMed]
2. Bassetti, M.; Merelli, M.; Temperoni, C.; Astilean, A. New antibiotics for bad bugs: Where are we? *Ann. Clin. Microbiol. Antimicrob.* **2013**, *12*, 22. [CrossRef] [PubMed]
3. Leucuta, S.E. Nanotechnology for delivery of drugs and biomedical applications. *Curr. Clin. Pharmacol.* **2010**, *5*, 257–280. [CrossRef] [PubMed]
4. Mahapatro, A.; Singh, D.K. Biodegradable nanoparticles are excellent vehicle for site directed in-vivo delivery of drugs and vaccines. *J. Nanobiotechnol.* **2011**, *9*, 55. [CrossRef]

5. Gunn, J.; Zhang, M. Polyblend nanofibers for biomedical applications: Perspectives and challenges. *Trends Biotechnol.* **2010**, *28*, 189–197. [CrossRef]
6. Vasita, R.; Katti, D.S. Nanofibers and their applications in tissue engineering. *Int. J. Nanomed.* **2006**, *1*, 15–30. [CrossRef]
7. Guo, G.; Fu, S.; Zhou, L.; Liang, H.; Fan, M.; Luo, F.; Qian, Z.; Wei, Y. Preparation of curcumin loaded poly(epsilon-caprolactone)-poly(ethylene glycol)-poly(epsilon-caprolactone) nanofibers and their in vitro antitumor activity against glioma 9l cells. *Nanoscale* **2011**, *3*, 3825–3832. [CrossRef]
8. Yoo, J.J.; Kim, C.; Chung, C.W.; Jeong, Y.I.; Kang, D.H. 5-aminolevulinic acid-incorporated poly(vinyl alcohol) nanofiber-coated metal stent for application in photodynamic therapy. *Int. J. Nanomed.* **2012**, *7*, 1997–2005.
9. Lucio, D.; Martinez-Oharriz, M.C.; Gonzalez-Navarro, C.J.; Navarro-Herrera, D.; Gonzalez-Gaitano, G.; Radulescu, A.; Irache, J.M. Coencapsulation of cyclodextrins into poly(anhydride) nanoparticles to improve the oral administration of glibenclamide. A screening on c. Elegans. *Colloids Surf. B Biointerfaces* **2018**, *163*, 64–72. [CrossRef]
10. Martinez-Ortega, L.; Mira, A.; Fernandez-Carvajal, A.; Mateo, C.R.; Mallavia, R.; Falco, A. Development of a new delivery system based on drug-loadable electrospun nanofibers for psoriasis treatment. *Pharmaceutics* **2019**, *11*, 14. [CrossRef]
11. Mira, A.; Mateo, C.R.; Mallavia, R.; Falco, A. Poly (methyl vinyl ether-alt-maleic acid) and ethyl monoester as building polymers for drug-loadable electrospun nanofibers. *Sci. Rep.* **2017**, *7*, 17205. [CrossRef] [PubMed]
12. Iglesias, T.; de Cerain, A.L.; Irache, J.; Martín-Arbella, N.; Wilcox, M.; Pearson, J.; Azqueta, A. Evaluation of the cytotoxicity, genotoxicity and mucus permeation capacity of several surface modified poly (anhydride) nanoparticles designed for oral drug delivery. *Int. J. Pharm.* **2017**, *517*, 67–79. [CrossRef] [PubMed]
13. Ruiz-Gaton, L.; Espuelas, S.; Larraneta, E.; Reviakine, I.; Yate, L.A.; Irache, J.M. Pegylated poly(anhydride) nanoparticles for oral delivery of docetaxel. *Eur. J. Pharm. Sci.* **2018**, *118*, 165–175. [CrossRef] [PubMed]
14. Vazquez-Guillo, R.; Martinez-Tome, M.J.; Kahveci, Z.; Torres, I.; Falco, A.; Mallavia, R.; Mateo, C.R. Synthesis and characterization of a novel green cationic polyfluorene and its potential use as a fluorescent membrane probe. *Polymers* **2018**, *10*, 938. [CrossRef] [PubMed]
15. Vázquez-Guilló, R.; Falco, A.; Martínez-Tomé, M.J.; Mateo, C.R.; Herrero, M.A.; Vázquez, E.; Mallavia, R. Advantageous microwave-assisted suzuki polycondensation for the synthesis of aniline-fluorene alternate copolymers as molecular model with solvent sensing properties. *Polymers* **2018**, *10*, 215. [CrossRef] [PubMed]
16. Kahveci, Z.; Vazquez-Guillo, R.; Martinez-Tome, M.J.; Mallavia, R.; Mateo, C.R. New red-emitting conjugated polyelectrolyte: Stabilization by interaction with biomolecules and potential use as drug carriers and bioimaging probes. *ACS Appl Mater. Interfaces* **2016**, *8*, 1958–1969. [CrossRef]
17. Kumari, A.; Yadav, S.K.; Yadav, S.C. Biodegradable polymeric nanoparticles based drug delivery systems. *Colloids Surf. B Biointerfaces* **2010**, *75*, 1–18. [CrossRef]
18. Sharma, J.; Lizu, M.; Stewart, M.; Zygula, K.; Lu, Y.; Chauhan, R.; Yan, X.; Guo, Z.; Wujcik, E.K.; Wei, S. Multifunctional nanofibers towards active biomedical therapeutics. *Polymers* **2015**, *7*, 186–219. [CrossRef]
19. Arbos, P.; Wirth, M.; Arangoa, M.A.; Gabor, F.; Irache, J.M. Gantrez an as a new polymer for the preparation of ligand-nanoparticle conjugates. *J. Control. Release* **2002**, *83*, 321–330. [CrossRef]
20. Cockerill, F.; Wikler, M.; Alder, J.; Dudley, M.; Eliopoulos, G.; Ferraro, M.; Hardy, D.; Hecht, D.; Hindler, J.; Patel, J. *Methods for Dilution Antimicrobial Susceptibility Tests for Bacteria That Grow Aerobically: Approved Standard*; Clinical and Laboratory Standards Institute: Wayne, PA, USA, 2012.
21. Goke, K.; Lorenz, T.; Repanas, A.; Schneider, F.; Steiner, D.; Baumann, K.; Bunjes, H.; Dietzel, A.; Finke, J.H.; Glasmacher, B.; et al. Novel strategies for the formulation and processing of poorly water-soluble drugs. *Eur. J. Pharm. Biopharm.* **2018**, *126*, 40–56. [CrossRef]
22. Yu, D.G.; Li, J.J.; Williams, G.R.; Zhao, M. Electrospun amorphous solid dispersions of poorly water-soluble drugs: A review. *J. Control. Release* **2018**, *292*, 91–110. [CrossRef] [PubMed]
23. Singh, A.; Rath, G.; Singh, R.; Goyal, A.K. Nanofibers: An effective tool for controlled and sustained drug delivery. *Curr. Drug. Deliv.* **2018**, *15*, 155–166. [CrossRef] [PubMed]
24. Son, Y.J.; Kim, W.J.; Yoo, H.S. Therapeutic applications of electrospun nanofibers for drug delivery systems. *Arch. Pharm. Res.* **2014**, *37*, 69–78. [CrossRef] [PubMed]
25. Shen, X.; Yu, D.; Zhu, L.; Branford-White, C.; White, K.; Chatterton, N.P. Electrospun diclofenac sodium loaded eudragit(r) l 100-55 nanofibers for colon-targeted drug delivery. *Int. J. Pharm.* **2011**, *408*, 200–207. [CrossRef]

26. Samprasit, W.; Akkaramongkolporn, P.; Ngawhirunpat, T.; Rojanarata, T.; Kaomongkolgit, R.; Opanasopit, P. Fast releasing oral electrospun pvp/cd nanofiber mats of taste-masked meloxicam. *Int. J. Pharm.* **2015**, *487*, 213–222. [CrossRef]
27. Nezarati, R.M.; Eifert, M.B.; Cosgriff-Hernandez, E. Effects of humidity and solution viscosity on electrospun fiber morphology. *Tissue Eng. Part C Methods* **2013**, *19*, 810–819. [CrossRef]
28. Reda, R.I.; Wen, M.M.; El-Kamel, A.H. Ketoprofen-loaded eudragit electrospun nanofibers for the treatment of oral mucositis. *Int. J. Nanomed.* **2017**, *12*, 2335. [CrossRef]
29. Canbolat, M.F.; Celebioglu, A.; Uyar, T. Drug delivery system based on cyclodextrin-naproxen inclusion complex incorporated in electrospun polycaprolactone nanofibers. *Colloids Surf. B Biointerfaces* **2014**, *115*, 15–21. [CrossRef]
30. Irache, J.M.; Huici, M.; Konecny, M.; Espuelas, S.; Campanero, M.A.; Arbos, P. Bioadhesive properties of gantrez nanoparticles. *Molecules* **2005**, *10*, 126–145. [CrossRef]
31. Salman, H.H.; Azcarate, I.G. Nanoparticles Comprising Esters of Poly (Methyl Vinyl Ether-Co-Maleic Anhydride) and Uses Thereof. U.S. Patent No. 9,351,940, 31 May 2016.
32. Kaur, I.P.; Bhandari, R.; Bhandari, S.; Kakkar, V. Potential of solid lipid nanoparticles in brain targeting. *J. Control. Release* **2008**, *127*, 97–109. [CrossRef]
33. Hunter, R.J. *Zeta Potential in Colloid Science: Principles and Applications*; Academic Press: Cambridge, MA, USA, 2013; Volume 2.
34. Kovacevic, A.; Savic, S.; Vuleta, G.; Muller, R.H.; Keck, C.M. Polyhydroxy surfactants for the formulation of lipid nanoparticles (sln and nlc): Effects on size, physical stability and particle matrix structure. *Int. J. Pharm.* **2011**, *406*, 163–172. [CrossRef]
35. Agüeros, M.; Zabaleta, V.; Espuelas, S.; Campanero, M.; Irache, J. Increased oral bioavailability of paclitaxel by its encapsulation through complex formation with cyclodextrins in poly (anhydride) nanoparticles. *J. Control. Release* **2010**, *145*, 2–8. [CrossRef] [PubMed]
36. Araujo, R.S.; Garcia, G.M.; Vilela, J.M.C.; Andrade, M.S.; Oliveira, L.A.M.; Kano, E.K.; Lange, C.C.; Brito, M.; Brandao, H.M.; Mosqueira, V.C.F. Cloxacillin benzathine-loaded polymeric nanocapsules: Physicochemical characterization, cell uptake, and intramammary antimicrobial effect. *Mater. Sci. Eng. C Mater. Biol. Appl.* **2019**, *104*, 110006. [CrossRef] [PubMed]
37. Brandhonneur, N.; Hatahet, T.; Amela-Cortes, M.; Molard, Y.; Cordier, S.; Dollo, G. Molybdenum cluster loaded plga nanoparticles: An innovative theranostic approach for the treatment of ovarian cancer. *Eur. J. Pharm. Biopharm.* **2018**, *125*, 95–105. [CrossRef]
38. Lopalco, A.; Ali, H.; Denora, N.; Rytting, E. Oxcarbazepine-loaded polymeric nanoparticles: Development and permeability studies across in vitro models of the blood-brain barrier and human placental trophoblast. *Int. J. Nanomed.* **2015**, *10*, 1985–1996.
39. Calleja, P.; Espuelas, S.; Vauthier, C.; Ponchel, G.; Irache, J.M. Controlled release, intestinal transport, and oral bioavailablity of paclitaxel can be considerably increased using suitably tailored pegylated poly(anhydride) nanoparticles. *J. Pharm. Sci.* **2015**, *104*, 2877–2886. [CrossRef]
40. Sabaeifard, P.; Abdi-Ali, A.; Soudi, M.R.; Gamazo, C.; Irache, J.M. Amikacin loaded plga nanoparticles against pseudomonas aeruginosa. *Eur. J. Pharm. Sci.* **2016**, *93*, 392–398. [CrossRef]
41. Zaki, N.M.; Hafez, M.M. Enhanced antibacterial effect of ceftriaxone sodium-loaded chitosan nanoparticles against intracellular salmonella typhimurium. *AAPS PharmSciTech* **2012**, *13*, 411–421. [CrossRef]
42. Mushtaq, S.; Khan, J.A.; Rabbani, F.; Latif, U.; Arfan, M.; Yameen, M.A. Biocompatible biodegradable polymeric antibacterial nanoparticles for enhancing the effects of a third-generation cephalosporin against resistant bacteria. *J. Med. Microbiol.* **2017**, *66*, 318–327. [CrossRef]
43. Sonam; Chaudhary, H.; Kumar, V. Taguchi design for optimization and development of antibacterial drug-loaded plga nanoparticles. *Int. J. Biol. Macromol.* **2014**, *64*, 99–105. [CrossRef]
44. Natan, M.; Banin, E. From nano to micro: Using nanotechnology to combat microorganisms and their multidrug resistance. *FEMS Microbiol. Rev.* **2017**, *41*, 302–322. [CrossRef] [PubMed]

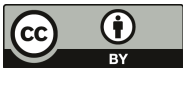

nanomaterials

MDPI

Article

Micro- and Nanostructures of Agave Fructans to Stabilize Compounds of High Biological Value via Electrohydrodynamic Processing

Carla N. Cruz-Salas [1], Cristina Prieto [2], Montserrat Calderón-Santoyo [1], José M. Lagarón [2] and Juan A. Ragazzo-Sánchez [1,*]

[1] Laboratorio Integral de Investigación en Alimentos, Tecnológico Nacional de México/Instituto Tecnológico de Tepic, Av. Tecnológico 2595, Tepic C.P. 63175, Nayarit, Mexico; ccruz@ittepic.edu.mx (C.N.C.-S.); montserratcalder@gmail.com (M.C.-S.)

[2] Novel Materials and Nanotechnology Group, IATA-CSIC, Calle Catedrático Agustín Escardino Benlloch 7, 46980 Paterna, Spain; cprieto@iata.csic.es (C.P.); lagaron@iata.csic.es (J.M.L.)

* Correspondence: arturoragazzo@hotmail.com or jragazzo@ittepic.edu.mx; Tel.: +52-311-2119400 (ext. 233)

Received: 24 October 2019; Accepted: 12 November 2019; Published: 21 November 2019

Abstract: This study focuses on the use of high degree of polymerization agave fructans (HDPAF) as a polymer matrix to encapsulate compounds of high biological value within micro- and nanostructures by electrohydrodynamic processing. In this work, β-carotene was selected as a model compound, due to its high sensitivity to temperature, light and oxygen. Ultrafine fibers from HDPAF were obtained via this technology. These fibers showed an increase in fiber diameter when containing β-carotene, an encapsulation efficiency (EE) of 95% and a loading efficiency (LE) of 85%. The thermogravimetric analysis (TGA) showed a 90 °C shift in the β-carotene decomposition temperature with respect to its independent analysis, evidencing the HDPAF thermoprotective effect. Concerning the HDPAF photoprotector effect, only 21% of encapsulated β-carotene was lost after 48 h, while non-encapsulated β-carotene oxidized completely after 24 h. Consequently, fructans could be a feasible alternative to replace synthetic polymers in the encapsulation of compounds of high biological value.

Keywords: HDPAF; electrospinning; micro-nanofibers; β-carotene; thermoprotection; photoprotection

1. Introduction

Obtaining micro- and nanostructures in the food industry represents a viable option for the incorporation and stabilization of compounds of high biological value (CHBV). The production of these structures containing CHBV is based on the encapsulation processes in which the bioactive is surrounded by polymeric materials that act as matrices and help to preserve their properties. Currently, there is a huge interest in the use of biopolymers that replace synthetic polymers in the encapsulation and transport processes of compounds of high biological value, as well as expanding their use in biomedical and pharmaceutical technologies [1,2]. Fructans are a new class of heterodispersed biopolymers that are found in various plants, such as the *Agave tequilana* from the Agavaceae family, and serve as an important source of reserve carbohydrates in the plant. Five types of fructans have been identified in nature so far, which are classified into inulins, neo-inulins, levans, neo-levans and mixed fructans, depending on the type of bond [3,4]. Agave fructans are characterized by the presence of fructose units with a terminal glucose connected by bonds β (2-1) and β (2-6) and can present different degrees of polymerization, which are determined by the species [5–7] as well as the environmental conditions in which the agave is produced, stored and processed [8,9].

Toriz et al. (2007) [10] propose a chemical structure for the fructans of *Agave tequilana* Weber var. Azul, based on the combination of permethylation and reductive rupture techniques for identification.

They mainly propose the distribution of two monomers, the β-D fructofuranose terminal type (22%), 1-linked (30.8%), 6-linked (21.2%), 1-6 linked (19.8%) and the α-D terminal glucopiranose (7.3%).

The use of high degree of polymerization agave fructans (HDPAF) has been implemented in recent years as a wall material in encapsulation processes such as spray drying, obtaining remarkable results. Ortiz-Basurto et al. (2017) [11] microencapsulated pitanga juice (*Eugenia uniflora* L.) by spray drying with HDPAF and maltodextrin as encapsulants. These authors reported similar behaviors between both materials. Alternatively, Farías Cervantes et al. (2016) [12] used 50% agave fructans, as an encapsulant to obtain blackberry powder by spray drying, mentioning that agave fructans, in addition to increasing the encapsulation efficiency, could add prebiotic properties and improve the physico-chemical characteristics of the powder.

However, conventional encapsulation processes, such as spray drying, require the use of high temperatures or toxic reactives that could affect the CHBV or compromise its application in a food or pharmaceutical product. The electrohydrodynamic processing, electrospinning or electrospraying, has demonstrated to be a promising alternative to encapsulate and stabilize compounds of high biological value, since it does not require severe conditions of temperature, pressure or aggressive chemicals [13]. This technology allows obtaining structures called fibers or particles at the micron, submicron or nano scale [14]. This technique uses a potential difference for the electro-stretching of a drop of polymer solution from a charged electrode (capillary or free surface) to a collector. Once the drop has gained enough electrical charge to overcome the surface tension and viscosity of the polymer, the drop is stretched, causing ultra-fine fibers to emerge from the polymer drop, forming the so-called Taylor cone [15]. The extent of each phase, whether direct or in drag motion, depends on the operating parameters as well as the physical properties of the polymer, such as surface tension, conductivity and viscosity [16]. The difference between electrospinning and electrospraying (electrohydrodynamic spraying) is based on the degree of molecular cohesion, which can be easily controlled by variation in the concentration of the polymer solution [17]. Ramos-Hernández et al. (2018) [18] managed to obtain spherical structures with a size distribution of 440 to 880 nm, as well as the thermostability and photostability of β-carotene encapsulated by electrospraying, using solutions with concentrations from 10% to 50% of HDPAF.

Electro-spun nanofibers have also been used in CHBV encapsulation processes, such as the encapsulation of bioactive compounds in zein fibers with application in food and pharmaceutical products [19]; however, up to our knowledge, the production of electro-spun micro-nanofibers of HDPAF has not been reported yet. This material could be a feasible alternative to replace synthetic polymers in the encapsulation of compounds of high biological value, as well as expanding their use in biomedical and pharmaceutical products.

Antioxidants are a good example of CHBV due to the high number of health benefits attributed to them and their high sensitivity to physico-chemical factors [20]. Carotenoids are an important member of the antioxidant family, being natural organic pigments present in plants and some photosynthetic organisms. Their consumption is associated with health benefits by reducing the incidence of cancer and heart disease, as well as improving ocular health [21]. β-carotene is one of the most common carotenoids in the functionality of food, supplements and pharmaceuticals due to its high, pro-vitamin A activity and antioxidant capacity. However, its use is sometimes limited due to its sensitivity to oxidation, especially when exposed to high temperatures, light, oxygen, acidic conditions, etc. [19,22].

The aim of this study was to evaluate the feasibility of agave fructans to obtain micro-nanofibers through the electrospinning process, using β-carotene as a model compound, with properties and characteristics, as a first approach, and to provide stability to compounds of high biological value for further applications in the food and pharmaceutical areas.

2. Materials and Methods

2.1. Materials

High degree of polymerization agave fructans (HDPAF) were obtained in the Laboratorio Integral de Investigación en Alimentos (LIIA) of Tecnológico Nacional de México/Instituto Tecnológico de Tepic, Nayarit, México, from native fructans provided by the company Campos Azules Co. (Mexico City, Mexico); β-carotene (>97.0% UV, C40H56) (Sigma Aldrich, Steinheim, Germany), 96% ethyl alcohol (CTR Scientific, Monterrey N.L, Mexico), Chloroform (trichloromethane) HPLC grade (Fermon Episolv, Monterrey N.L, Mexico), Tego® SML (Evonik Industries AG, Essen, Germany).

2.2. Preparation and Characterization of Polymer Solutions

Polymeric solutions were prepared with 70% (*w*/*w*) of HDPAF in hydroalcoholic solution (ethanol-water, at 10% *w*/*w*) and 1% (*w*/*w*) of Tego® SML as surfactant was added. The solution was homogenized under magnetic stirring for 45 min at room temperature. In the alcoholic fraction of the solution, β-carotene was added (1% *w*/*w*), protecting the mixture from light during the homogenization period with dark paper.

The characterization of the solutions consisted in determining the electrical conductivity, viscosity and surface tension. The electrical conductivity was analyzed with a multiparameter potentiometer Hanna Instruments HI-4521 (Melrose, MA, USA). The viscosity (η) was determined with a Discovery HR-1 Hybrid rheometer (TA Instruments, New Castle, DE, USA), equipped with geometry Smart Swap ™ with automatic detection. The cone and plate geometry option was selected (2°, 60 mm of diameter, 64 μm of gap) and the Peltier system for temperature stabilization was used. The surface tension was measured with the equipment Force tensiometer model K20 EasyDyne (KRÜSS GmbH, Hamburg, Germany), with the Wilhelmy Plate method.

2.3. Obtaining Fibers by Electrospinning

The electrospinning process was performed in a machine LE-10 brand Fluidnatek® from BIOINICIA company (Valencia, Spain), which has a voltage power supply of 19 kV. The injector is based on a syringe pump with a flow from 200 μL/h, and has a distance from the injector to the collector of 20 cm, the collector is cylindrical stainless steel and it has a variable rotation speed from 500 rpm. The process parameters such as voltage, flow, distance and rotation speed of the collector were adjusted in preliminary tests according to the characterization and stability of the solutions.

2.4. Morphology Analysis through SEM

The morphology and size of the fibers obtained were both determined with the scanning electron microscopy (SEM) technique with a Hitachi-S-4800 device (Hitachi High-Technologies Corporation, Tokyo, Japan). Approximately 1.5 mg of sample was fixed with double-sided tape on the sample holder, coated with gold-palladium for 2 min, and an acceleration voltage of 10 kV was used. The determination of the size distribution based on the diameters of the structures was made with the SEM system software (Hitachi High-Technologies Corporation, Tokyo, Japan) with at least 100 measurements per sample.

2.5. Loading and Encapsulation Efficiency

The loading efficiency (LE) of β-carotene in the fibers was determined considering the amount of total extract and final extract by weight difference, obtained with thermogravimetry analysis (TGA) using the TRIOS software (TA Instruments, New Castle, DE, USA) and applying Equation (1). Where the total extract corresponds to the amount of extract added to the fibers, the final extract represents the amount of extract determined by TGA. Regarding the encapsulation efficiency (EE), initially the amount of extract loaded was determined with the application of Equation (2).

Subsequently, the amount of surface was calculated, performing a superficial washing of the fibers with a solvent related to β-carotene and not to the polymer, in order to determine the content of compounds of high biological value (CHBV) on the fiber surface. To this end, 1 mg of fibers was taken and suspended in 1 mL of trichloromethane, centrifuging at 10,000 rpm for 1 min, analyzing the supernatant obtained absorbance at 466 nm in a Varian brand Cary® 50 UV-Vis spectrophotometer (Sydney, Australia). The β-carotene content is calculated according to the calibration curve performed, y = 3.6298x + 0.0059 (R^2 = 0.9998). Finally, knowing the values of loading and surface extract, Equation (3) was applied to determine the encapsulation efficiency (EE).

Loading efficiency (LE)

$$\%LE = \left(1 - \left(\frac{total\ extract - final\ extract}{total\ extract}\right)\right) \times 100 \quad (1)$$

Loading extract

$$Loading\ extract = \frac{\%EC * total\ extract}{100} \quad (2)$$

Encapsulation efficiency (EE)

$$\%EE = \frac{loading\ extract - surface\ extract}{loading} \times 100 \quad (3)$$

2.6. Thermogravimetric Analysis (TGA)

The thermogravimetric analysis to determine the decomposition temperature of each component of the fiber, as well as to determine the LE and to demonstrate the thermoprotective effect of the materials on β-carotene, was performed on a TGA 550 (TA Instruments, New Castle, DE, USA) in a nitrogen atmosphere (N_2), with a heating ramp of 25 to 600 °C at a speed of 5 °C/min. The results were analyzed with the TRIOS software (TA Instruments, New Castle, DE, USA).

2.7. UV Photostability

In order to analyze the oxidation kinetics of β-carotene, the fibers obtained were exposed to a simulator of sunlight. An Osram Ultra-vitalux lamp (300 W) (OSRAM, Munich, Germany) was utilized, which generates a mixture of radiation, using a quartz discharge tube and a tungsten filament [19]. It was placed in a sample holder 1 mg of standard β-carotene, and samples of the fibers with and without β-carotene, which were exposed to ultraviolet (UV) radiation for 48 h at 37 °C. Samples were taken every 6 h. A central segment of the exposed material was cut and dissolved in distilled water at a ratio of 1 mg/mL with magnetic stirring for 1 min. Subsequently, 1 mL of chloroform was added and centrifuged (10,000 rpm, 1 min). The absorbance of the organic phase at 466 nm was measured with the Varian brand Cary® 50 UV-Vis spectrophotometer (Sydney, Australia). Chloroform was used as the target. The results, obtained in relation to oxidation, are reported based on the relative content of β-carotene (% absorbance).

2.8. Statistic Analysis

Data analysis was performed using the least significant digit (LSD) test for comparison of means with STATISTICA version 10 (StatSoft, Inc. (2011), (Tulsa, OK, USA)). All tests were performed in triplicate.

3. Results and Discussion

3.1. Physicochemical Characterization of Polymer Solutions

First, the physicochemical properties of the polymer solutions were evaluated, since the stability of the electrohydrodynamic process and the morphology obtained are highly related to them.

The solutions presented viscosity values of 3.69 ± 0.05 and 3.36 ± 0.03 Pa·s without and with β-carotene, respectively, as shown is Table 1. These results are in the same order of magnitude as those obtained by Kutzli et al. (2019) [23], at high concentrations of maltodextrin combined with whey protein isolated (WPI) or soy protein isolated (SPI). They obtained values of apparent viscosity of 4.85 ± 0.14 Pa·s (WPI 80:5), 5.88 ± 0.18 Pa·s (WPI 80:10), 5.14 ± 0.09 Pa·s (SPI 80:5) and 7.77 ± 0.12 Pa·s (SPI 80:10), respectively. The similarity of fructans with maltodextrin with respect to this property is mainly due to their structural conformation. Concerning the surface tension, similar values in the solutions with and without β-carotene were obtained (29.6 ± 0.2 and 30.1 ± 0.1 mN/m), showing that the β-carotene incorporation does not modify the penetration resistance of the solution ($p \leq 0.05$). Ramos-Hernández et al. (2018) [18] analyzed the surface tension of HDPAF solutions at different concentrations, obtaining a value of 23.46 mN/m for a 50% solution of the polymer, which differs from those obtained in this study. The difference could be associated with the type of surfactant used, but mainly at the concentration of the biopolymer (70%). In contrast, the addition of β-carotene to the polymer solution caused a significant increase in electrical conductivity from 5.54 ± 0.01 to 7.30 ± 0.03 mS/cm, and this can be attributed to the functional group loads of β-carotene (Table 1).

Table 1. Physicochemical characterization of the 70% high degree of polymerization agave fructans (HDPAF) polymer solution with and without β-carotene.

Parameter	70% HDPAF without β-Carotene	70% HDPAF with β-Carotene
Viscosity [1] (Pa·s)	3.69 ± 0.05 [a]	3.36 ± 0.03 [a]
Surface tension (mN/m)	30.1 ± 0.1 [b]	29.6 ± 0.2 [b]
Electrical conductivity (mS/cm)	5.54 ± 0.01 [c]	7.30 ± 0.03 [d]

Different letters within the same row indicate significant differences among samples ($\alpha = 0.05$). The average values were obtained from the analysis of three replicas. [1] Viscosity values were read at a shear rate of 39.8 s^{-1}.

In the electrospinning process, the high concentrations of HDPAF allowed the increase of intermolecular interactions of the polymer with the solvent, and in the same way, the polymer–polymer crosslinking, favoring the stability of the flow [17]. In addition, polymer chain interactions have a close relationship with concentration and viscosity [24]. However, a high viscosity can cause clogging of the injector partially or totally, but it can also affect the morphology of the fibers due to the presence of artifacts in the structures.

3.2. Micro-Nanofiber Formation Process

The stabilization of the electrospinning process was achieved with a voltage of 19 kV, 200 µL/h feed flow of the polymer solution, 20 cm distance from the injector to the collector with 500 rpm rotation. A concentration of the polymer of 70% (*w*/*w*) was used, which allowed the formation of a network of polymer chains and enough entanglement to electro-stretch the solution, obtaining continuous fibers (Figure 1).

In preliminary studies, the electrospinning process was carried out with a 60% solution (*w*/*w*) of HDPAF concentration. The presence of structures, with artifacts that cannot be considered as spheres or fibers, was observed (Figure 1a). On the contrary, for a concentration of 70% of HDPAF, it was possible to obtain a homogeneous film on the collector. This is directly related to the increase in concentration, the structure of high-polymerization fructans and the molecular arrangement of the terminal chains and interactions that occur during the electrospinning process.

Despite not finding references in literature about fiber formation with HDPAF, some authors such as Lee et al. (2009) [25]; Kai et al. (2015) [26] reported the use of polysaccharides such as alginate, cellulose, chitosan, starch in the formation of fibers by electrospinning, which could be used as natural encapsulants in the area of medicine. HDPAFs have just been used so far for the production of spherical nanocapsules ([18]), which were obtained using a HDPAF concentration of 30% through the

electrospraying process to encapsulate β-carotene. The possibility of obtaining fibers could increase the application field of agave fructans to medicine or biomaterials.

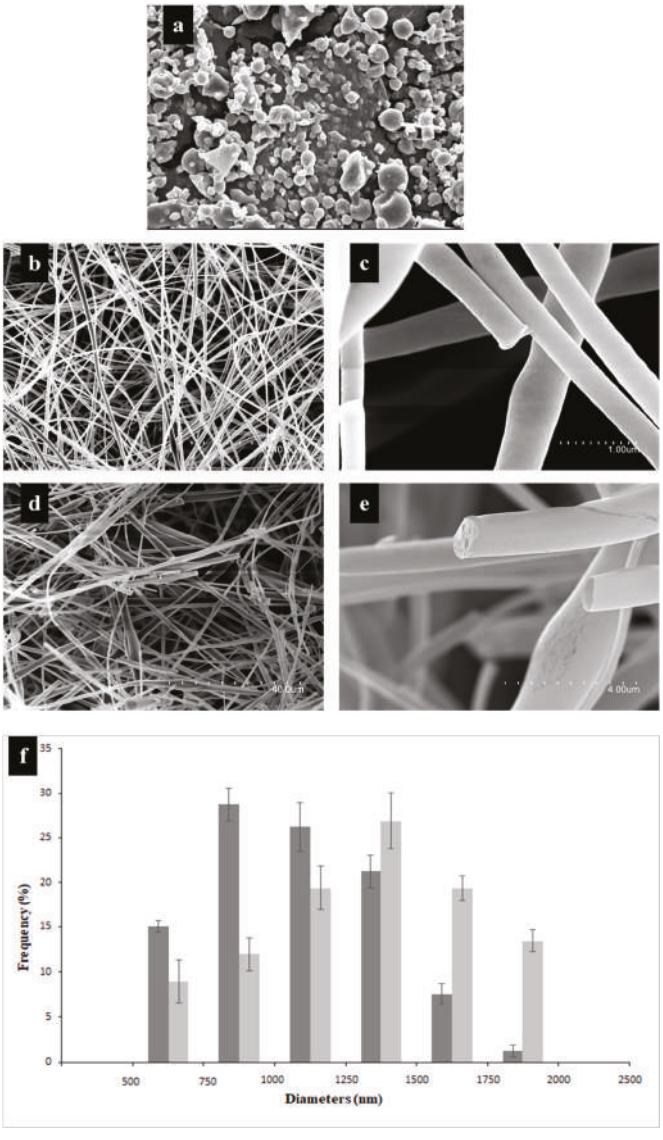

Figure 1. Scanning electron microscopy (SEM) micrographs show structures obtained with (**a**) 60% HDPAF, (**b**,**c**) fibers obtained with 70% HDPAF without β-carotene at different magnification, (**d**,**e**) fibers obtained with 70% HDPAF loaded with β-carotene at different magnification, (**f**) distribution of micro-nanofiber diameters obtained with the 70% HDPAF formulation (■) without and (■) with β-carotene. The average values and standard deviation (SD) were obtained from the analysis of three replicas.

3.3. Morphology Analysis

Fibers obtained with solutions without β-carotene presented a smooth and continuous surface (Figure 1d) with a larger distribution of diameters, in the range of 750 to 1000 nm (Figure 1f). Structures obtained with β-carotene showed smooth, continuous surface fibers, with a slight fragmentation of some structures. This is possibly associated with the applied voltage and its effect on the breaking of the cross-links of the polymer chains. An increase in the diameter size distribution was observed, being in the range between 1250 and 1500 nm. The presence of pores and widenings in some segments was observed, which could be due to the lipophilic nature of β-carotene that limits cross-linking with the polymer or the relative humidity and vapor pressure of the solvent used. The high hygroscopicity of the HDPAF could also affect the diameter of the fibers. Bak et al. (2016) [27] analyzed the effect of relative humidity (30% and 60%) in the manufacture of collagen nanofibers. These authors reported that the quantity of humidity affects the morphological characteristics of the fibers obtained, and therefore concluded that at lower humidity the diameter of the fibers decreases.

3.4. Loading and Encapsulation Efficiency (LE and EE)

The encapsulation efficiency of the β-carotene inside the ultrathin fibers of HDPAF was 95%. This indicates that almost all the loaded compound was encapsulated in the center of the fibers. This value differs with the encapsulation efficiencies obtained with other polysaccharides, such as chitosan, where an encapsulation efficiency of β-carotene of 36% was obtained in the encapsulation by nanomicelles. However, it is similar to the encapsulation efficiency reported for the encapsulation of anthocyanins in xanthan gum in combination with starch (96%) by spray drying [28,29]. HDPAFs show similarities in their entrapment capacity compared to some proteins. In this sense, López-Rubio and Lagaron (2012) [30] report a 90% of encapsulation efficiency for the encapsulation of β-carotene in whey protein. Gomez-Estaca et al. (2012) [31] obtain an encapsulation efficiency between 85 and 90% in encapsules of curcumin into zein by electrospraying. The branched structure of the HDPAF favors the entrapment of the bioactive compound due to its available functional groups, forming bonds such as hydrogen bonds that stabilize the nucleus and maintain the compound of interest in the fiber. The loading efficiency was of 85% in the fibers based on thermogravimetric analysis.

3.5. Thermogravimetric Analysis

A thermogravimetric analysis was performed to the fibers as well as to each of the materials used to make the fibers, in order to study the thermal stability of the β-carotene inside the polymeric wall of HDPAF. The β-carotene displayed an initial decomposition temperature of 138 °C and a final temperature of 367 °C (Figure 2b), similar to the temperatures reported by Peinado et al. (2016) [32] when analyzing this powder compound with a maximum peak of decomposition at approximately 120 °C. In addition, there were two important variations in mass, which are related to the breakdown of the basic structure due to thermal energy, generating the formation of volatile organic compounds including 2-methyl-2-hepten-6-yne, 2-methyl-2-hepten-4-yne and β cyclocitral.

The thermal stability of the fibers in the absence of β-carotene (Figure 2b) was characterized by presenting a first weight loss of 5.0% at 100 °C, which is associated with the humidity content. The second variation occurred between 167 to 307 °C, attributed to HDPAF (57.91%), reaching the maximum decomposition temperature at 209 °C. This temperature is similar to that presented by the individually analyzed HDPAFs, which explains that the surfactant used does not modify the thermal properties of the polymer. Espinosa-Andrews and Urias-Silvas (2012) [33] reported decomposition temperatures of 200 to 222 °C for commercial agave fructans, with a similar thermal behavior to that reported in this study. Regarding the fibers with β-carotene, the thermogram showed three mass variations (Figure 2b).

The first corresponds to humidity (4.0%), the second, between 174 to 232 °C, is attributed to the breakdown of HDPAF according to Figure 2a, the third was in the temperature range of 232 to 288 °C, which was related with the breakdown of β-carotene, a higher degree of polymerization fructans and surfactant according to Figure 2b. This can be explained due to the nature of the compounds and their affinity between β-carotene and HDPAF. Likewise, the fibers with β-carotene showed a displacement of 90 °C in the initial decomposition temperature of this compound, demonstrating the thermoprotective effect of HDPAF.

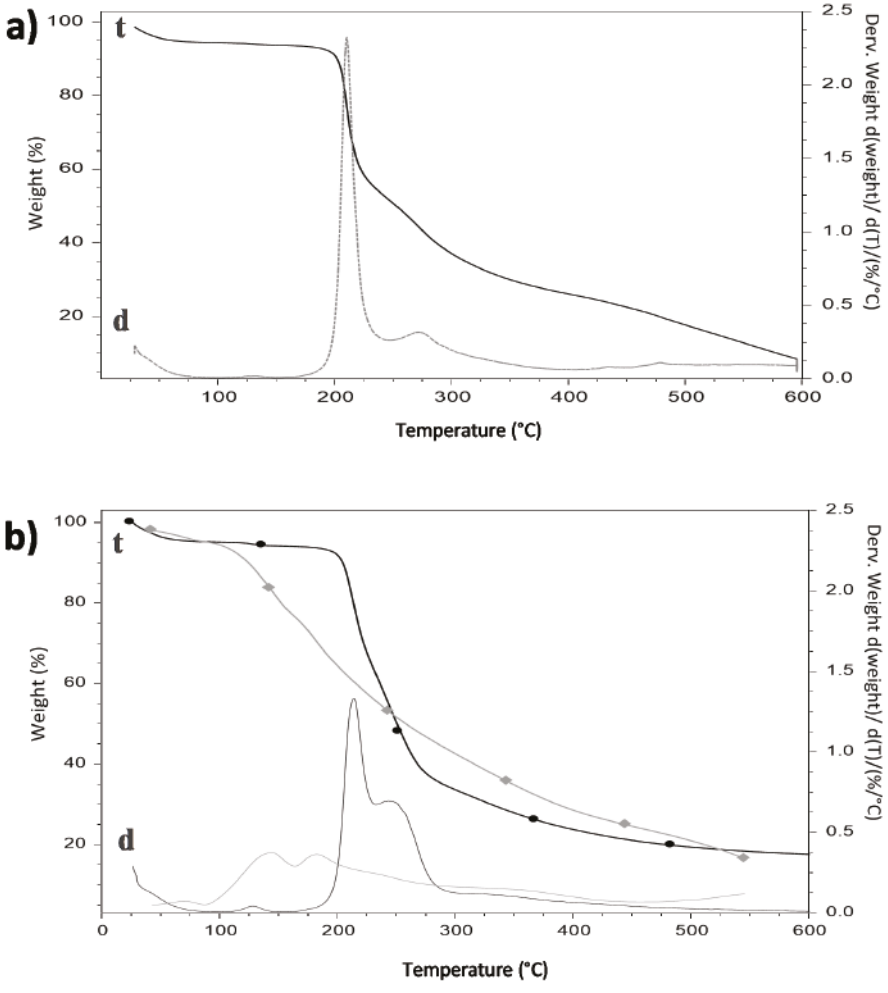

Figure 2. Thermograms of (**a**) HDPAF and (**b**) comparative (♦) β-carotene (●) fibers with β-carotene. (t, indicates thermograms and d, the derivatives of the thermograms).

3.6. Photostability Analysis

The need to evaluate the protection capacity of polymers used in encapsulation processes arises due to the susceptibility of photosensitive compounds to structural modification, such as β-carotene. The photostability of the fibers was evaluated under exposure of the fibers to ultraviolet A (UVA)

light. According to the results, the photooxidation of uncapsulated β-carotene was presented from the beginning of the exposure, becoming total at 24 h.

On the contrary, when β-carotene was encapsulated within the fibers, the loss of its relative content was only 21% until 48 h (Figure 3). This behavior shows the ability of HDPAFs to reduce the photooxidation process, thus, prolonging the stability of β-carotene. Ramos-Hernández et al. (2018) [18] prepared capsules with HDPAF using a polymer concentration of 30% and 0.1% of β-carotene, and the results in the oxidation of β-carotene encapsulated with the electrospraying method showed a loss of 10% in capsules within 48 h. If the protective effect of both morphologies is compared, it is possible to observe that the fibers show twice the oxidation than the capsules, although the β-carotene content is 10 times higher in the fibers. The loss of photostability could be attributed to a reduced biopolymer-bioactive ratio, as well as to an effect of morphology, since the fibers have a larger surface exposed to light. For this reason, taking into account the amount of encapsulated β-carotene and the encapsulation efficiency obtained, the photostabilizing effect of the fiber could be considered very adequate.

In comparison with synthetic polymers, the behavior of the fibers with β-carotene is similar to that presented with the use of HDPAF. Peinado et al. (2016) [32] report a 20% loss of the relative content of the bioactive compound when exposed to UVA fibers made with polyethylene oxide (PEO) attributed to the stability of β-carotene once encapsulated, reflecting the polymer ability to limit oxygen diffusion and reduce exposure to light. On the other hand, de Freitas Zômpero et al. (2015) [34] obtain a 20% reduction after 6 h of exposure to UV light in fibers made with polyvinyl alcohol (PVOH) loaded with nanoliposomes, with the aim of analyzing the stability of the β-carotene. Whereas, the fibers in the present study show a reduction of 7% in the same period of time, which proves that HDPAFs have the ability to protect photosensitive compounds.

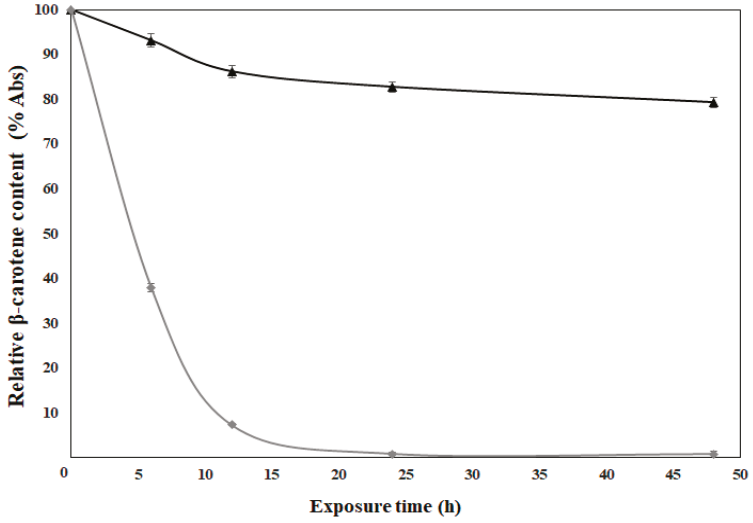

Figure 3. Photostability kinetics of the β-carotene (♦) and 70% HDPAF micro-nanofibers loaded with β-carotene (▲).

4. Conclusions

To the best of our knowledge, this paper reports for the very first time the possibility of generating continuous micro- and nanometric scale fibers from agave fructans of high degree of polymerization in 70% (*w*/*w*) solutions. This document also reports the possibility to encapsulate a bioactive model

compound, such as β-carotene inside the fibers, obtaining a high encapsulation efficiency as well as providing stability to both temperature and UVA radiation.

The good results provided by fructans could suppose the expansion of its use and exploitations, since they could be a feasible alternative to replace synthetic polymers in the encapsulation of compounds of high biological value, as well as expanding their use in biomedical and pharmaceutical products. In this spirit, it is of important interest to consider the study of possible complexes with other polymers that help enhance their characteristics and properties, such as its high hygroscopicity, and structures more homogeneous, as well as their incursion into new applications.

Author Contributions: Conceptualization by J.A.R.-S. and J.M.L.; methodology, validation, and formal analysis was carried out by C.N.C.-S., J.A.R.-S., M.C.-S., C.P., and J.M.L.; investigation, resources, data curation, writing—original draft preparation and writing—review and editing was performed by C.N.C.-S., J.A.R.-S., M.C.-S., C.P., and J.M.L.; visualization, supervision, project administration, funding acquisition was carried out by J.A.R.-S. and J.M.L.

Funding: This study was supported by the Consejo Nacional de Ciencia y Tecnoligía (CONACyT, Mexico) for the scholarship granted (Number 702624) to Carla Norma Cruz Salas; CYTED thematic network code 319RT0576 and Spanish Ministry of Science, Innovation and Universities (proyect code RTI2018-097249-B-C21).

Acknowledgments: We thank Rosa Isela Ortiz-Basurto for providing the high degree of polymerization Agave fructans (HDPAF), Jorge Alberto Ramos-Hernandez and Elda Margarita Gonzalez-Cruz for your technical assistance.

Conflicts of Interest: The authors declare no conflict of interest.

References

1. Apolinário, A.C.; De Lima Damasceno, B.P.G.; De Macêdo Beltrão, N.E.; Pessoa, A.; Converti, A.; Da Silva, J.A. Inulin-Type Fructans: A Review on Different Aspects of Biochemical and Pharmaceutical Technology. *Carbohydr. Polym.* **2014**, *101*, 368–378. [CrossRef]
2. Saénz, C.; Tapia, S.; Chávez, J.; Robert, P. Microencapsulation by Spray Drying of Bioactive Compounds from Cactus Pear (Opuntia Ficus-Indica). *Food Chem.* **2009**, *114*, 616–622. [CrossRef]
3. Moreno-Vilet, L.; Bostyn, S.; Flores-Montaño, J.L.; Camacho-Ruiz, R.M. Size-Exclusion Chromatography (HPLC-SEC) Technique Optimization by Simplex Method to Estimate Molecular Weight Distribution of Agave Fructans. *Food Chem.* **2017**, *237*, 833–840. [CrossRef] [PubMed]
4. Waleckx, E.; Gschaedler, A.; Colonna-Ceccaldi, B.; Monsan, P. Hydrolysis of Fructans from Agave Tequilana Weber Var. Azul during the Cooking Step in a Traditional Tequila Elaboration Process. *Food Chem.* **2008**, *108*, 40–48. [CrossRef]
5. García Gamboa, R.; Ortiz Basurto, R.I.; Calderón Santoyo, M.; Bravo Madrigal, J.; Ruiz Álvarez, B.E.; González Avila, M. In Vitro Evaluation of Prebiotic Activity, Pathogen Inhibition and Enzymatic Metabolism of Intestinal Bacteria in the Presence of Fructans Extracted from Agave: A Comparison Based on Polymerization Degree. *LWT Food Sci. Technol.* **2018**, *92*, 380–387. [CrossRef]
6. Farías-Cervantes, V.S.; Chávez-Rodríguez, A.; Delgado-Licon, E.; Aguilar, J.; Medrano-Roldan, H.; Andrade-González, I. Effect of Spray Drying of Agave Fructans, Nopal Mucilage and Aloe Vera Juice. *J. Food Process. Preserv.* **2017**, *41*, e13027. [CrossRef]
7. Lopez, M.G.; Mancilla-Margalli, N.A.; Mendoza-Diaz, G. Molecular Structures of Fructans from Agave Tequilana Weber Var. Azul. *J. Agric. Food Chem.* **2003**, *51*, 7835–7840. [CrossRef]
8. Da Fonseca Contado, E.W.N.; de Rezende Queiroz, E.; Rocha, D.A.; Fraguas, R.M.; Simao, A.A.; Botelho, L.N.S.; de Fatima Abreu, A.; de Abreu, M.A.B.C.M.P. Extraction, Quantification and Degree of Polymerization of Yacon (Smallanthus Sonchifolia) Fructans. *Afr. J. Biotechnol.* **2015**, *14*, 1783–1789. [CrossRef]
9. Carranza, C.O.; Fernandez, A.Á.; Bustillo Armendáriz, G.R.; López-Munguía, A. *Processing of Fructans and Oligosaccharides from Agave Plants*; Elsevier Inc.: Amsterdam, The Netherlands, 2014. [CrossRef]
10. Toriz, G.; Delgado, E.; Zúñiga, V. A Proposed Chemical Structure for Fructans from Blue Agave Plant (Tequilana Weber Var. Azul). *Rev. Electrónica Y Tecnológica e-Gnosis* **2007**, *5*, 1.
11. Ortiz-Basurto, R.I.; Rubio-Ibarra, M.E.; Ragazzo-Sanchez, J.A.; Beristain, C.I.; Jiménez-Fernández, M. Microencapsulation of Eugenia Uniflora L. Juice by Spray Drying Using Fructans with Different Degrees of Polymerisation. *Carbohydr. Polym.* **2017**, *175*, 603–609. [CrossRef]

12. Farías Cervantes, V.S.; Delgado Lincon, E.; Solís Soto, A.; Medrano Roldan, H.; Andrade González, I. Effect of Spray Drying Temperature and Agave Fructans Concentration as Carrier Agent on the Quality Properties of Blackberry Powder. *Int. J. Food Eng.* **2016**, *12*, 451–459. [CrossRef]
13. Wen, P.; Zong, M.H.; Linhardt, R.J.; Feng, K.; Wu, H. Electrospinning: A Novel Nano-Encapsulation Approach for Bioactive Compounds. *Trends Food Sci. Technol.* **2017**, *70*, 56–68. [CrossRef]
14. Anu Bhushani, J.; Anandharamakrishnan, C. Electrospinning and Electrospraying Techniques: Potential Food Based Applications. *Trends Food Sci. Technol.* **2014**, *38*, 21–33. [CrossRef]
15. Haider, A.; Haider, S.; Kang, I.K. A Comprehensive Review Summarizing the Effect of Electrospinning Parameters and Potential Applications of Nanofibers in Biomedical and Biotechnology. *Arab. J. Chem.* **2018**, *11*, 1165–1188. [CrossRef]
16. Le Corre-Bordes, D.; Hofman, K.; Hall, B. Guide to Electrospinning Denatured Whole Chain Collagen from Hoki Fish Using Benign Solvents. *Int. J. Biol. Macromol.* **2018**, *112*, 1289–1299. [CrossRef] [PubMed]
17. Ghorani, B.; Tucker, N. Fundamentals of Electrospinning as a Novel Delivery Vehicle for Bioactive Compounds in Food Nanotechnology. *Food Hydrocoll.* **2015**, *51*, 227–240. [CrossRef]
18. Ramos-Hernández, J.; Ragazzo-Sánchez, J.; Calderón-Santoyo, M.; Ortiz-Basurto, R.; Prieto, C.; Lagaron, J. Use of Electrosprayed Agave Fructans as Nanoencapsulating Hydrocolloids for Bioactives. *Nanomaterials* **2018**, *8*, 868. [CrossRef]
19. Fernandez, A.; Torres-Giner, S.; Lagaron, J.M. Novel Route to Stabilization of Bioactive Antioxidants by Encapsulation in Electrospun Fibers of Zein Prolamine. *Food Hydrocoll.* **2009**, *23*, 1427–1432. [CrossRef]
20. Ozkan, G.; Franco, P.; De Marco, I.; Xiao, J.; Capanoglu, E. A Review of Microencapsulation Methods for Food Antioxidants: Principles, Advantages, Drawbacks and Applications. *Food Chem.* **2019**, *272*, 494–506. [CrossRef]
21. Fu, D.; Deng, S.; McClements, D.J.; Zhou, L.; Zou, L.; Yi, J.; Liu, C.; Liu, W. Encapsulation of β-Carotene in Wheat Gluten Nanoparticle-Xanthan Gum-Stabilized Pickering Emulsions: Enhancement of Carotenoid Stability and Bioaccessibility. *Food Hydrocoll.* **2019**, *89*, 80–89. [CrossRef]
22. González-Reza, R.M.; Quintanar-Guerrero, D.; Flores-Minutti, J.J.; Gutiérrez-Cortez, E.; Zambrano-Zaragoza, M.L. Nanocapsules of β-Carotene: Thermal Degradation Kinetics in a Scraped Surface Heat Exchanger (SSHE). *LWT Food Sci. Technol.* **2015**, *60*, 124–130. [CrossRef]
23. Kutzli, I.; Gibis, M.; Baier, S.K.; Weiss, J. Electrospinning of Whey and Soy Protein Mixed with Maltodextrin—Influence of Protein Type and Ratio on the Production and Morphology of Fibers. *Food Hydrocoll.* **2019**, *93*, 206–214. [CrossRef]
24. Hulsey, S.; Absar, S.; Choi, H. Comparative Study of Polymer Dissolution Techniques for Electrospinning. *Procedia Manuf.* **2017**, *10*, 652–661. [CrossRef]
25. Lee, K.Y.; Jeong, L.; Kang, Y.O.; Lee, S.J.; Park, W.H. Electrospinning of Polysaccharides for Regenerative Medicine. *Adv. Drug Deliv. Rev.* **2009**, *61*, 1020–1032. [CrossRef] [PubMed]
26. Kai, D.; Liow, S.S.; Loh, X.J. Biodegradable Polymers for Electrospinning: Towards Biomedical Applications. *Mater. Sci. Eng. C* **2015**, *45*, 659–670. [CrossRef] [PubMed]
27. Bak, S.Y.; Yoon, G.J.; Lee, S.W.; Kim, H.W. Effect of Humidity and Benign Solvent Composition on Electrospinning of Collagen Nanofibrous Sheets. *Mater. Lett.* **2016**, *181*, 136–139. [CrossRef]
28. Cai, X.; Du, X.; Cui, D.; Wang, X.; Yang, Z.; Zhu, G. Improvement of Stability of Blueberry Anthocyanins by Carboxymethyl Starch/Xanthan Gum Combinations Microencapsulation. *Food Hydrocoll.* **2019**, *91*, 238–245. [CrossRef]
29. Ge, W.; Li, D.; Chen, M.; Wang, X.; Liu, S.; Sun, R. Characterization and Antioxidant Activity of β-Carotene Loaded Chitosan-Graft-Poly (Lactide) Nanomicelles. *Carbohydr. Polym.* **2015**, *117*, 169–176. [CrossRef]
30. López-Rubio, A.; Lagaron, J.M. Whey Protein Capsules Obtained through Electrospraying for the Encapsulation of Bioactives. *Innov. Food Sci. Emerg. Technol.* **2012**, *13*, 200–206. [CrossRef]
31. Gomez-Estaca, J.; Balaguer, M.P.; Gavara, R.; Hernandez-Munoz, P. Formation of Zein Nanoparticles by Electrohydrodynamic Atomization: Effect of the Main Processing Variables and Suitability for Encapsulating the Food Coloring and Active Ingredient Curcumin. *Food Hydrocoll.* **2012**, *28*, 82–91. [CrossRef]
32. Peinado, I.; Mason, M.; Romano, A.; Biasioli, F.; Scampicchio, M. Stability of β-Carotene in Polyethylene Oxide Electrospun Nanofibers. *Appl. Surf. Sci.* **2016**, *370*, 111–116. [CrossRef]

33. Espinosa-Andrews, H.; Urias-Silvas, J.E. Thermal Properties of Agave Fructans (Agave Tequilana Weber Var. Azul). *Carbohydr. Polym.* **2012**, *87*, 2671–2676. [CrossRef]
34. De Freitas Zômpero, R.H.; López-Rubio, A.; de Pinho, S.C.; Lagaron, J.M.; de la Torre, L.G. Hybrid Encapsulation Structures Based on β-Carotene-Loaded Nanoliposomes within Electrospun Fibers. *Colloids Surf. B Biointerfaces* **2015**, *134*, 475–482. [CrossRef] [PubMed]

nanomaterials

MDPI

Article

Preparation, Characterization and Properties of Porous PLA/PEG/Curcumin Composite Nanofibers for Antibacterial Application

Feifei Wang †, Zhaoyang Sun †, Jing Yin † and Lan Xu *

National Engineering Laboratory for Modern Silk, College of Textile and Engineering, Soochow University, 199 Ren-ai Road, Suzhou 215123, China; ffwang@stu.suda.edu.cn (F.W.); zhaoyangsun1991@163.com (Z.S.); 20184215040@stu.suda.edu.cn (J.Y.)

* Correspondence: lanxu@suda.edu.cn; Tel.: +86-512-65884521

† F.W., Z.S. and J.Y. contributed equally to this paper.

Received: 23 February 2019; Accepted: 21 March 2019; Published: 2 April 2019

Abstract: Polylactide/polyethylene glycol/curcumin (PLA/PEG/Cur) composite nanofibers (CNFs) with varying ratios of PEG were successfully fabricated by electrospinning. Characterizations of the samples, such as the porous structure, crystalline structure, pore size, wetting property and Cur release property were investigated by a combination of scanning electron microscopy (SEM), Fourier-transform infrared (FTIR) spectroscopy, X-ray diffraction (XRD) and UV spectrophotometer. The antibacterial properties of the prepared porous CNFs against *Escherichia coli* bacteria were studied. The results showed that with the decrease of PEG in the CNFs, there appeared an evident porous structure on the CNF surface, and the porous structure could enhance the release properties of Cur from the CNFs. When the weight ratio (PEG:PLA) was 1:9, the pore structure of the nanofiber surface became most evident and the amount of Cur released was highest. However, the antibacterial effect of nonporous CNFs was better due to burst release over a short period of time. That meant that the porous structure of the CNFs could reduce the burst release and provide better control over the drug release.

Keywords: electrospinning; curcumin; PLA/PEG/curcumin nanofiber; drug release; porous nanofiber

1. Introduction

Electrospinning has been recognized as a simple and efficient technique for the fabrication of composite nanofibers (CNFs). The application of electrospun nanofibers can be improved by increasing the specific surface area and porosity of the nanofibers. Because of high porosity, high specific surface area and high surface activity, porous nanofibers have many existing and potential applications in drug delivery, tissue engineering, electronic engineering, and so on [1–5].

Curcumin (Cur) is a polyphenol compound extracted from the rhizome of the plant *Curcuma longa*. Recently, it was reported that Cur has a wide range of pharmacologic activities, such as anti-inflammation, anti-human immunodeficiency virus (HIV), anti-microbial, anti-oxidant, anti-parasitic, anti-mutagenic and anti-cancer, with low or no intrinsic toxicity [6–8]. Polylactic acid (PLA) has been widely used in biomedical and tissue engineering because of its excellent biocompatibility and biodegradability [9]. Lu et al. [10] investigated the effects of electrospraying a solution system and concentration of polyethylene oxide (PEO) on the morphologies of the single-drug and dual-drug loaded nanocomposites. Zhang et al. [11] reported that the polyethylene glycolation (PEGylation) modification could afford a faster release profile of the encapsulated drug than pure poly(lactic-co-glycolic acid) (PLGA) nanofibers, and the drug-loaded PLGA-PEG nanofibers were able to inhibit the growth of a model bacterium, *Staphylococcus aureus*. Ramírez-Agudelo et al. [12] found that composite nanofibers were easier to obtain an antibacterial property compared to a single polymer system. And the antibacterial

composite with bacterial cellulose could prolong the antimicrobial activity against both *E. coli* and *S. aureus* [13]. Phan et al. [14] prepared and characterized a series of polymeric micellar formulations of Cur for targeted cancer therapy. Aytac et al. [15] designed core-shell nanofibers via coaxial-electrospinning using an inclusion complex of curcumin with cyclodextrin in the core and polylactide (PLA) in the shell. Zhong et al. [16] prepared PLA and a PLA-b-PEG composite porous scaffold loaded with a high dose of aspirin, using the solvent casting/particulate leaching technique, and found that the amphiphilic block polymer could efficiently enhance the dispersion property and stabilize the release of hydrophilic drugs. Shaik et al. [17] investigated the preventive role of orally administered *Aloe vera* supplemented probiotic *lassi* (APL) on *Shigella dysenteriae* infection in mice, and found that the immunoprotective effects of APL against *Shigella dysenteriae* induced infection in mice. Feng et al. [18] used tea polyphenol (TP) as an additive to develop to inhibit the spoilage of fish fillet during cold storage.

In this paper, electrospun PLA/PEG/Cur porous CNFs were fabricated by controlling the weight ratio of PEG:PLA. The effects of this ratio on the morphology and porous structure of CNFs were studied by scanning electron microscopy (SEM) and capillary flow porometry. Successful entrapments of Cur in the PEG/PLA CNFs were validated by Fourier-transform infrared (FTIR) spectroscopy and X-ray diffraction (XRD). Then, the properties of these CNFs with various PEG:PLA ratios were investigated by a contact angle (CA) measurement apparatus, UV spectrophotometer and shaking incubator. The results showed the CA and the cumulative release of Cur increased with the decrease of PEG, due to the appearance of a porous structure on the nanofiber surface. However, the antibacterial effect of the nonporous composite nanofiber membranes (CNFMs) was better due to burst release over a short period of time. The initial burst release of Cur was prevented by the porous structure of the porous CNFs compared to nonporous CNFs. That meant that the porous structure of CNFs could reduce the burst release and allow better control of the drug release.

2. Experimental

2.1. Materials

Polylactic acid (PLA), with an average molecular weight of 22,000 g/mol, was purchased from Anqing chemical Co. Ltd. (Anhui, China). The polyethylene glycol (PEG) with an average molecular weight of 400 g/mol was supplied by Sangon Biotech Co. Ltd. (Shanghai, China). The *N*,*N*-Dimethylformamide (DMF) (Analytical Reagent), chloroform (CF) (Analytical Reagent) and phosphate buffered saline (PBS) (Analytical Reagent, pH 7.4) were purchased from Shanghai Chemical Reagent Co. Ltd. (Shanghai, China). The curcumin (Cur) ($\geq$95.0% purity) was purchased from Shanghai Yuanye Biotechnology Co. Ltd. (Shanghai, China). *E. coli* for antibacterial tests were obtained from Soochow University (Suzhou, China). The nutrient broth medium and nutrient agar medium were purchased from SCAS Ecoscience Technology Inc. (Shanghai, China). All chemicals were used without further purification.

2.2. Preparation of PLA/PEG/Cur CNFs

The concentration was measured by weight. PEG and PLA with various weight ratios of 1:1, 1:3, 1:5, 1:7 and 1:9 were respectively dissolved in a solvent mixture of DMF and CF, with a weight ratio of 1:9. The concentrations of mixed solutions (PEG and PLA weight ratio to solution) were all 8 wt%. Then, a certain amount of Cur was added into the PEG/PLA solutions and the weight ratio of Cur to PEG/PLA was 3:100. The prepared solutions were magnetically stirred for 3 h to ensure homogeneous mixing.

The obtained spinning solution was dropped into a 10 mL syringe. According to our previous work [1,5], the electrospinning parameters were set as follows: The flow rate was 0.6 mL/h, the applied voltage was 15 kV, and the working distance from the needle tip to the collector was 14 cm. All electrospinning experiments were carried out at room temperature (20 °C) and a humidity of 60%.

2.3. Characterizations and Measurements

The electrical conductivity and viscosity of spinning solutions were determined respectively by a conductivity meter (DDS-307, Shanghai instrument & electric Scientific Instrument Co., Ltd., Shanghai, China) and a viscometer (NDJ-5S, Shanghai Nirun Intelligent Technology Co., Ltd., Shanghai, China). The measurement was repeated three times.

The surface morphologies of PLA/PEG/Cur CNFs were carried out using a scanning electron microscopy (SEM, Hitachi S-4800, Tokyo, Japan) at an acceleration voltage of 3 KV. The diameter distribution of the nanofibers was characterized by Image J software (National Institute of Mental Health, Bethesda, MD, USA). Twenty SEM images of 50 nanofibers in each SEM image were chosen at random for diameter distribution analysis.

The mixture, consisting of 1 mg of shredded PLA/PEG/Cur CNFMs and 200 mg of KBr powder, was pressed into a flaky sample, which was used in the Fourier-transform infrared (FTIR) analysis. The sample was characterized using FTIR spectroscopy (Nicolet 5700, Thermo Fisher Scientific, Waltham, WA, USA). The FTIR spectrum of the sample was obtained by the performance of 32 scans with the wavenumber range of 400–4000 cm^{-1} and a resolution of 4 cm^{-1}.

X-ray diffraction (XRD) analyses were performed to illustrate the crystalline structures of Cur powders and PLA/PEG/Cur CNFs using a Philips X'Pert-Pro MPD with a 3 KW ceramic tube as the X-ray source (Cu-Kα) and an X'Celerator detector. Cu-Kα radiation was used with a diffraction angle range of 10–60° at 40 kV and 200 mA at a scanning rate of 10°/min.

The pore size distributions of PLA/PEG/Cur CNFMs were determined using capillary flow porometry (Porometer 3G, Quantachrome Instruments, Boynton, FL, USA), which employed the technique of expelling a wetting liquid, Porofil, from through-pores in the sample. All samples were circular membranes with a diameter of 25 mm and a thickness of 10 μm.

The wettability of the PLA/PEG/Cur CNFMs was characterized using an optical contact angle (CA) measurement instrument (Krüss DSA100, Krüss Company, Hamburg, Germany). The volume of the deionized water droplet used for static CA measurement was 6 μL. The CAs were measured by the sessile drop method [19]. Moreover, the average CAs were determined by measuring six different positions of the same sample.

2.4. In Vitro Release of Cur

Electrospun PLA/PEG/Cur CNFs (10 mg) were dispersed in 3 mL of PBS (PH 7.4) as a release medium and then placed in 25 mL centrifuge tubes (Shanghai Hongsheng Biotech Co. Ltd., Shanghai, China). These centrifuge tubes were incubated in a shaking incubator (FLY-100/200, Shanghai Shenxian Thermostatic Equipment Factory, Shanghai, China) at 37.4 °C with a shaking speed of 60 rpm. At desired intervals, 1 mL of the release medium was withdrawn for Cur release rate analysis, and an equal volume of fresh PBS was replenished for sustaining the incubation. The released amounts of Cur were measured by UV spectrophotometer (Cary 5000, Agilent Technologies, Santa Clara, CA, USA).

2.5. Antimicrobial Tests

The PLA/PEG/Cur CNFMs were cut into 5 mm × 5 mm shreds and were sterilized for 30 min, at a temperature of 125 °C and a pressure of 10^3 KPa. The antibacterial effects of these PLA/PEG/Cur CNFMs on a bacterial strain, *E. coli*, were investigated. Overnight cultures of *E. coli* derived from a single colony and cultivated in nutrient broth medium were used in the study. Each culture solution (1 mL) was inoculated into 9 mL of PBS, resulting in a concentration of 3×10^5–5×10^5 colony forming units (CFUs/mL). These bacterial solutions with a concentration of 3×10^5–5×10^5 CFUs/mL were used for the antibacterial tests, and bacterial solutions incubated in pure PBS only served as controls.

In a conical flask, 375 mg of shredded PLA/PEG/Cur CNFMs were dispersed in 35 mL of PBS, and then 5 mL of bacterial solutions with a concentration of prepared 3×10^5–5×10^5 CFUs/mL were added. The conical flask was shaken in a constant temperature incubator shaker (IS-RDV1,

Crystal Technology & Industries, Inc., Dallas, TX, USA) at 25 °C with a shaking speed of 300 rpm for 20 h. Aliquots (1 mL) of the obtained samples were placed on nutrient agar plates in multiple replicates. Each sample was prepared separately in a triplicate. The growth of the *E. coli* was evaluated by counting CFUs after incubation for 24 h at 37 °C. The inhibition rate was calculated according to the following equation [20]:

$$\text{Inhibition rate } (\%) = \frac{\text{CFUcontrol group} - \text{CFUexperimental group}}{\text{CFUcontrol group}} \times 100\%$$

3. Results and Discussion

3.1. Properties Characterization of Spinning Solutions

The electrical conductivity and viscosity of the spinning solutions with the different weight ratios (PEG:PLA) are shown in Table 1. It was obvious that as the content of the PLA increased, the viscosity of solutions increased due to increased average molecular weight [21], which resulted in a decrease of the electrical conductivity of the solutions [22]. The viscosity played an important role in determining the diameter of the electrospun nanofibers [1].

Table 1. Properties characterization of spinning solutions with the different weight ratio (polyethylene glycol:polylactide, or PEG:PLA).

PEG:PLA	Electrical Conductivity (μs/cm)	Viscosity (mPa·s)
1:1	0.455 ± 0.045	33 ± 2
1:3	0.432 ± 0.038	77 ± 4
1:5	0.421 ± 0.035	112 ± 3
1:7	0.267 ± 0.052	137 ± 3
1:9	0.249 ± 0.048	157 ± 4

3.2. Morphological Characterization of PLA/PEG/Cur CNFs (SEM)

The surface morphologies of the electrospun PLA/PEG/Cur CNFs with different weight ratios (PEG:PLA) were investigated by SEM. Figure 1 shows SEM images of the CNFs and the respective nanofiber diameter distributions. It could be seen that with the decrease in the weight ratio (PEG:PLA), the surface morphology of the CNFs changed from smooth to porous. A further decrease of PEG in the mixtures, with the weight ratio 1:5, resulted in the appearance of evident pores on the CNF surfaces. When the weight ratio (PEG:PLA) was 1:7 and 1:9, the pore structure of the nanofiber surfaces became very noticeable, and the diameters of the porous nanofibers increased due to an increased pore number. This could be explained by the plastic deformation of PLA in water, which led to the formation of the pore structure, due to the solvent volatilization at a suitable humidity in the electrospinning process. Therefore, as the PLA content increased to a certain proportion, evident pore structures appeared on the nanofiber surfaces.

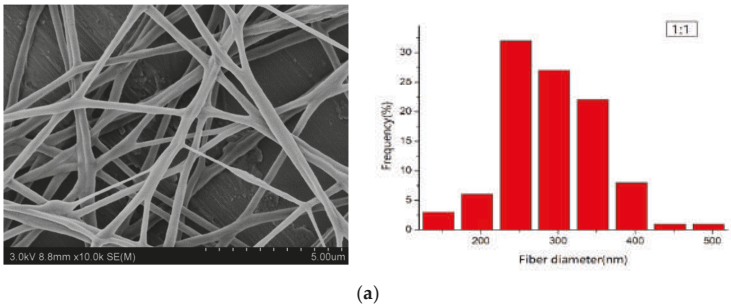

(**a**)

Figure 1. *Cont.*

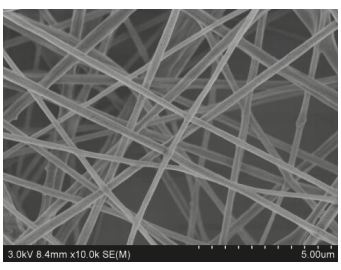

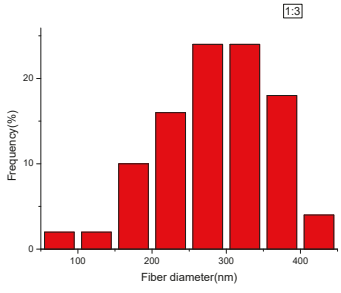

(**b**)

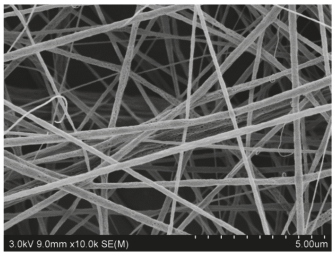

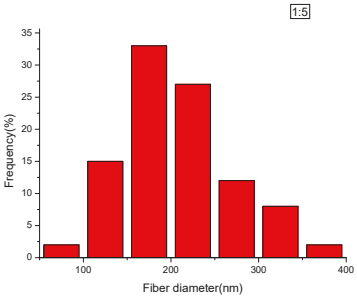

(**c**)

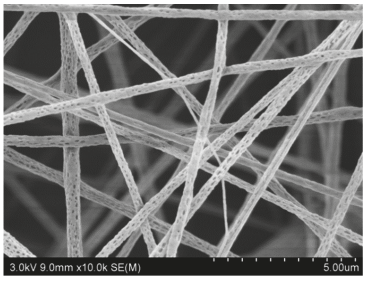

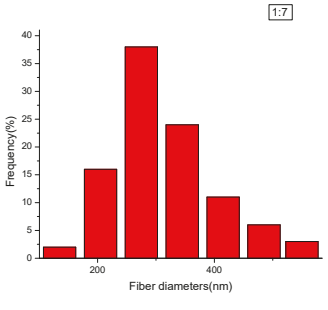

(**d**)

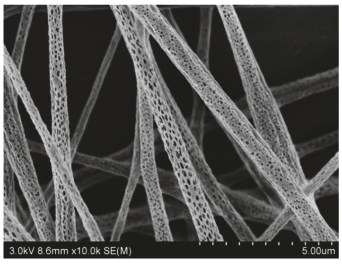

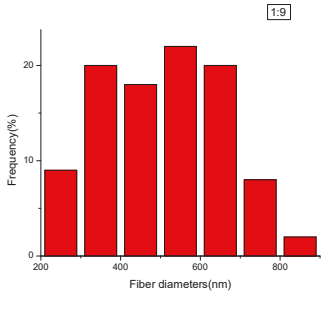

(**e**)

Figure 1. SEM pictures of the electrospun polylactide/polyethylene glycol/curcumin (PLA/PEG/Cur) carbon nanofibers (CNFs) with different weight ratios (PEG:PLA). The right figures were the according diameter distribution: (**a**) 1:1, (**b**) 1:3, (**c**) 1:5, (**d**) 1:7, (**e**) 1:9.

In addition, the relationship between the weight ratio (PEG:PLA) and the average diameters of the electrospun CNFs is shown in Table 2, with the confidence intervals calculated according to Reference [1]. Table 2 illustrates that with the decrease of the weight ratio (PEG:PLA), the average diameters of the CNFs decreased. This was firstly due to better spinnability of the spinning solution, which increased rapidly with a weight ratio of 1:7, due to the formation of pores [21]. When the contents of PEG were too much, such as 1:1 and 1:3 (mass ratios to PLA), the viscosity of the spinning solution was too low, which resulted in poor spinnability of the solution.

Table 2. The relationship between the weight ratio (PEG:PLA) and the average diameters of CNFs.

PEG:PLA	Average Diameter ($\bar{D}$) (nm)	Standard Deviation (σ) (nm)	Confidence Interval (nm)
1:1	290.60	64.08	±12.56
1:3	287.70	74.39	±16.91
1:5	205.16	59.43	±11.64
1:7	308.73	91.25	±17.89
1:9	552.81	195.53	±38.32

3.3. Fourier-Transform Infrared (FTIR) and Raman Spectrum Analysis

The presences of Cur in the PEG/PLA CNFs with the different weight ratios (PEG:PLA) were confirmed by Fourier-transform infrared (FTIR) spectroscopy, as shown in Figure 2. The FTIR spectra of these PLA/PEG/Cur CNFs displayed characteristic absorption bands at 1754 cm^{-1} and 1087 cm^{-1}, which represented the backbone ester group of PLA [4], and also showed a CH_3 asymmetric bending peak at 1454 cm^{-1}, a C-O stretching peak at 1182 cm^{-1} and a O-H bending peak at 1047 cm^{-1} of PLA. In addition, the absorption peak at 1128 cm^{-1} could be attributed to C-O-C characteristic vibration of PEG [23]. Moreover, it was obvious that a sharp peak appeared at 1272 cm^{-1} due to the C-O stretching vibration in -C-OCH_3 of the phenyl ring of Cur [24]. As seen in Figure 2, Cur was encapsulated in the CNFs, and the intensity of the peaks corresponding to PLA in FTIR spectra of samples increased as the PLA contents increased.

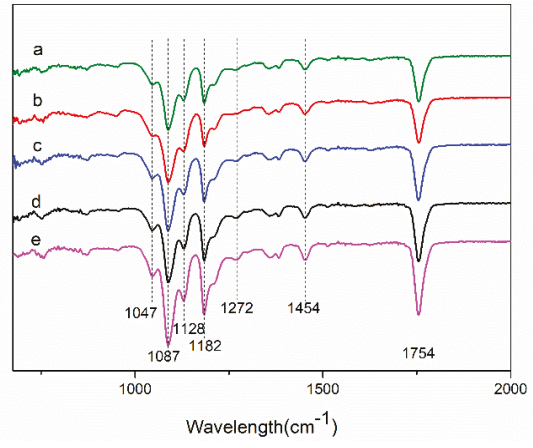

Figure 2. Fourier-transform infrared (FTIR) spectra of PLA/PEG/Cur CNFs with different weight ratios (PEG:PLA): (**a**) 1:1; (**b**) 1:3; (**c**) 1:5; (**d**) 1:7; (**e**) 1:9.

3.4. X-ray Diffraction (XRD) Spectrum Analysis

XRD patterns with distinctive crystalline peaks of Cur and PLA/PEG/Cur CNFs with different weight ratios (PEG:PLA) are shown in Figure 3. As seen in Figure 3A, the XRD spectrum of Cur

displayed sharp and intense peaks of crystallinity, which suggested a highly crystalline nature. Figure 3B shows the XRD spectra of the CNFs with different weight ratios (PEG:PLA). It could be observed that the peaks at 2θ = 16.88° and 22.58° could be assigned as (010) crystal planes of PEG and (015) crystal planes of PLA, respectively. With the decrease of PEG, the XRD spectra of the CNFs showed a reduction of peak intensity, as compared to the Cur, which indicated decreased crystallinity or changes into an amorphous phase of the drug [6]. The principal peak of Cur at 2θ = 17.08° did not appear due to the low ratio of Cur with respect to the polymer composite.

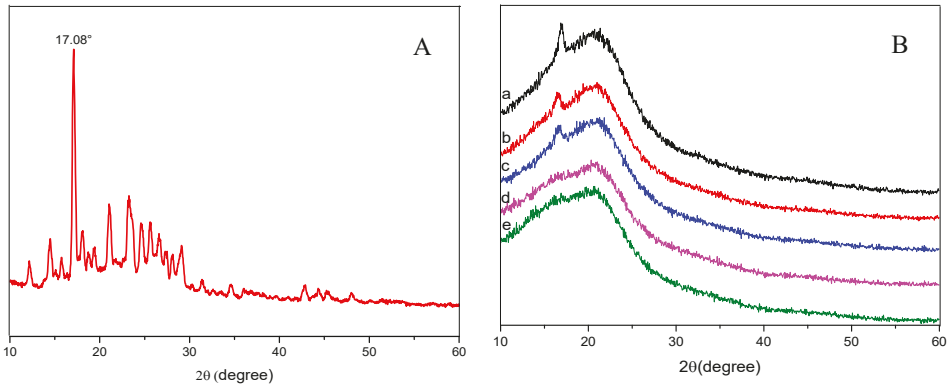

Figure 3. XRD spectra of Cur (**A**). XRD spectra of PLA/PEG/Cur CNFs with the different weight ratio (PEG:PLA): (**a**) 1:1; (**b**) 1:3; (**c**) 1:5; (**d**) 1:7; (**e**) 1:9 (**B**).

3.5. Measuring Pore Size Distribution Composite Membranes

Figure 4 illustrates the pore size distributions of the PLA/PEG/Cur CNFMs with varying PEG weight ratios, measured by a capillary flow porometry, and Table 3 shows the size and number of pores. It could be seen that as the PEG weight ratio decreased, the pore size of the CNFMs increased, and the respective pore number of the CNFMs decreased. Moreover, the pore distributions of the CNFMs with the weight ratios 1:7 and 1:9 (PEG:PLA) demonstrated more uniformity. These results were in agreement with the SEM images, as illustrated in Figure 1.

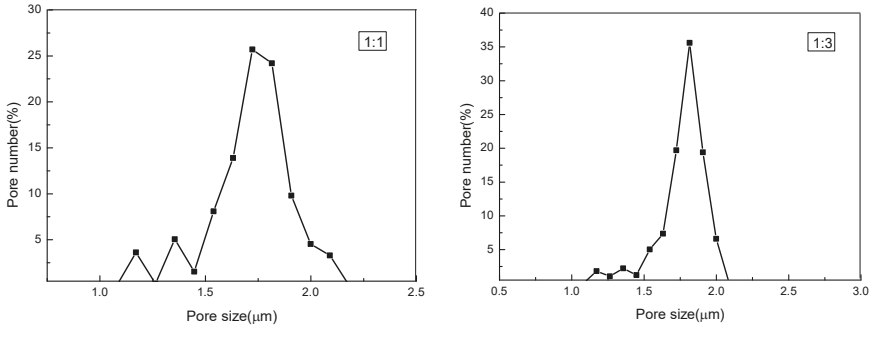

Figure 4. *Cont.*

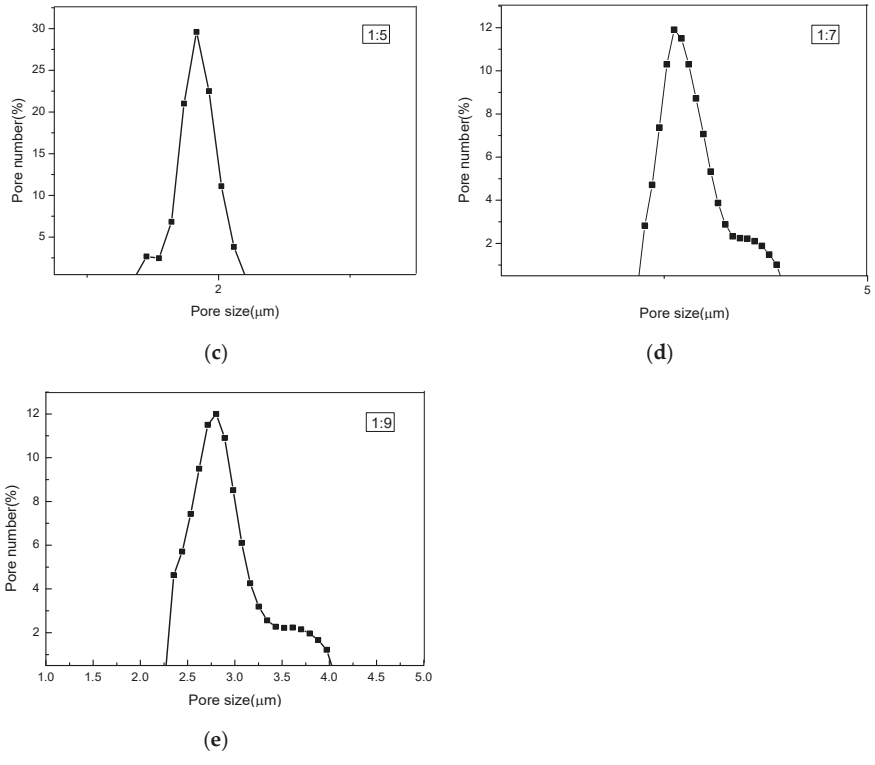

Figure 4. The pore size distributions of PLA/PEG/Cur nonporous composite nanofiber membranes (CNFMs) with different weight ratios (PEG:PLA): (**a**) 1:1; (**b**) 1:3; (**c**) 1:5; (**d**) 1:7; (**e**) 1:9.

Table 3. The analysis of pore size distributions of the CNFMs with different weight ratios (PEG:PLA).

PEG:PLA	Pore Size (μm)	Maximum Pore Number (/cm^2) /The According Pore Size (μm)	Pore Number (/cm^2)
1:1	1.39–2.11	4.3×10^7/1.769	1.68×10^8
1:3	1.41–2.18	4.13×10^7/1.861	1.15×10^8
1:5	1.55–2.39	2.2×10^7/1.879	7.4×10^7
1:7	2.35–3.93	5.6×10^6/2.668	5.1×10^7
1:9	2.44–4.04	5.5×10^6/2.848	4.5×10^7

3.6. Wetting Properties

The CA values of the PLA/PEG/Cur CNFMs with different weight ratios (PEG:PLA) were obtained by an optical (CA) measurement instrument (Table 4). It was obvious that the CNFMs with the weight ratio 1:1 (PEG:PLA) were hydrophilic due to the hydrophilicity of PEG, and with the increase of the PLA weight ratio, the CA increased gradually due to the hydrophobicity of PLA. When the weight ratio was up to 1:3, the CA of the CNFMs increased to 125.4°. With the continuous increase of the PLA weight ratio, the CNFMs were highly hydrophilic. This might be due to the increase of hydrophobic PLA and pores of the CNFs. The pore structure could further enlarge the surface area and enhance the hydrophobicity of the CNFMs [25].

Table 4. Contact angles of PLA/PEG/Cur CNFMs with different weight ratios (PEG:PLA).

Ratio	1:1	1:3	1:5	1:7	1:9
Contact angles	47.1 ± 1.1°	125.4 ± 2.6°	130.2 ± 1.1°	134.6 ± 2.0°	139.0 ± 1.7°

3.7. In Vitro Cur Release

The released amounts of Cur in PBS from the electrospun CNFs were determined spectrophotometrically at 425 nm by a UV spectrophotometer. The standard curve of Cur concentration was calculated according to $y = 14.26087x - 0.06634$ (R = 0.997), where x is the Cur concentration (μg/mL), y is the optical density (OD) value measured. Based on the standard curve, the cumulative release of Cur was calculated. Figure 5 illustrates the cumulative release of Cur from the porous and nonporous CNFs with the different Cur contents, which were prepared with a weight ratio of 1:7 (PEG:PLA), at a humidity of 60% (porous) and 30% (nonporous), respectively. It could be seen that after 240 h the cumulative release rates of Cur from the porous CNFs with varying Cur percentages from 1% to 5%, were 92.17%, 81.23%, 82.89%, 58.36%, and 57.62%, respectively, were higher than those from the according nonporous CNFs, which were 88.51%, 63.83%, 58.10%, 58.35% and 56.66%. This may have been due to the higher specific surface area of the porous nanofibers and the porous structure could promote the release of the drug [4]. In addition, the cumulative release rate of Cur from the CNFs with 1% Cur was highest, and when the Cur percentage was higher than 3%, the cumulative release rate of Cur was at a low level. This may have been due to the fact that Cur could be dissolved less in the spinning solution when the Cur percentage was at a higher level. Therefore, 3% Cur was selected as the experimental parameter in the following study.

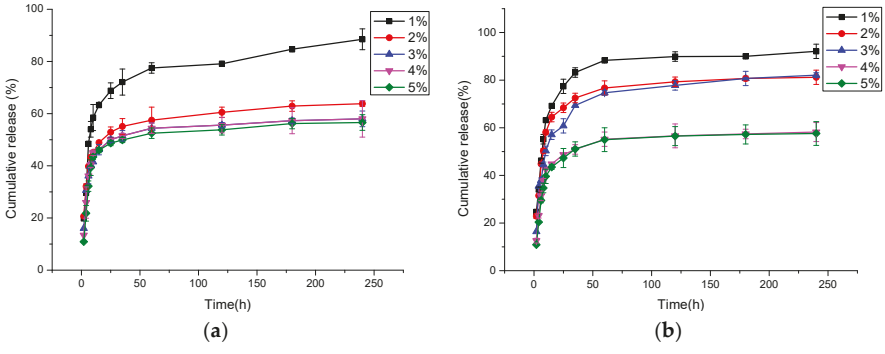

Figure 5. Cumulative release of Cur from porous and nonporous PLA/PEG/Cur CNFs with the different Cur contents: (**a**) Nonporous CNFs; (**b**) Porous CNFs.

Figure 6 shows the cumulative release of Cur from the PLA/PEG/Cur CNFs with 3% Cur and different weight ratios (PEG:PLA). It was evident that after 80 h, the Cur release of CNFs with different weight ratios (PEG:PLA), such as 1:1, 1:3, 1:5, 1:7 and 1:9, reached 48.40%, 53.58%, 55.75%, 66.08% and 69.41%, respectively. That meant the Cur release increased as the PLA weight ratio increased, due to the appearance and increase of pores on the CNFs. The results also demonstrated that the porous structure of the CNFs could absorb more Cur and promote the release of Cur. Therefore, the PLA/PEG/Cur porous CNFs exhibited an improved drug release property.

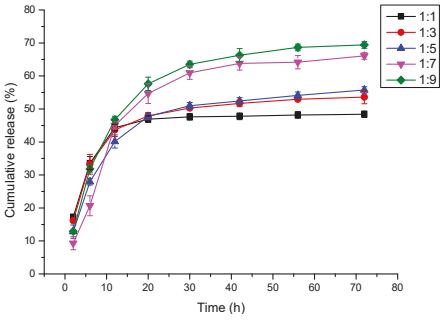

Figure 6. Cumulative release of Cur from PLA/PEG/Cur CNFs with the different weight ratio (PEG:PLA).

3.8. Effects of Porous Structure on Antibacterial Properties

Figure 7 and Table 5 present the antibacterial properties of the PLA/PEG/Cur CNFMs with 3% Cur and different weight ratios (PEG:PLA), and the PEG/PLA CNFMs with a weight ratio (PEG:PLA) of 1:7 used as a comparative sample. It could be seen that the antibacterial effect of the PEG/PLA CNFMs with a weight ratio of 1:7 was poor, and the inhibition rates of the PLA/PEG/Cur CNFMs were all beyond 97%. The antibacterial effect of the PLA/PEG/Cur CNFMs was as good as that of other antibacterial materials in Reference [26]. However, the inhibition rates decreased as the PLA weight ratio increased. To illustrate the results of the antibacterial tests, the initial burst releases of Cur from the PLA/PEG/Cur CNFMs with 3% Cur and different weight ratios (PEG:PLA) for about 20 h were investigated. The standard curve of the Cur concentration was calculated according to $y = 186.428x - 3.3719$ (R = 0.997). According to the standard curve, the cumulative releases of Cur were calculated, as displayed in Figure 8.

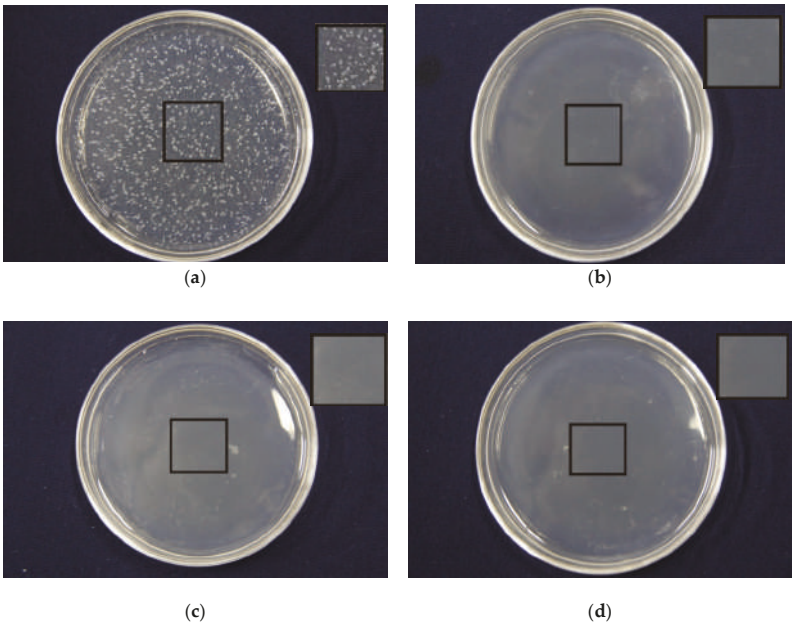

(**a**) (**b**)

(**c**) (**d**)

Figure 7. *Cont.*

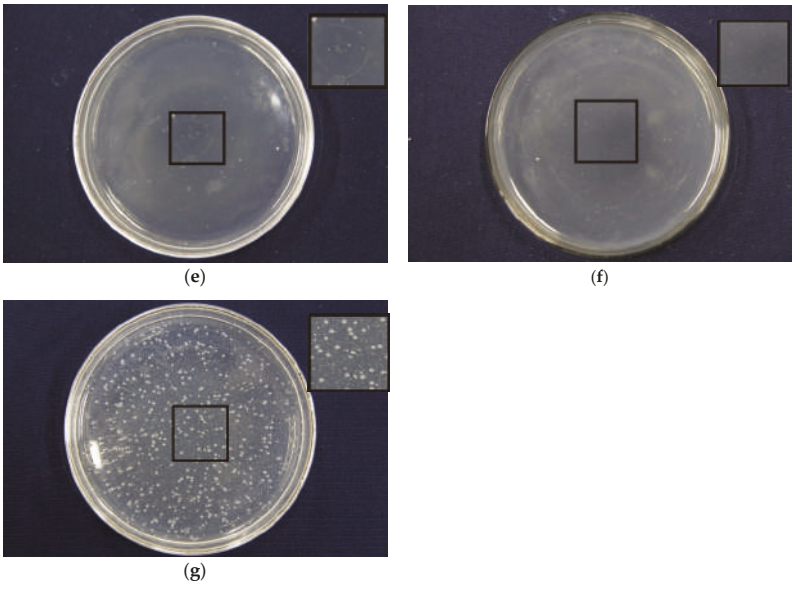

Figure 7. Effects of different composite ratio on antibacterial properties of PLA/PEG/Cur nanofibers membranes: (**a**) PEG:PLA = 1:7 (0% Cur); (**b**) PEG:PLA = 1:1 (3% Cur); (**c**) PEG:PLA = 1:3 (3% Cur); (**d**) PEG:PLA = 1:5 (3% Cur); (**e**) PEG:PLA = 1:7 (3% Cur); (**f**) PEG/PLA = 1:9 (3% Cur); (**g**) cotton.

Table 5. Effects of different composite ratio on antibacterial properties of PLA/PEG/Cur nanofiber membranes.

PEG/PLA	Inhibition Rates (%)
1:1	99.97
1:3	99.96
1:5	99.93
1:7	98.77
1:9	97.61

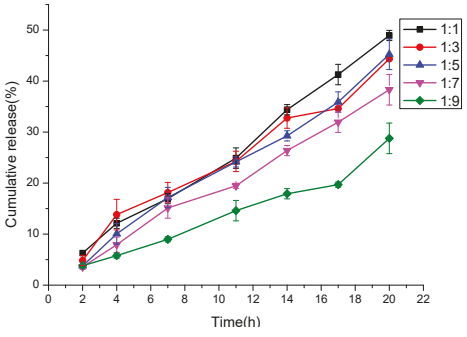

Figure 8. Initial burst release of Cur from PLA/PEG/Cur CNFMs with different weight ratios (PEG:PLA).

As seen in Figure 8, as the PLA weight ratio increased, the initial burst release rate of Cur decreased due to the appearance and increase of pores on the CNFs, which resulted in the decrease of the inhibition rates of the CNFMs. The results showed that the antibacterial effect of the nonporous

CNFs was better due to burst release over a short period of time. This meant that the porous structure of the CNFs could reduce the initial burst release and better control drug release. This could be explained using a modified Fickian diffusion equation, which is presented in our previous work [4]. According to the equation, the porous nanofibers had a longer diffusion path than the nonporous nanofibers, and as the diffusion path increased, the concentration gradient of the drug would become smaller. As a result, the diffusion flux would decrease and lead to the slow release of the drug [4].

4. Conclusions

In the present study, electrospun PLA/PEG/Cur porous CNFs with different weight ratios (PEG:PLA) were successfully prepared by controlling the electrospinning parameters. The electrical conductivity and viscosity of the spinning solutions with different weight ratios (PEG:PLA) were investigated. The results indicated that with the decrease in the weight ratio, the electrical conductivity of spinning solutions decreased, and accordingly, the viscosity of the solutions increased.

The effects of the weight ratio (PEG:PLA) on the morphology and structure of the CNFs were studied systematically. SEM images displayed that as the weight ratio decreased, the morphology of the CNFs changed from smooth to porous. And when the weight ratio increased to 1:7, the pore structure of the nanofiber surfaces became very evident. FTIR and XRD data indicated that Cur was encapsulated successfully in the CNFs. Pore size analysis displayed that with the decrease of the weight ratio, the pore size of the CNFMs increased, and the respective pore number of the CNFMs decreased. CA measurements illustrated that the CA of the CNFMs increased as the weight ratio decreased.

Property characterizations—such as the wetting property, drug release property and antibacterial property—of the PLA/PEG/Cur CNFMs showed that with the decrease of the weight ratio, the CA and the Cur cumulative release of the CNFMs increased due to the appearance of pores on the CNFs. In addition, the antibacterial effect of the CNFMs decreased, as the initial burst release of Cur was prevented by the porous structure of the CNFs. Therefore, the porous structure of the CNFs could improve the drug release property, and the PLA/PEG/Cur porous CNFMs could have great potential for biomedical applications, such as drug delivery, biological scaffold, medical dressing and antibacterial materials.

Author Contributions: L.X. and Z.S. designed the experiments. F.W., Z.S. and J.Y. performed the experiments and the characterizations, and analyzed the data. Z.S. and F.W. drafted the paper. L.X. supervised data analysis and revised the paper.

Funding: This research was funded by National Natural Science Foundation of China: No. 11672198, Six Talent Peaks Project of Jiangsu Province: GDZB-050, and Foundation project of Jiangsu Advanced Textile Engineering Technology Center: No. XJFZ/2018/15.

Acknowledgments: The work was supported financially by National Natural Science Foundation of China (Grant No. 11672198), Six Talent Peaks Project of Jiangsu Province (Grant No. GDZB-050), PAPD (A Project Funded by the Priority Academic Program Development of Jiangsu Higher Education Institutions), and Foundation project of Jiangsu Advanced Textile Engineering Technology Center: No. XJFZ/2018/15.

Conflicts of Interest: The authors declare no conflict of interest.

References

1. Sun, Z.; Fan, C.; Tang, X.; Zhao, J.; Song, Y.; Shao, Z.; Xu, L. Characterization and antibacterial properties of porous fibers containing silver ions. *Appl. Surf. Sci.* **2016**, *387*, 828–838. [CrossRef]
2. Kanehata, M.; Ding, B.; Shiratori, S. Nanoporous ultra-high specific surface inorganic fibres. *Nanotechnology* **2007**, *18*, 1–7. [CrossRef]
3. Liu, P.; Zhu, Y.; Ma, J.; Yang, S.; Gong, J.; Xu, J. Preparation of continuous porous alumina nanofibers with hollow structure by single capillary electrospinning. *Colloids Surf. A-Physicochem. Eng. Asp.* **2013**, *436*, 489–494. [CrossRef]
4. Wang, Y.; Xu, L. Preparation and characterization of porous core-shell fibers for slow release of tea polyphenols. *Polymers* **2018**, *10*, 144. [CrossRef]

5. Zhao, J.; Si, N.; Xu, L. Experimental and theoretical study on the electrospinning nanoporous fibers process. *Mater. Chem. Phys.* **2016**, *170*, 294–302. [CrossRef]
6. Yang, C.; Chen, H.; Zhao, J.; Pang, X.; Xi, Y.; Zhai, J. Development of a folate-modified curcumin loaded micelle delivery system for cancer targeting. *Colloids Surf. B-Biointerfaces* **2014**, *121*, 206–213. [CrossRef]
7. Heni, R.; Yanda, Y.; Rahma, A.; Mase, N. Curcumin-Loaded PLA Nanoparticles: Formulation and Physical Evaluation. *Sci. Pharm.* **2016**, *84*, 191–202. [CrossRef]
8. Lv, L.; Shen, Y.; Li, M.; Xu, X.; Li, M.; Guo, S.; Huang, S. Novel 4-Arm Poly(Ethylene Glycol)-Block-Poly(Anhydride-Esters) Amphiphilic Copolymer Micelles Loading Curcumin: Preparation, Characterization, and In Vitro Evaluation. *Biomed. Res. Int.* **2013**, 1–11. [CrossRef]
9. Bhattarai, N.; Li, Z.; Gunn, J.; Leung, M.; Cooper, A.; Edmondson, D.; Veiseh, O.; Chen, M.; Zhang, Y.; Ellenbogen, R.; et al. Natural-Synthetic Polyblend Nanofibers for Biomedical Applications. *Adv. Mater.* **2009**, *21*, 2792–2797. [CrossRef]
10. Lu, H.; Qiu, Y.; Wang, Q.; Li, G.; Wei, Q. Nanocomposites prepared by electrohydrodynamics and their drug release properties. *Mater. Sci. Eng. C* **2018**, *91*, 26–35. [CrossRef]
11. Zhang, L.; Wang, Z.; Xiao, Y.; Liu, P.; Wang, S.; Zhao, Y.; Shen, M.; Shi, X. Electrospun PEGylated PLGA nanofibers for drug encapsulation and release. *Mater. Sci. Eng. C* **2018**, *91*, 255–262. [CrossRef]
12. Ramírezagudelo, R.; Scheuermann, K.; Galagarcía, A.; Monteiro, A.; Pinzóngarcía, A.D.; Cortés, M.E.; Sinisterra, R.D. Hybrid nanofibers based on poly-caprolactone/gelatin/hydroxyapatite nanoparticles-loaded Doxycycline: Effective anti-tumoral and antibacterial activity. *Mater. Sci. Eng. C* **2018**, *83*, 25–34. [CrossRef]
13. Ma, B.; Huang, Y.; Zhu, C.; Chen, C.; Chen, X.; Fan, M.; Sun, D. Novel Cu@SiO2/bacterial cellulose nanofibers: Preparation and excellent performance in antibacterial activity. *Mater. Sci. Eng. C* **2016**, *62*, 656–661. [CrossRef]
14. Phan, Q.; Mai, H.; Le, T.; Tran, T.; Xuan, P.; Ha, P. Characteristics and cytotoxicity of folate-modified curcumin-loaded PLA-PEG micellar nano systems with various PLA: PEG ratios. *Int. J. Pharm.* **2016**, *507*, 32–40. [CrossRef]
15. Aytac, Z.; Uyar, T. Core-shell nanofibers of curcumin/cyclodextrin inclusion complex and polylactic acid: Enhanced water solubility and slow release of curcumin. *Int. J. Pharm.* **2017**, *518*, 177–184. [CrossRef]
16. Zhong, T.; Jiao, Y.; Guo, L.; Ding, J.; Nie, Z.; Tan, L.; Huang, R. Investigations on porous PLA composite scaffolds with amphiphilic block PLA-b-PEG to enhance the carrying property for hydrophilic drugs of excess dose. *J. Appl. Polym. Sci.* **2017**, *134*, 1–7. [CrossRef]
17. Hussain, S.A.; Patil, G.R.; Reddi, S.; Yadav, V.; Pothuraju, R.; Singh, R.R.B.; Kapila, S. Aloe vera (Aloe barbadensis Miller) supplemented probiotic lassi, prevents Shigella, infiltration from epithelial barrier into systemic blood flow in mice model. *Microb. Pathog.* **2017**, *102*, 143–147. [CrossRef] [PubMed]
18. Feng, X.; Ng, V.K.; Mikš-Krajnik, M.; Yang, H. Effects of Fish Gelatin and Tea Polyphenol Coating on the Spoilage and Degradation of Myofibril in Fish Fillet During Cold Storage. *Food Bioprocess Technol.* **2017**, *10*, 1–14. [CrossRef]
19. Serrano-Aroca, A.; Iskandar, L.; Deb, S. Green synthetic routes to alginate-graphene oxide composite hydrogels with enhanced physical properties for bioengineering applications. *Eur. Polym. J.* **2018**, *103*, 198–206. [CrossRef]
20. Ma, M.; Wan, R.; Gong, H.; Lv, X.; Chu, S.; Li, D.; Peng, C. Study on the In Vitro and In Vivo Antibacterial Activity and Biocompatibility of Novel TiN/Ag Multilayers Immobilized onto Biomedical Titanium. *J. Nanosci. Nanotechnol.* **2019**, *19*, 3777–3791. [CrossRef]
21. Xu, L.; Si, N.; Lee, E.W.M. Effect of humidity on the surface morphology of a charged jet. *Heat Transf. Res.* **2013**, *44*, 441–445. [CrossRef]
22. Achoh, A.; Zabolotsky, V.; Melnikov, S. Conversion of water-organic solution of sodium naphtenates into naphtenic acids and alkali by electrodialysis with bipolar membranes. *Sep. Purif. Technol.* **2019**, *212*, 929–940. [CrossRef]
23. Yan, C.; Yu, Z.; Yang, B. Improvement of thermoregulating performance for outlast/silk fabric by the incorporation of polyurethane microcapsule containing paraffin. *Fibers Polym.* **2013**, *14*, 1290–1294. [CrossRef]
24. Li, J.; Wang, X.; Li, C.; Fan, N.; Wang, J.; He, Z.; Sun, J. Viewing Molecular and Interface Interactions of Curcumin Amorphous Solid Dispersions for Comprehending Dissolution Mechanisms. *Mol. Pharm.* **2017**, *14*, 2781–2792. [CrossRef] [PubMed]

25. Xu, L.; Si, N.; Liu, H.Y. Fabrication and characterization of chinese drug-loaded nanoporous materials. *J. Nano Res.* **2014**, *27*, 103–109. [CrossRef]
26. Frıgols, B.; Martı, M.; Salesa, B.; Herna´ndezOliver, C.; Aarstad, O.; Teialeret Ulset, A.-S.; Inger Sætrom, G.; Lillelund Aachman, F.; Serrano-Aroca, A. Graphene oxide in zinc alginate films: Antibacterial activity, cytotoxicity, zinc release, water sorption/diffusion, wettability and opacity. *PLoS ONE* **2019**, *14*, e0212819. [CrossRef] [PubMed]